

**Polynuclear Metallocene Complexes incorporating
Ansa-Chromocene and Ferrocene Units**

Dissertation

to receive the Degree of a Doctor
in Natural Sciences

Presented by

Dipl.-Chem. Ralph Zehnder

from Bergneustadt

Handed in at Fachbereich 8
of the Universität-Gesamthochschule Siegen
Siegen 2002

urn:nbn:de:hbz:467-296

Day of oral examination: 04.02.2003

Examiners:

Prof. Dr. Wenclawiak

Prof. Dr. Shapiro

Prof. Dr. Deiseroth

Abstract

Novel bimetallic and trimetallic complexes containing *ansa*-chromocene units have been synthesized by a ligand substitution approach. The carbonyl ligands of the corresponding *ansa*-chromocene carbonyl complexes were substituted by the mono- and diisocyanide species ferrocenylisocyanide, ferrocenyldiisocyanide, and 1,4-phenylene diisocyanide in order to form polymetallic complexes that might exhibit mixed valence behavior. The heteronuclear complexes containing a ferrocene unit show a remarkable stability against thermolysis and photolysis. Crystallographic data show that the C-N-C bond angles and Cr-C bond distances of these species follow the trend of other *ansa*-chromocene isocyanides that show a moderate dependence of the Cr^{2+/3+} redox potential on the substituents of the isocyanide groups. In contrast, the heteronuclear complexes do not follow such a trend in respect to their electronic properties. Interestingly, these complexes can modulate the electron density at the Cr metal centers, which enables them to keep their redox potentials constant.

Neuartige *ansa*-Chromocenkomplexe mit zwei bzw. drei Metallzentren wurden mittels Ligandensubstitution synthetisiert. Die Carbonyl-Liganden der entsprechenden *ansa*-Chromocencarbonylkomplexe wurden von den Isocyanidderivaten Ferrocenisocyanid, Ferrocendiisocyanid und 1,4-Phenyldiisocyanid substituiert, um mehrkernige Komplexe zu erhalten, die eventuell gemischtvalente Eigenschaften aufweisen könnten. Die heteronuklearen *ansa*-Chromocenkomplexe mit einer Ferroceneinheit zeigen eine beachtliche Stabilität in Bezug auf Photolyse und Thermolyse. Kristallografische Daten zeigen, dass die C-N-C Bindungswinkel und Cr-C Bindungslängen dem Trend anderer Isocyanide folgen, die eine gewisse Abhängigkeit des Cr^{2+/3+} Redoxpotentials von der Art der Substituenten an den Isocyanidgruppen aufweisen. Im Kontrast dazu folgen die heteronuklearen Komplexe nicht solch einem Trend in Bezug auf ihre elektronischen Eigenschaften. Interessanterweise können diese Komplexe die Elektronendichte an den Cr Metallzentren regulieren, was es ihnen ermöglicht, ihre Redoxpotentiale konstant zu halten.

Table of Contents

1. Introduction.....	1
1.1. <i>The Historical Development of Metallocene Complexes of the Early Transition Metals</i>	1
1.2. <i>The Goal of this Work</i>	13
1.2.1. <i>Ansa-Chromocene(III) Complexes</i>	13
1.2.2. <i>Polynuclear Ansa-Chromocene(II) isocyanide Complexes</i>	13
2. Analytical Methods.....	15
2.1. <i>NMR-Spectroscopy</i>	15
2.2. <i>IR-Spectroscopy</i>	18
2.3. <i>UV-VIS-NIR Spectroscopy</i>	22
2.4. <i>Cyclic Voltammetry</i>	25
2.5. <i>Magnetic Susceptibility</i>	29
2.5.1. <i>Association of Magnetic Susceptibility and Magnetic Moment</i>	29
2.5.2. <i>The Johnson Matthey Magnetic Susceptibility Balance</i>	32
2.5.3. <i>The Evans NMR Method</i>	35
3. Experimentals	36
3.1. <i>General Considerations</i>	36
3.2. <i>Preparation of the Starting Materials</i>	38
3.3. <i>Preparation of all new Polynuclear Ansa-Chromocene isocyanide Complexes</i>	39
3.3.1. <i>{1,1'-(trans-1,2-diphenylethano) dicyclopentadienyl} (ferrocenyliisocyanide) chromium(II)</i>	39
3.3.2. <i>Bis {1,1'-(trans-1,2-diphenylethano) dicyclopentadienyl} (1,1'-ferrocenyldiisocyanide) chromium(II)</i>	40
3.3.3. <i>Bis {1,1'-(tetramethylethano) dicyclopentadienyl} (1,1'-ferrocenyldiisocyanide) chromium(II)</i> ...	41
3.3.4. <i>Bis {1,1'-(tetramethylethano) dicyclopentadienyl} (1,4-phenylene diisocyanide) chromium(II)</i> ...	41
3.4. <i>Chemical Oxidation of Heteronuclear Complexes</i>	42
3.4.1. <i>Oxidation of {1,1'-(trans-1,2-diphenylethano) dicyclopentadienyl} (ferrocenyliisocyanide) chromium(II)</i>	42
3.4.2. <i>Oxidation of Bis {1,1'-(trans-1,2-diphenylethano) dicyclopentadienyl} (1,1'-ferrocenyldiisocyanide) chromium(II)</i>	43
3.5. <i>Determination of the Effective Magnetic Moments</i>	44
3.5.1. <i>Johnson Matthey Magnetic Susceptibility Balance</i>	44
3.5.2. <i>Evans Method using the NMR Device</i>	45
3.5.3. <i>Correction Values</i>	46

4. Results	47
4.1. <i>Electrochemistry of Ansa-Chromocene Complexes</i>	47
4.2. <i>Generation of ansa-Chromocene(III) halide Complexes</i>	49
4.3. <i>Synthesis, Physical and Electronic Properties of Hetero nuclear and Homobinuclear Ansa-Chromocene isocyanide Complexes</i>	54
4.3.1. Synthesis of Ferrocenyliisocyanide Derivatives.....	54
4.3.1.1. Synthesis of Ferrocenyliisocyanide	54
4.3.1.2. Synthesis of Ferrocenyldiisocyanide:	56
4.3.2. New Synthetic Route to <i>Ansa-Chromocene isocyanides</i>	57
4.3.3. Synthesis of Neutral Polynuclear <i>Ansa-Chromocene isocyanides</i>	59
4.3.4. Characterization with NMR- and IR-Spectroscopy.....	60
4.3.5. Ligand Exchange with CO	67
4.3.6. Electrochemistry and X-Ray Single Crystal Structures	68
4.3.7. UV-VIS Spectroscopy.....	76
4.4. <i>Chemical Oxidation of Heteronuclear Ansa-Chromocene isocyanide Complexes</i>	77
4.4.1. Oxidation of 3 and 4a with the Ferrocenylum Cation as well as Benzoquinone.....	77
4.4.2. Determination of the Effective Magnetic Moments	82
5. Discussion	85
6. Conclusions	91
7. Future Work	93
8. References	94
9. Appendix	101
9.1. <i>Magnetic Susceptibility</i>	101
9.1.1. Determination of the Effective Magnetic Moment using the Evans NMR Method	101
9.1.2. Determination of the Effective Magnetic Moment using the Evans Matthey Johnson Magnetic Susceptibility Balance	103
9.2. <i>X-Ray Single Crystal Structure Data</i>	106

1. Introduction

1.1. The Historical Development of Metallocene Complexes of the Early Transition Metals

Over the last five decades metallocene chemistry has grown to a big and important field in organometallic chemistry. The first so called sandwich complex, ferrocene $[(\eta^5\text{-Cp})_2\text{Fe}]$ ($\text{Cp}=\text{C}_5\text{H}_5$), was discovered serendipitously in 1951 by Pauson and Kealy [1] when they tried to synthesize dihydrofulvalene by coupling two molecules of CpMgBr in the presence of iron(III) chloride. They obtained an orange crystalline compound with the composition $\text{C}_{10}\text{H}_{10}\text{Fe}$ that was diamagnetic and remarkably stable. Independently, Miller and Tebboth obtained ferrocene by reacting cyclopentadiene with freshly reduced iron at $300\text{ }^\circ\text{C}$ [2]. Pauson and Kealy proposed a linear structure for the new compound. Shortly after that Woodward and Wilkinson ruled out the linear structure of this compound [3], and Wilkinson proposed the sandwich structure of ferrocene [4]. By collecting X-ray structural data on Cp_2Fe , Pepinsky [5] and Fisher [6] finally confirmed independently the sandwich structure in 1952. For Fisher this was the first step to the 1973 Nobel Prize in chemistry that he and Wilkinson were awarded. Woodward suggested that ferrocene was aromatic and later he showed together with Whiting and Rosenblum that ferrocene undergoes Friedel Crafts acylation readily [7,8].

After the discovery of this prototype sandwich compound, over the last five decades many other transition metal sandwich compounds and other compounds containing metal atoms π -bonded to cyclic organic ligands were developed and their reaction chemistry was characterized. Therefore it is often stated that the modern era of organometallic chemistry began with the discovery of ferrocene. Ferrocene, as the first sandwich complex, shows a remarkable stability and scientists have been able to learn a lot about the frontier orbitals within these kinds of complexes. In general, the molecular orbitals in metallocenes are arranged in such a way that the metal atom in-

between the two Cp rings exhibits bonds to each of the 10 carbon atoms. The bonding orbital shown in Figure 1-1 exhibits the lobes of the d_{yz} orbital of the metal merging with the lobes of the cyclopentadienyl group orbital towards which they point [9].

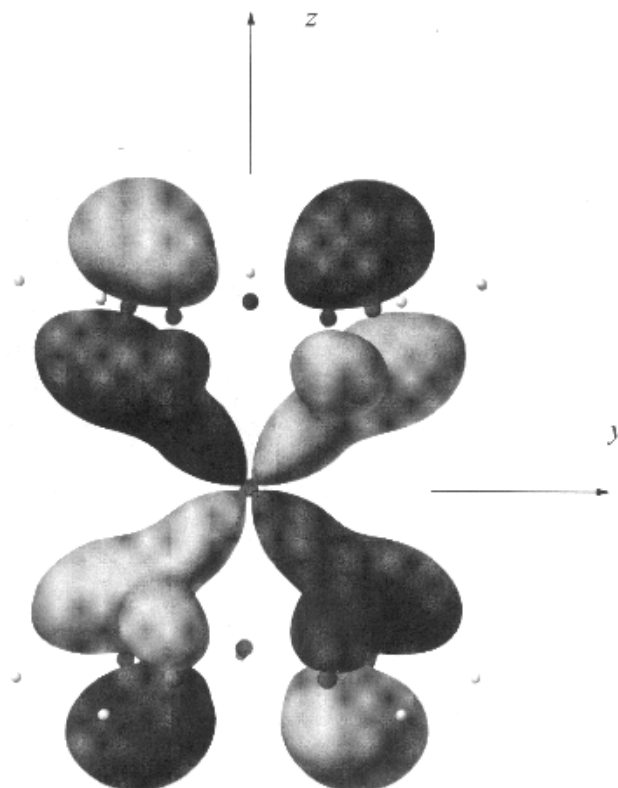


Figure 1-1: Bonding molecular orbital formed from d_{yz} orbital of iron in ferrocene, taken from [9]

The complete energy level diagram for all of the resulting molecular orbitals is shown in Figure 1-2 [10]. The orbitals possessing the greatest d-character are the most interesting ones and they are highlighted in the box in Figure 1-2. These are the orbitals where the form of occupation as well as the number of accommodated electrons govern the chemical and physical properties of the corresponding metallocenes. Ferrocene, for example, is an 18 electron complex; thus, it satisfies the 18 electron rule. The molecular orbitals resulting from the d_{xz} and d_{yz} bonding interactions (e_{1g}) are occupied, whereas the antibonding counterparts (e^*_{1g}), remain empty.

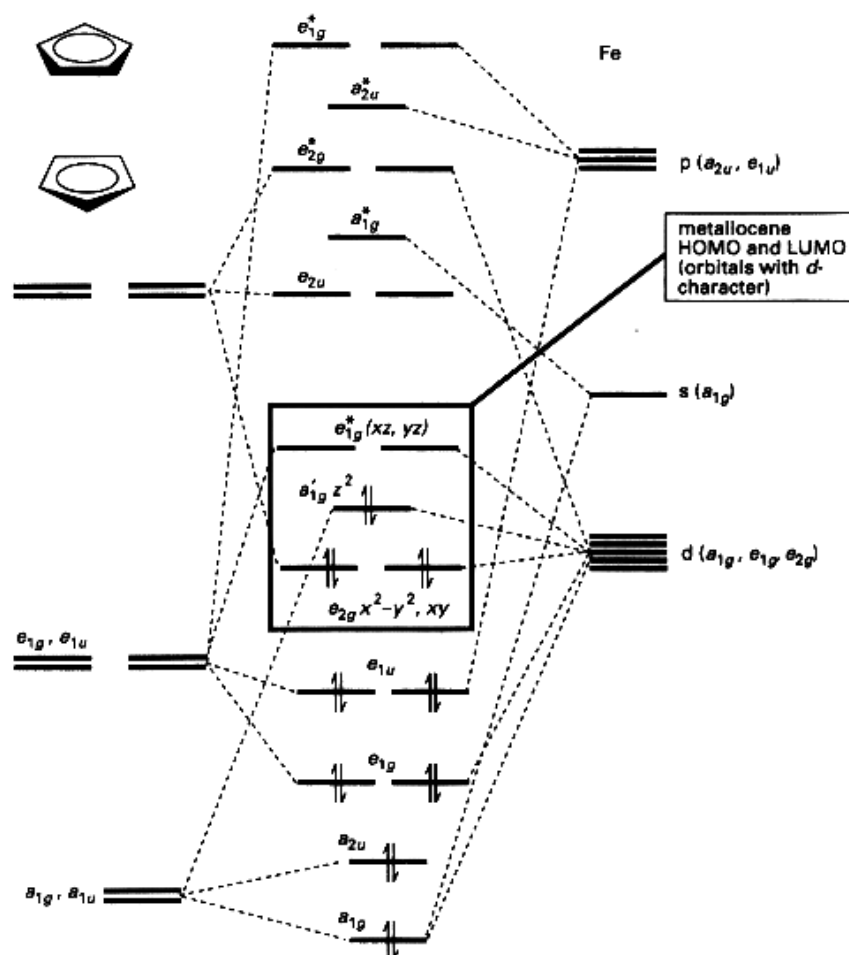
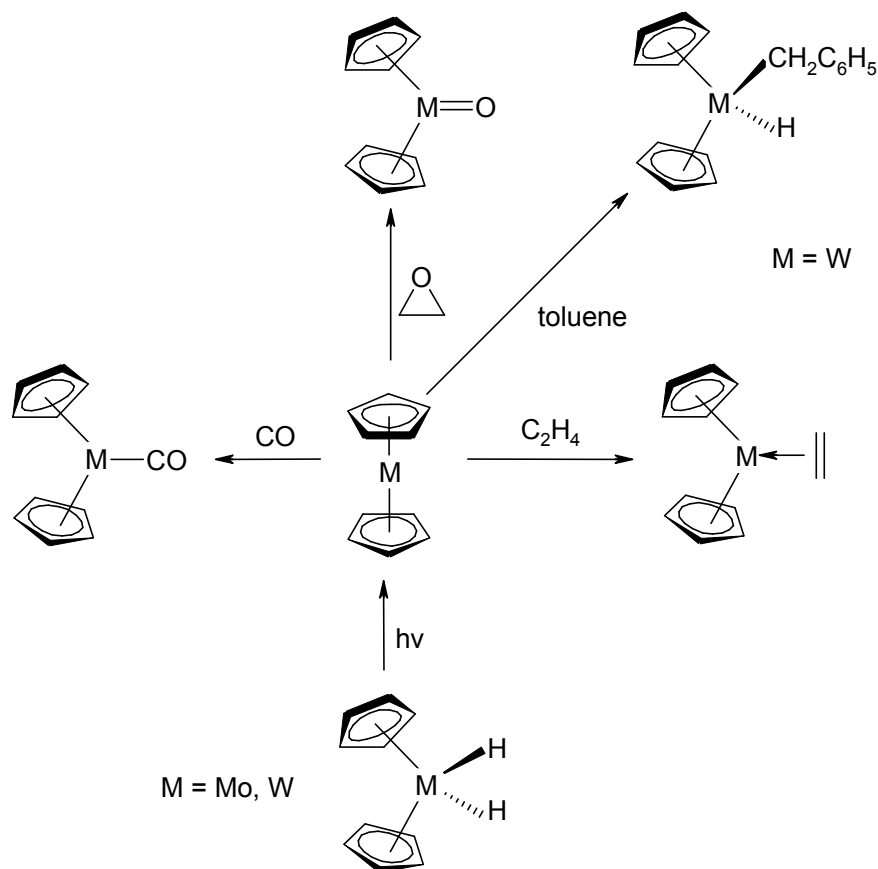


Figure 1-2: Molecular orbital energy levels in ferrocene, taken from [10]

Also, the essentially non-bonding d_{xy} , $d_{x^2-y^2}$ and the d_{z^2} orbitals are occupied. This is the reason why 18 electron metallocenes are relatively inert, diamagnetic compounds. A 19th and 20th electron, however, destabilizes the complex, as in cobaltocene and nickelocene. In cobaltocene the antibonding e^*_{1g} orbitals are occupied with one electron. In nickelocene they are occupied with two unpaired electrons. This causes these two complexes to be paramagnetic and also to be good reducing agents. Once cobaltocene reaches the 1+ oxidation state, it exhibits the same electron configuration and therefore stability as ferrocene. Nickelocene is the only 20 valence electron (VE) metallocene and can be easily oxidized to the nickelocenium ion (19 VE), which is also not very stable.

Geiger et. al. [11] observed its further oxidation to an 18 VE di-cation at low temperatures and also its irreversible reduction to a 21 VE monoanion. Metallocenes with fewer than 18 electrons try to achieve the 18 VE state by complexation of additional electron donor ligands. This results in versatile chemistry for many metallocene species [12].

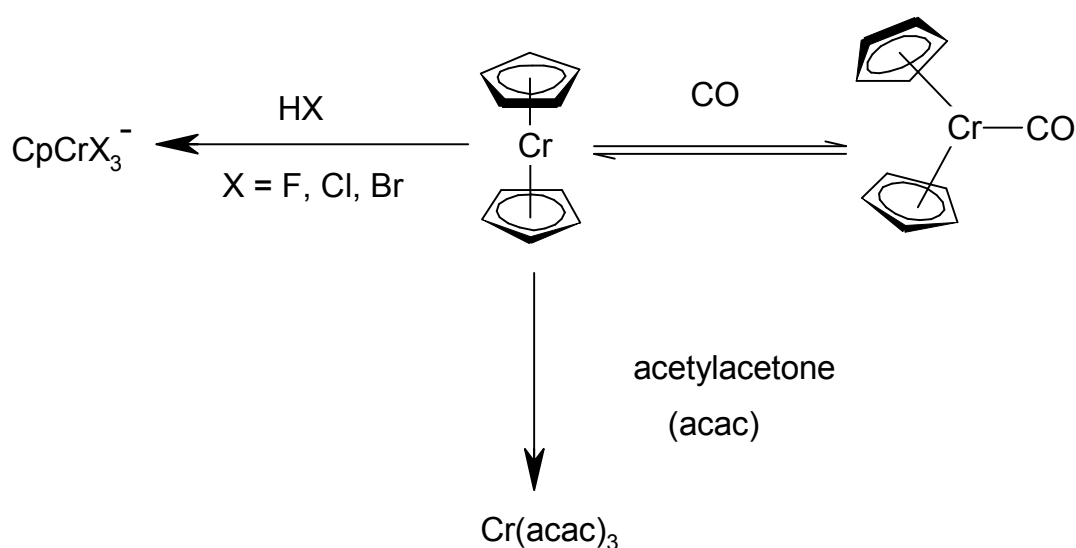
Metallocenes of the group 6 metals Mo and W desire to receive two more electrons from an appropriate donor ligand. Therefore, tungstenocene and molybdocene show a very rich chemistry by complexing additional ligands to the metal center, as can be seen in Scheme 1-1. The 16 VE species with the original parallel ring structure readily complex two electron donor ligands like ethylene and carbon monoxide. They also insert into the C-H bond of aromatic molecules, e.g. toluene, and abstract oxygen from epoxides.



Scheme 1-1: Reactions of molybdocene and tungstenocene complexes

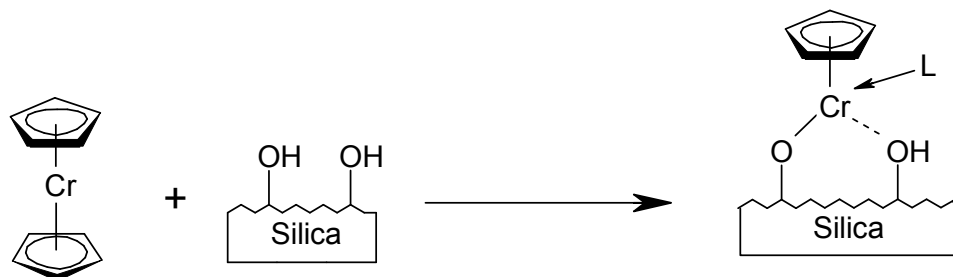
The resulting complexes exhibit a bent structure, so that the frontier orbitals assume an appropriate symmetry to overlap with the corresponding ligand orbitals. The fact that the Cp rings bend back changes the symmetries and energies of the frontier orbitals in the highlighted box of Figure 1-2. Tungstenocene and molybdocene both form thermally stable 18 electron adducts with the neutral two electron donor ligand carbon monoxide.

Chromocene as the first row analogue of group 6 metallocenes does not show such a rich chemistry. Brintzinger et. al. showed that chromocene prefers the 16 VE coplanar ring structure over the bent 18 VE chromocene carbonyl complex [13]. They observed the formation of the CO adduct under an atmosphere of carbon monoxide at low temperatures. But this product was not thermally stable and decomposed under the liberation of CO as well as the regeneration of chromocene at ambient temperature. The formation of NH_3 adducts has been observed in liquid ammonia; however, at ambient temperature chromocene is again regenerated as in the case of the carbonyl adduct [14,15]. As Scheme 1-2 shows, in other reactions chromocene undergoes ring loss, forming either half sandwich complexes with halides as ligands or ordinary chelates with acetylacetonone for instance.



Scheme 1-2:Reaction chemistry of chromocene

However, chromocene possesses catalytic potential in association with silica. The so-called Union Carbide Catalyst can be generated easily by the surface reaction of chromocene with silica (Scheme 1-3). This product is a highly active catalyst for the polymerization of olefins [16,17]. It is remarkable that it does not need any co catalysts or high pressures to accomplish the polymerization.



Scheme 1-3: Formation of the Union Carbide Catalyst

Another example of a chromium based olefin polymerization catalyst is the Phillips Catalyst [18]. However, the chemistry of these heterogeneous catalysts is not yet very well understood. This is the reason why over recent years more and more attention has been drawn to the creation of homogeneous chromium(III) based catalysts [19] as well as compounds that can serve as model systems to elucidate the processes that take place at the catalytic sites of the classical heterogeneous catalysts [20,21]. This branch of organometallic chemistry resulted in the formation of several organometallic chromium (III) complexes and Cr(III) half sandwich complexes that were found to exhibit catalytic activity in olefin polymerization reactions [22,23]. To find an explanation for the different chemical behavior between chromocene and its second and third row analogues, Brintzinger et. al. examined the CO adducts of all three metallocene complexes by using the extended Hückel molecular orbital method (EHMO) [24]. The three CO adducts show nearly identical CO stretching frequencies, implying similar binding in all three complexes. The difference in reactivity however was attributed to the repulsion between the d electrons that needs to be overcome to form the respective CO complex. The metallocene exhibits a triplet ground state, whereas the CO complex exhibits a singlet ground state. The energy difference between the

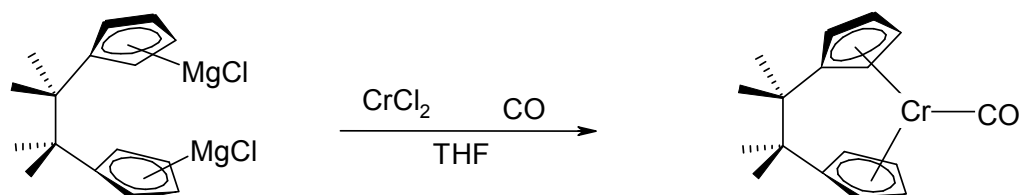
triplet ground state and the singlet excited state is larger for the first row metallocene. Thus, there is a larger energy input to form CrCp_2CO and therefore a bigger energy gain upon its decomposition. Green performed density functional theory (DFT) calculations on the orbital structure and the geometry of bent metallocenes depending on the number of d electrons [25,26]. She was able to confirm Brintzinger's previous results with her theoretical approach.

Her calculations on the enforced bent back structure of tungstenocene complexes is also consistent with experimental results [27]. A significant difference can be observed between *ansa*-bridged and non *ansa*-bridged group 6 metallocene complexes [28]. The non *ansa*-bridged dihydride WCp_2H_2 photochemically eliminates dihydrogen, generating a triplet tungstenocene intermediate that can insert into the C-H bonds of aromatic molecules [29]. However the *ansa*-bridged analogue $\text{W}[(\eta^5\text{-C}_5\text{H}_4)_2\text{CMe}_2]\text{H}_2$ is photochemically inert. In the case of WCp_2MeH , methane can be eliminated thermally, whereas $\text{W}[(\eta^5\text{-C}_5\text{H}_4)_2\text{CMe}_2]\text{MeH}$ is thermally stable up to a temperature of 110 °C.

The reductive elimination from the tungstenocene derivatives is enabled by the formation of a coplanar ring structure for the d^4 configuration metallocene product. If a bent back structure of the Cp rings is enforced by an *ansa*-bridge, relaxation of the complex to this parallel ring geometry is prohibited. As a result, the 18 e- species are stabilized against reductive elimination. Similar stabilization of 18 VE chromocene complexes can be achieved by constraining the Cp rings with a transannular bridging system.

This was accomplished by Brintzinger et al., who in 1983 generated the first thermally stable chromocene carbonyl derivative by introducing a 1,1'-tetramethylethano bridge between the two Cp rings [30]. This was a key step that opened the door to the *ansa*-chromocene chemistry.

To obtain the 1,1'-tetramethylethano chromocene carbonyl complex, Brintzinger et. al. reacted chromium(II) chloride with the di-Grignard compound $(\text{CH}_3)_4\text{C}_2(\text{CpMgCl})_2 \cdot 4\text{THF}$ [31] in THF under an atmosphere of CO. With this approach they produced the desired species in ca. 50% yield.



Scheme 1-4: Synthesis of 1,1'-tetramethylethano chromocene carbonyl

However in the hands of the Shapiro group it was never possible to obtain such a yield. They developed another route to obtain the 18 electron *ansa*-chromocene complex in good yields by synthesizing the corresponding *ansa*-calcocene species as precursor, previously described by Edlmann and co-workers [32]. The *ansa*-calcocene was converted to the *ansa*-chromocene species by reaction with chromium (II) chloride [33] under CO atmosphere. Later they modified the *ansa*-bridge by synthesizing different calcocene complexes by reductive coupling of fulvenes with activated calcium [34]. By employing different fulvene species [35], it is possible to obtain a wide range of different calcocene complexes [36]. To change the design of the *ansa*-bridge was an interesting aspect to compare the physical properties and the reaction chemistry of the resulting complexes.

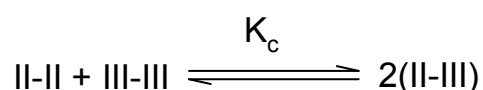
The Shapiro group also generated new 18 VE *ansa*-chromocene complexes by replacing the carbonyl ligand with the isoelectronic *tert*-butyl isocyanide species [33]. As we will see in chapter 4, the formal $\text{Cr}^{2+/3+}$ redox potential in *ansa*-chromocene complexes is profoundly influenced by the electronic properties of the 2 electron donor ligand that is complexed to the metal center [37]. Electrochemical experiments, which will be described later, revealed that the *tert*-butyl isocyanide ligand causes the $\text{Cr}^{2+/3+}$ redox potential to shift to more negative values compared to the carbonyl ligand. The main advantage of the isocyanide ligand over the carbonyl ligand is that there exists a wide

variety of different isocyanide species. This opens the door to new 18 VE *ansa*-chromocene isocyanide complexes with diverse ligand designs. One interesting aspect is to examine the physical properties and the reaction chemistry of *ansa*-chromocenes in association with alkyl isocyanides, aromatic isocyanides or with isocyanide species that could link the Cr metal center with another metal center.

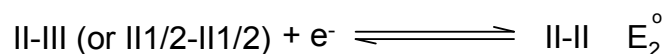
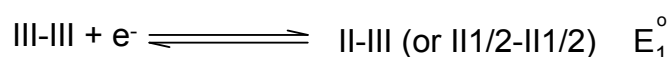
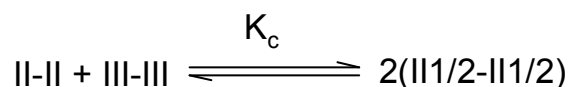
Such polynuclear organometallic complexes have been subject of intense research over recent years. Often it can be observed that these kinds of complexes exhibit electronic communication between their metal centers. One classical example of such a so called mixed valence complex is the Creutz Taube ion [38]. Two Ru centers with different oxidation states are linked by a pyrazine system [39]. These metal centers electronically communicate to a certain extent. This results in the delocalization of the positive charge over the whole molecule, so that both metal centers actually exhibit the same oxidation states. Mixed valence complexes fall into one of three categories: class III complexes, whose ground state is entirely delocalized [40], class II complexes that show delocalization to a certain extent, and class I complexes, in which the metal centers are electronically independent from each other [41]. The extent of delocalization can be monitored using cyclic voltammetry. The electrochemistry should show two reversible redox systems, for instance, if a homobimetallic complex with electronic interactions is investigated. This separation of redox potentials is due to the delocalization of the positive charge generated by the oxidation of the first metal center. The delocalized charge causes a decrease of electron density at the second metal center. Therefore, the second metal center is harder to oxidize and this can be detected by a second redox peak system in the CV. Besides electrochemistry, metal-metal coupling generally can be detected as a broad electronic absorption band in the NIR region, which is caused by a strong metal-to-metal charge transfer (MMCT) transition.

However, it often turns out to be difficult to make definite assignments of which mixed valence class is present in a complex. For example the Creutz Taube ion was first assumed to be localized, while later its category was changed to a class III complex. In many cases there is no clear distinction between class II and class III complexes [42].

The stability of a mixed-valence species [III, II] relative to its oxidized and reduced forms can be recognized by the comproportionation equilibrium constant K_c [43]. The comproportionation reaction for a class II system is:



Whereas the corresponding reaction for a class III system is:



K_c and the free energy change for the comproportionation ΔG_c° can be calculated from the difference in the III/II reduction potentials of the oxidized complexes [44,45]:

$$K_c = \exp\left(\frac{\Delta E_c^\circ \times F}{R \times T}\right) \quad \text{equation 1-1}$$

$$\Delta G_c^\circ = \Delta E_c^\circ \times F \quad \text{equation 1-2}$$

F is the Faraday constant, ΔE_c° is the difference between E_1° and E_2° , which expresses the degree of electronic interactions between the metal centers [46].

The bridge as the link between the metal centers has a profound influence on the extent of metal-metal coupling [47-52]. If the bridge is very short, the metals can interact directly and/or over the bridge with each other. If the distance is longer, the metals can only interact over the bridge with each other. Then the interactions depend directly on the electronic properties of the bridge. The metal centers can be connected with each other in three different ways [53]:

1) Linking the Cp systems of two metallocene moieties

(0.0) Ferrocenophane, for instance, is a valence III complex that shows a significant separation of the formal redox potential in the CV [41]. Biferrocene shows quite similar properties. The monocations of both species show a broad absorption band in the NIR spectrum. In diferrocenylmethane however the coupling is not as intensive as observed for the two former species. The presence of an insulating CH₂ unit between the ferrocene moieties leads to a decrease of the metal-metal interactions [50]. Metallocenes linked with longer saturated bridges show almost unresolvable separations between oxidations. If the linking bridges are olefinic, one can observe larger metal-metal interactions than those found for analogues with saturated bridges [53]. Acetylene bridges show similar effects to C=C bridges. Thus, more π -conjugation via the bridge results in greater metal-metal interactions.

2) Linking the metal center of one moiety with the Cp system of the other one

Peris and co-workers [54], for instance, used ferrocenyl-based conjugated ligands in order to obtain bimetallic and heterometallic push-pull complexes [55-57]. Another example are the electronic interactions of ferrocenyl-capped ruthenium(II) bis(acetylide) complexes and their function as models for organometallic molecular wires [58,59]. It was found that the integration of a metal center in-between the capping metallocene units significantly increases the electronic interactions in these molecules [60].

3) Linking the metal centers directly with each other

These complexes have recently received a lot of attention [61-65]. The Creutz Taube ion [38] is the classical prototype of this group of compounds. McCleverty and co-workers examined quite extensively the role of the bridging ligand to control the electronic and magnetic properties in such complexes [66,67]. Strong interactions can be observed even over long distances if the symmetry and energy terms of the conjugated bridging systems match well to the corresponding terms of the relevant metal orbitals [68]. 1,4-phenylene diisocyanide has been employed as a self-assembled monolayer (SAM) of oligomers onto metals [69], and it was found that it enables the electronic transport between two gold layers [70].

The interest in polynuclear mixed valence complexes has grown tremendously during recent years [71] because of their role in biochemistry [72], their utility in modeling intramolecular electron-transfer reactivity [73], their potential in molecular electronics [74], as well as their role as test systems for theoretical approaches [75].

1.2. The Goal of this Work

1.2.1. *Ansa*-Chromocene(III) Complexes

Many transition metal-containing metallocene complexes show strong potential as catalysts [12]. Since several organometallic chromium (III) complexes and Cr(III) half sandwich complexes were found to exhibit catalytic activity in olefin polymerization reactions [20,22,23], new *ansa*-chromocene(III) analogues could be potential candidates exhibiting catalytic activity as well. One goal of this work was to synthesize such new 17 VE *ansa*-chromocene(III) complexes and examine their reaction chemistry along with their potential to exhibit catalytic activity. As a first step we pursued the synthesis of corresponding *ansa*-chromocene(III) halide complexes. The resulting paramagnetic compounds were to be structurally elucidated using IR-spectroscopy, elemental analyses and X-ray crystallography. Electrochemical experiments were expected to reveal if the 4+ oxidation state is accessible in any of these complexes. The halide complexes were sought as starting materials for diverse new *ansa*-chromocene(III) species.

1.2.2. Polynuclear *Ansa*-Chromocene(II) isocyanide Complexes

The potential ability of ferrocenyl-capped metal complexes [58,59] and 1,4-phenylene diisocyanide to act as molecular wires [70] opens interesting new aspects about the association of such ligand systems with *ansa*-chromocene complexes. Since polynuclear mixed valence complexes are of interest for their potential application to nanotechnology and molecular devices [76], as the second goal of this work, we sought to create new polynuclear 18 VE *ansa*-chromocene isocyanide complexes that incorporate appropriate ligand systems that could possibly enable the metal centers to electronically communicate with each other. Heterobinuclear and heterotrinnuclear *ansa*-chromocene complexes were synthesized by complexing ferrocenylisocyanide

derivatives to the Cr metal centers. A homobinuclear complex was also obtained by linking two *ansa*-chromocene units with 1,4-phenylene diisocyanide.

The physical and structural properties of the resulting compounds were characterized with $^1\text{H-NMR}$, $^{13}\text{C-NMR}$, UV-VIS-NIR, and IR spectroscopies. In some cases crystals of the complexes were grown and their X-ray structures elucidated. The electronic and redox properties were investigated using cyclic voltammetry in order to determine if, on one hand, a perturbation of the $\text{Cr}^{2+/3+}$ redox potential can be correlated with a change of the electronic properties of the isocyanide ligand, and, on the other hand, if the resulting complexes can be converted into mixed valence class II or III complexes. Chemical oxidation reactions were also performed in order to obtain the cationic counterparts that would potentially exhibit intermetallic communication. These cationic species were then subjected to the same kinds of analytical experiments as their neutral parent compounds.

2. Analytical Methods

2.1. NMR-Spectroscopy

NMR-spectroscopy is a very important analytical technique to elucidate the structure of molecules. It provides evidence for the surrounding electronic structure of nuclei. The nuclear magnetic resonance (NMR) experiment is based on the resonant absorption of radiofrequency radiation by nuclei that are exposed to a magnetic field. Only nuclei that provide an odd number of protons or neutrons are eligible for this analytical method since they possess a spin angular momentum and therefore have a magnetic moment. Thus, to some extent they behave like small bar magnets. For instance, ^1H , ^{13}C , ^{19}F , ^{31}P are nuclei with the spin quantum number $I = 1/2$, possessing magnetic moments. If such a nucleus with the spin quantum number $1/2$ is exposed to a homogenous magnetic field its spin may adopt either of two orientations. The spin might adopt the orientation parallel to the magnetic field with the state $m_I = +1/2$ which is denoted α , or it might adopt the orientation antiparallel to the magnetic field with the state $m_I = -1/2$ denoted as β . In a magnetic field these orientations of the nucleus have different energies. The β state lies above the α state and there are slightly more α spins than β spins. If a variable radiofrequency radiation is applied perpendicular to the magnetic field, the energy separations come into resonance with the radiation when the frequency satisfies the resonance condition:

$$\Delta E = h \times \nu = \left(\frac{h}{2 \times \pi} \right) \times \gamma \times H_0 \quad \text{equation 2-1}$$

$$\text{or} \quad \nu = \frac{\gamma \times H_0}{2 \times \pi} \quad \text{equation 2-2}$$

Where γ , an experimentally determined quantity, is the magnetogyric ratio of the respective nucleus, and H_0 is the magnetic field. At resonance conditions there is strong

coupling between the nuclear spins and the radiation, which results in strong absorption as the spins make the transition $\alpha \rightarrow \beta$. In an NMR spectrometer a magnet produces a uniform, intense field. Modern NMR spectrometers possess a superconducting magnet capable of producing fields of the order of 2 T and more. Nuclear magnetic moments interact with the local magnetic field. In general the local field differs from the applied field because the latter induces electronic orbital angular momentum, which causes a small additional magnetic field $-\sigma \times B$ at the nucleus. This additional field is proportional to the applied field. σ is called the shielding constant of the nucleus. Therefore, the resulting local magnetic field that is experienced by the nucleus is dependent on the electronic structure near the magnetic nucleus. Thus, nuclei in different chemical groups have different shielding constants that change the resonance condition resulting in the incorporation of the shielding constant into the following expression:

$$\nu = (1 - \sigma) \frac{\gamma \times H_0}{2 \times \pi} \quad \text{equation 2-3}$$

The result is that the same kind of nuclei surrounded by different electron densities with a fixed frequency of radio radiation will absorb at different strengths of the magnetic field and thus possess their own specific absorption signal. This effect is called the chemical shift because it is dependent on the chemical surrounding of the observed nucleus. In order to compare the chemical shift of different nuclei one needs to use a fixed absorption frequency of a standard compound. For ^1H -NMR spectroscopy this standard compound is tetramethylsilane (TMS). TMS possesses 12 identical protons that are shielded to a relatively large extent, which causes the absorption signal to occur at a high field. The following definition makes it possible to compare chemical shifts of protons independently of the applied radio frequency:

$$\delta = (v_{comp.} - v_{st.}) \times \frac{10^6}{v_0} \quad \text{equation 2-4}$$

Where ν_0 is the applied radio frequency and $\delta_{(\text{TMS})} = 0$. The strength of the local field experienced by a certain proton is not just dependent on the electron density around this particular proton but also on the spin orientation of the neighboring proton. This effect is called spin-spin coupling and it causes the splitting of the absorption signals into multiplets, also known as the fine structure. For the ^1H resonance a group consisting of n equivalent protons causes a splitting into $(n+1)$ fine structure signals for the neighboring atoms, whereby the intensities of these signals correspond to the numbers of the Pascal triangle. The distance of these fine structure signals is called the coupling constant and denoted J . The value of this constant is dependent on the number as well as the type of bonds between the two neighboring atoms. The following information can be obtained from an NMR spectrum of a molecule:

- The number of different resonance signals reveals the number of different characteristic groups within the compound.
- The chemical shifts of different resonance signals correspond to certain kinds of characteristic groups.
- The intensity of the resonance signals is proportional to the number of the signal causing protons.
- Fine structure signals give evidence about the number of protons at a neighboring atom.
- The coupling constant corresponds to the bond strength as well as the hybridization of the atoms.

The shape of the resonance signals is dependent on the relaxation time of the nuclei. Even in the case of resonance, the excited nuclei try to restore the normal Boltzmann distribution by relaxation. This causes a portion of the absorbed energy of the radiofrequency field to be transferred to the environment. The longer the relaxation times, the sharper the resonance signals, and with decreasing relaxation time a broadening of the resonance lines can be observed. This is a significant problem for the examination of paramagnetic compounds. Paramagnetic centers close to the excited nuclei accelerate the relaxation. Therefore, compounds that are paramagnetic, in general, are difficult to investigate by NMR-spectroscopy.

For the study of the properties of diamagnetic molecules containing magnetic nuclei a sample is brought into a homogeneous magnetic field. The sample is surrounded by an inductive coil that applies a high frequency electromagnetic field of 300 MHz or 500 MHz perpendicular to the magnetic field. At certain strengths of the magnetic field the resonance condition is satisfied and the absorption is recorded as a resonance signal [77-79].

2.2. IR-Spectroscopy

Infrared Spectroscopy (IR) is a very commonly used method of instrumental analysis that is based on the absorption of radiation in the infrared region between 2000 nm and 15000 nm. In general, in infrared spectroscopy, one uses the wavenumber scale (ν , 5000 - 700 cm^{-1}). The wavenumber expressed in cm^{-1} is the number of waves in a 1 cm-long wavetrain

$$\nu = \frac{1}{\lambda}$$

Spectra are plotted with wavenumber as the x-axis (decreasing wave numbers to the right) and either absorbance or percent transmittance as the y-axis. Infrared radiation is absorbed when there is a match between the radiant energy and the frequency of a specific molecular motion, usually bond bending and stretching. IR spectroscopy can be applied to elucidate structural data of molecules and assign observed vibrations and the respective wave numbers to certain characteristic functional groups. Atoms within a diatomic molecule are constantly moving relative to each other, vibrating about the connecting bonds at constant frequencies. This motion of alternately stretching and compressing resembles that of two spheres held together by a spring. However, in molecules consisting of more than two atoms the atoms proceed in a motion where they constantly change the bond angle as well. Unlike a spring holding together two masses that can vibrate at any frequency and amplitude, the vibration of atoms in a

molecule is quantized. Only specific frequencies, known as vibrational states are possible. Only when the energy of the photons matches the energy gap between a vibrational state and the next higher one will infrared light be absorbed. Most of the molecules exist in the lowest energy state. Absorption of light that causes an infrared spectrum is the result of raising molecules to the next higher state.

To absorb infrared radiation, a net change in dipole moment as a consequence of the vibrational or rotational motion of a molecule must take place. This is required because only a vibrating dipole can interact with an electromagnetic field whereby absorption of energy from the field becomes possible. A molecule consisting of N atoms possesses $3N$ degrees of freedom because every atom has three degrees of freedom in motion. Six degrees of freedom are needed to describe the translational motion as well as the rotational motion. The remaining $3N-6$ degrees of freedom involve interatomic motion and thus represent the number of possible vibrations within the molecule. A linear molecule, however, possesses only two degrees of freedom in rotational motion; thus, these kinds of molecules have $3N-5$ modes of vibration. Each of these $3N-6$ or $3N-5$ vibrations is called a normal mode. One has to distinguish between two kinds of normal modes:

1. Symmetric and asymmetric vibrations in which the distances between the atoms change.
2. Deformational vibrations where atoms vibrate within the plane (scissoring) and out of plane (twisting), changing the bond angles.

Besides vibrations, infrared absorption also causes rotations to occur. Due to this effect the bands within the spectrum tend to be broad and overlapping. To appreciate the energies of vibrations, it is quite useful to work with the model of the harmonic oscillator. Assuming that two atoms are connected with a covalent bond, in case of absorption of infrared light the atoms move apart. That causes, according to the Hook law, a force to rise which drives the atoms back to a closer distance ($F = -k \times X$). With Newton's second law ($F = m \times a$) and the formula for the harmonic oscillator one obtains the following equation for the wave numbers of the vibrations:

$$\nu_s = \frac{1}{2 \times \pi \times c} \times \sqrt{\frac{k}{\mu}} \quad \text{equation 2-5}$$

Where ν_s is the wavenumber of an absorption peak, μ is the reduced mass ($m_1 \times m_2 / (m_1 + m_2)$), c is the speed of light and k is the force constant for the bond. The force constant is an important representation of bonds. A larger force constant corresponds to a larger bond strength. Certain groups of atoms absorb within narrow regions at similar wave numbers. Therefore information about a carbon scaffold as well as the existence of certain functional groups can be obtained from an IR-spectrum [77, 80-82].

Table 2-1: Functional groups and their corresponding absorption frequencies:

Functional group			Functional group		
group	Band (cm ⁻¹)	intensity	group	Band (cm ⁻¹)	intensity
<i>C-H</i>	2960-2850	medium	<i>RO-H</i>	3650-3400	strong
<i>C=C-H</i>	3100-3020	medium	<i>-C-O-</i>	1150-1050	strong
<i>C=C</i>	1680-1620	medium	<i>C=O</i>	1780-1640	strong
<i>C≡C-H</i>	3350-3300	strong	<i>R₂N-H</i>	3500-3300	medium
<i>R-C≡C-R'</i>	2260-2100	medium	<i>-C-N-</i>	1230-1030	medium
<i>Ar-H</i>	3030-3000	medium	<i>-C≡N</i>	2260-2210	medium
benzene	1600, 1500	strong	<i>RNO₂</i>	1540	strong

The identification of unknown compounds is often accomplished by comparison of the recorded spectrum with reference spectra or values reported in the literature.

In recent years Fourier Transform Infrared Spectrometers (FT-IR) have replaced the dispersive instruments in the market of commercial mid-infrared devices. These instruments are equipped with a Michelson Interferometer, unlike the dispersive ones that were equipped with a monochromator. Figure 2-1 shows a schematic diagram of a Fourier transform spectrometer with a Michelson Interferometer. The radiation beam is

led from the source to a semi-permeable beamsplitter, where it is separated into two partial beams that are reflected on a fixed and on a movable mirror back to the beamsplitter where they recombine and interfere. The movable mirror changes the optical pathlength in the interferometer arm. Thereby the phase difference between both partial beams results and thus a change of the interference amplitude.

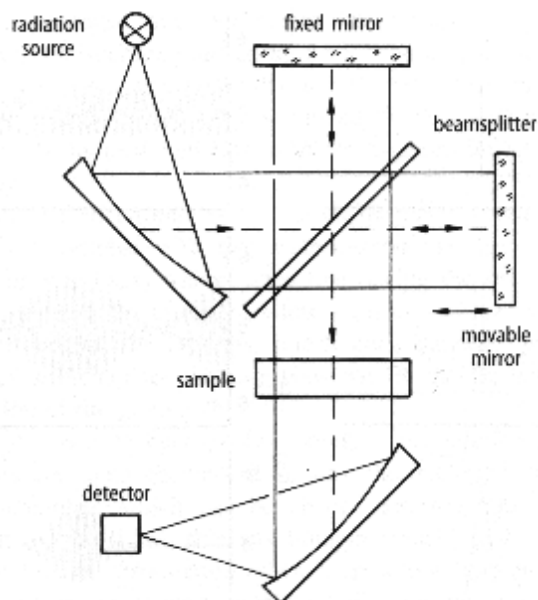


Figure 2-1: Schematic diagram of a Fourier Transform IR Spectrometer with a Michelson Interferometer, taken from [71]

For a monochromatic radiation source a cosine signal is obtained at the detector as a function of the optical path difference. In the case of the same optical path in both arms of the interferometer, the two partial beams are in phase, resulting in constructive interference. If the movable mirror shifts by $\lambda/4$, the path difference, which is called retardation, between both partial beams is $\lambda/2$ and a quenching interference results at the detector. If a radiation source with several wavelengths is applied, the interference pattern corresponds to the sum of the cosine signals of all individual frequencies. The symmetrical interferograms are converted into the spectrum by a Fourier transformation. The sample is brought into the beam before it reaches the detector. Often the sample is examined as a mull in Nujol between two NaCl or KBr windows [82].

2.3. UV-VIS-NIR Spectroscopy

In contrast to IR Spectroscopy, which is based on vibrational transitions of molecules, Ultraviolet-Visible Spectroscopy (UV-VIS) detects the electronic transitions of molecules. In general, electrons that experience an electromagnetic field matching the energy difference between the Highest Occupied Molecular Orbital (HOMO) and the Lowest Unoccupied Molecular Orbital (LUMO) undergo a transition. In most of the cases, such transitions take place at wavelengths between 200 and 800 nm, but for certain molecules also between 800 and 2200 nm, the Near Infrared Region (NIR). One distinguishes different electronic transitions according to their absorption of electromagnetic radiation in different regions of the UV-VIS spectrum [81]:

$\sigma \rightarrow \sigma^*$ Transitions: In this case electrons of bonding σ orbitals are excited to the corresponding antibonding orbital. The energy required for this kind of transition is high and corresponds to the vacuum ultraviolet region. For instance $\sigma \rightarrow \sigma^*$ transitions for C-H bonds exhibit an absorption maximum at 125 nm, whereas C-C bonds appear to absorb at around 135 nm. These are strong localized bonds, which require high energy radiation to undergo the electronic transition.

$n \rightarrow \sigma^*$ Transitions: Saturated compounds containing atoms with unshared electron pairs undergo $n \rightarrow \sigma^*$ transitions. These transitions generally require less energy than the $\sigma \rightarrow \sigma^*$ transitions and absorb between 150 and 250 nm.

$n \rightarrow \pi^*$ and $\pi \rightarrow \pi^*$ Transitions: Both transitions require the presence of an unsaturated functional group to provide the π orbitals. $n \rightarrow \pi^*$ transitions occur at carbonyl, carboxyl, amido groups etc. These groups absorb between 180 and 700 nm. $\pi \rightarrow \pi^*$ transitions occur in alkenes and alkynes as well as other multiple bond containing organic molecules. Alkenes and alkynes absorb at around 180 nm, conjugated organic molecules however absorb at lower energies. The more conjugation

a molecule has, the smaller the energy gap between its HOMO and LUMO. Thus, molecules with higher conjugation absorb at larger wavelengths.

Charge transfer: Complexes that have components of both electron donor and electron acceptor characteristics exhibit charge transfer spectra. Absorption of radiation involves transfer of an electron from the donor to an orbital that is largely associated with the acceptor. This is a very common feature in inorganic transition metal complexes as well as organometallic complexes. Metallocene complexes, for instance, can exhibit several absorption maxima at different energies. Ferrocene shows maxima at 225 nm, 330 nm and 440 nm. The intense charge transfer band at 225 nm has been assigned to a ligand to metal transition [83]. However, in some heteronuclear organometallic complexes, metal to metal charge transfer transitions can be observed as very low energy bands within the NIR region. This usually provides evidence for mixed valence behavior of these complexes. For instance, a broad intense metal-metal charge transfer band was observed within the region from 800 nm to 1900 nm for a binuclear Ru(II)/Ru(III) complex [48].

Many UV-VIS spectrophotometers work with two light beams. They possess one light source for the UV-region, using a deuterium lamp, and one light source for the VIS-region, using a tungsten lamp. Either one of the light sources is used depending on the wavelengths required for an experiment. The emitted polychromatic light is reflected by a mirror and led on a concave mirror. The concave mirror reflects the light to a monochromator, which breaks it down into its spectral pattern. From there the monochromatic light reaches another concave mirror. The beam is reflected by a further mirror and is separated into two identical light beams with the same intensity. Another mirror system leads the two beams through the chamber where they pass through the reference and the sample cuvettes. Behind these cuvettes the two light beams differ only in the intensity of light that was absorbed by the sample. To detect the difference, both beams are led to the detector separately by a scatterer.

Often, a photomultiplier detector is used in such a spectrophotometer. The absorption of light in the sample obeys Beer's law [84]. If I_0 is the intensity of the light before it reaches the sample cuvette, and I is the intensity after absorption by the sample, the decrease in intensity is proportional to the amount of intervening sample, thus the length of the cuvette (X):

$$-dI = k \times I_0 \times dx \quad \text{equation 2-6}$$

Integration of this equation between I_0 and I on the left as well as between 0 and l on the right leads to the following expression:

$$\ln\left(\frac{I_0}{I}\right) = k \times l \quad \text{equation 2-7}$$

Transformation to the decadic logarithm results in:

$$\log_{10}\left(\frac{I_0}{I}\right) = \alpha \times l \quad \text{equation 2-8}$$

The decadic logarithm of I_0/I is called the absorbance and denoted with an A . The relationship I/I_0 is called the transmission, α is the linear decadic absorbance coefficient. With $\alpha = \varepsilon \times c$, we obtain:

$$A = \log_{10}\left(\frac{I_0}{I}\right) = \varepsilon \times c \times l \quad \text{equation 2-9}$$

ε is the molar decadic absorbance coefficient, c is the molar concentration of the sample and l is the length of the cuvette. ε is a specific constant that can be determined experimentally.

2.4. Cyclic Voltammetry

Cyclic voltammetry (CV) is an important and versatile tool to study mechanisms and rates of oxidation/reduction processes, particularly in organic and organometallic systems. It helps to reveal the presence of intermediates in oxidation/reduction reactions. It can also be applied in routine quantitative analysis, to determine the redox potentials of metal containing molecules, and also to predict if certain chemical oxidation or reduction reactions are likely to proceed.

Cyclic voltammetry is a form of voltammetry that consists of cycling the potential of an electrode and measuring the resulting current. The electrode is immersed in an unstirred solution. The potential of this so called working electrode is controlled by a reference electrode that most commonly consists of a saturated calomel electrode (SCE), a silver/silver chloride electrode (Ag/AgCl) or a silver/silver nitrate electrode (Ag/AgNO₃). The excitation signal usually is generated by a linear potential scan with a triangular wave form (Figure 2-2):

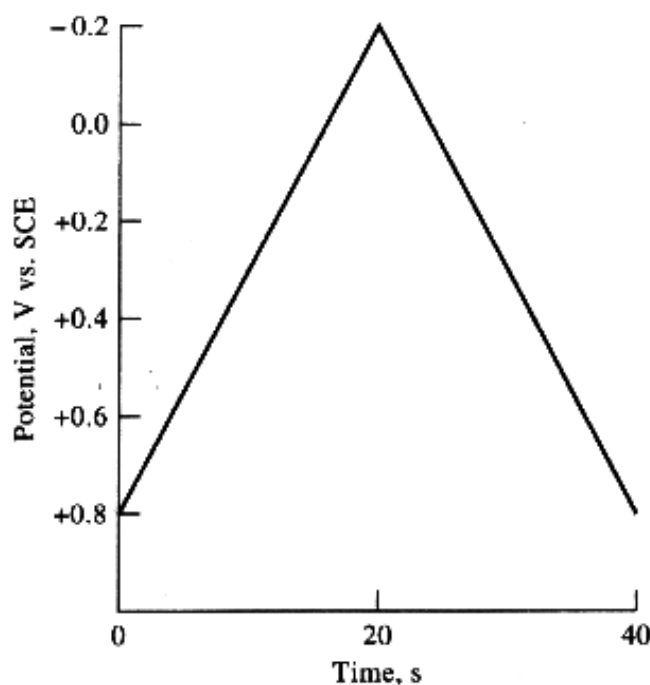


Figure 2-2: Cyclic voltammetric excitation signal, used to obtain voltammogram in Figure 2-3, taken from [70]

In this example, the potential is being swept linearly from + 0.8 V to – 0.15 V, then the scan direction is reversed and the potential is swept back linearly from -0.15 V to + 0.8 V. The scan rate in each direction is 50 mV/s. The current is proportional to the slope of the C-x profile at the electrode surface:

$$i = n \times F \times A \times D \times \left(\frac{\partial C}{\partial x} \right)_{x=0} = k \times \left(\frac{\partial C}{\partial x} \right)_{x=0} \quad \text{equation 2-10}$$

Where i is current, n is number of electrons transferred per ion (equivalents/mole), A is electrode area, D is diffusion coefficient, C is concentration and x is distance from the electrode. In Figure 2-3 the plot of the current versus the potential is shown for a solution that is 6 mM in $\text{K}_3\text{Fe}(\text{CN})_6$ and 1M in KNO_3 and that is subjected to the cyclic excitation signal shown in Figure 2-2.

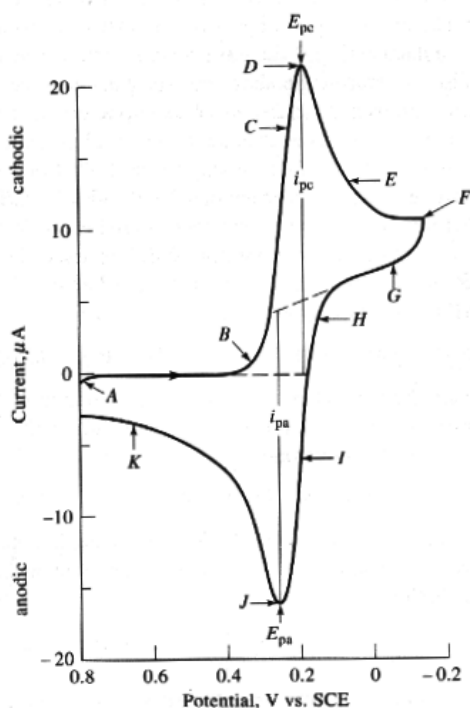
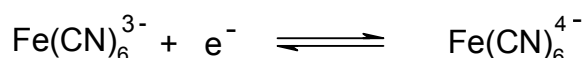


Figure 2-3: Cyclic voltammogram for a solution that is 6 mM in $\text{K}_3\text{Fe}(\text{CN})_6$ and 1M in KNO_3 , taken from [70]

The sweep starts at + 0.8 V (point A). No significant current is observed between the initial potential and + 0.4 V because no reducible or oxidizable species are present in this potential range.

Beyond + 0.4 V a cathodic current develops (point B) due to the reduction of the hexacyanoferrate(III) ion to the hexacyanoferrate(II) ion. The following reaction takes place at the cathode:



A rapid increase in the current can be observed between B and D as the surface concentration of Fe(CN)_6^{3-} becomes smaller and smaller. Two components make up the peak current:

- One is the initial current surge required to adjust the surface concentration of the reactant to its equilibrium concentration as given by the Nernst equation.
- The other one is the normal diffusion controlled current.

The current then decreases rapidly (points D to F) as the diffusion layer extends farther and farther away from the electrode surface. At -0.15 V (point F) the direction of the scan is switched. However the current remains cathodic because the potentials are still negative enough to cause reduction of Fe(CN)_6^{3-} . Once the potential reaches a point that this kind of reduction cannot occur anymore the current assumes the value zero and then becomes anodic. This is caused by the reoxidation of Fe(CN)_6^{4-} that has accumulated near the electrode surface during the forward scan. The anodic current peaks (point J) and then decreases because the Fe(CN)_6^{4-} becomes used up by the anodic reaction.

Important parameters in a cyclic voltammogram are the cathodic peak potential E_{pc} , the anodic peak potential E_{pa} , the cathodic peak current i_{pc} and the anodic peak current i_{pa} . A redox couple is called an electrochemically reversible couple when both species rapidly exchange electrons with the working electrode. The formal oxidation-reduction potential (E^0) is centered between E_{pa} and E_{pc} :

$$E^{o'} = \left(\frac{E_{pa} + E_{pc}}{2} \right) \quad \text{equation 2-11}$$

The numbers of electrons (n), exchanged in the electrode reaction for a reversible couple can be determined from the separation between the peak potentials:

$$\Delta E_p = E_{pa} - E_{pc} = \frac{0.059}{n} \quad \text{equation 2-12}$$

If the electron exchange taking place at the electrode surface is slow, the separation of the peak potentials increases and the process is considered electrochemically irreversible. The peak current for a reversible system is expressed by the Randles-Sevcik equation for the forward sweep of the first cycle:

$$i_p = 2.69 \times 10^5 \times \sqrt[3]{n} \times A \times \sqrt{D} \times C \times \sqrt{v} \quad \text{equation 2-13}$$

Where i_p is peak current, n is electron stoichiometry, A is electrode area, D is diffusion coefficient, C is concentration and v is scan rate. Accordingly the peak currents increase with the square root of the scan rate and are directly proportional to the concentration. In the case of a reversible electrode reaction, anodic and cathodic peak currents have approximately the same absolute values with opposite signs.

A cyclic voltammetric device consists of a voltammetric analyzer, which generates the appropriate sweep potentials and detects resulting currents using three electrodes:

The working electrode most commonly consists of platinum or glassy carbon. The reference electrode and the counter electrode consist of a silver or platinum wire. If an SCE is used as a reference electrode, all recorded potentials are referenced to the calomel redox potential. If a silver/silver nitrate electrode is used, the redox potential of ferrocene as standard is determined separately from the given experiment. This value is

then subtracted from the other experimentally obtained values. All values are then referenced to ferrocene as 0 V.

As mentioned at the beginning, cyclic voltammetry is commonly applied in organometallic chemistry. It can be used to determine shifts of redox potentials due to electronic effects caused by a variety of different ligands complexed to a metal center. This can be interesting if a derivative with a certain redox potential is required for a catalytic reaction. Then small amounts of a species produced on a very small scale are sufficient to perform a CV experiment and determine if it fulfills the requirements [81,85].

2.5. Magnetic Susceptibility

2.5.1. Association of Magnetic Susceptibility and Magnetic Moment

Compounds with unpaired electrons exhibit paramagnetism. Many transition metal, lanthanide and actinide complexes as well as free radicals are paramagnetic. In general, it is difficult to investigate paramagnetic compounds with NMR spectroscopy. Due to the short relaxation times of the nuclei, some paramagnetic systems do not show any resonance absorption signals. Only signals caused by parts of a complex that are far enough apart from the paramagnetic center can be seen as broad peaks. These peaks can only be assigned if additional knowledge about the investigated compounds exists in the form of other structural data. In other paramagnetic systems, the relaxation times are sufficiently long that resonance absorption signals can be observed. However, these signals are paramagnetically shifted, so that the chemical shifts of characteristic peaks can be very different from their values in diamagnetic systems [86].

The behavior of a paramagnetic molecule inside of a magnetic field can provide evidence about the number of unpaired electrons and the spin state of a complex. A paramagnetic substance exposed to a magnetic field B will experience a magnetic field B_{exp} that is more intense than the applied magnetic field B . To elucidate the induction of B_{exp} , a specific induction B' has to be added to B . B' is dependent on the substance and can be expressed as $B \times \chi_v$, where χ_v is called the magnetic susceptibility of a substance and can be defined as the quotient of the added part of induction and the applied magnetic field B [87]:

$$\chi_v = \frac{B'}{B} \quad \text{equation 2-14}$$

The magnetic susceptibility can be referenced to one cm^3 of a substance (volume susceptibility, χ_v), or to one gram of a substance (gram or mass susceptibility, χ_g).

$$\chi_v = \chi_g \times d; \quad (d = \text{density}). \quad \text{equation 2-15}$$

By multiplication of χ_v with the molar volume V_m or χ_g with the molar mass M one obtains the molar susceptibility χ_M :

$$\chi_M = \chi_g \times M \quad \text{equation 2-16}$$

Thus, the magnetic susceptibility is the ratio of the intensity of magnetism induced in a substance to the magnetizing force or intensity of field to which it is subjected. Therefore, the magnetic susceptibility of a paramagnetic substance possesses a positive value, and that of a diamagnetic substance possesses a negative value. Every paramagnetic substance possessing one or more unpaired electrons exhibits a magnetic moment that is called the effective magnetic moment, μ_{eff} . The calculation of the effective magnetic moment, in general, is sophisticated, because the orbital angular momentum has to be considered. However, for the 2+ and 3+ ions of the first row

transition metals the orbital angular momentum can be neglected because the orbital contribution is largely quenched by the field due to the surrounding ligands [88]. For these ions, the effective magnetic moment can be obtained from the spin-only equation:

$$\mu_{eff} = 2 \times \sqrt{S \times (S + 1)} \quad \text{equation 2-17}$$

S = spin quantum number = sum of the spin quantum numbers s of the unpaired electrons n. $s = \frac{1}{2}$, $S = n \times \frac{1}{2}$

$$\mu_{eff} = 2 \times \sqrt{\frac{n}{2} \times \left(\frac{n}{2} + 1\right)} \quad \text{equation 2-18}$$

$$\mu_{eff} = 2 \times \sqrt{n \times (n + 2)} \quad \text{equation 2-19}$$

Table 2-2 shows values for μ_{eff} as a function of n:

Table 2-2: Numbers of unpaired electrons and their corresponding effective magnetic moments:

n	μ_{eff}	n	μ_{eff}
1	1.73	4	4.90
2	2.83	5	5.92
3	3.87	6	6.93

χ_m and μ_{eff} are related by the expression:

$$\left(\mu_{eff}\right)^2 = \frac{3 \times k \times T \times \chi_M}{N \times \beta^2} \quad \text{equation 2-20}$$

N = Avogadro's number, β = the Bohr magneton, k = Boltzmann's constant, T = absolute temperature in K.

$$\mu_{\text{eff}} = 2.84 \times \sqrt{\chi_M \times T} \quad \text{equation 2-21}$$

If μ_{eff} is independent of the temperature for a substance, it obeys the Curie law. Each paramagnetic substance also experiences diamagnetic contributions from all other parts of the substance around the paramagnetic center. This is the reason why all diamagnetic values of ligands and atoms have to be added together and the value of this sum has to be added to the experimentally determined value of χ_M . The resulting corrected value of χ_M is applied to determine μ_{eff} . There are two commonly used methods to determine the magnetic susceptibility of compounds as well as their effective magnetic moment:

2.5.2. The Johnson Matthey Magnetic Susceptibility Balance

The magnetic balance can be used to determine the mass susceptibility of a complex in the solid state [88]. The sample tube is placed in-between one pair of movable magnets that are fixed to one end of a lever. Another pair of magnets is fixed to the other end of the lever. A coil is placed between these two other magnets. The source of a light beam is fixed to the middle part of the lever shining on optical sensors. As long as no sample is present, the system is balanced. Once the sample becomes introduced into the system, the magnets experience a force and move the lever. This causes the light beam to deflect. The movement of the light beam is optically detected. This causes an electric current to flow through the coil inducing another magnetic field, which causes the other pair of magnets to move the lever into the opposite direction. Once the light beam shines on the optical sensors in the same way as it did before the sample was introduced, the system is in balance again. The electric current flowing through the coil,

necessary to bring the system back to balance, is directly proportional to the force exerted by the sample and can be measured as a voltage drop [89]. The following expression for χ_g in cgs/g units results from the derivation shown below:

$$\chi_g = \frac{c \times l \times (R_{full} - R_0)}{m} \quad \text{equation 2-22}$$

Where R_0 = empty tube reading, R_{full} = reading obtained for tube plus sample, R = net value for $R_{full} - R_0$, l = sample length in cm, m = sample mass, and c is the calibration constant of the balance.

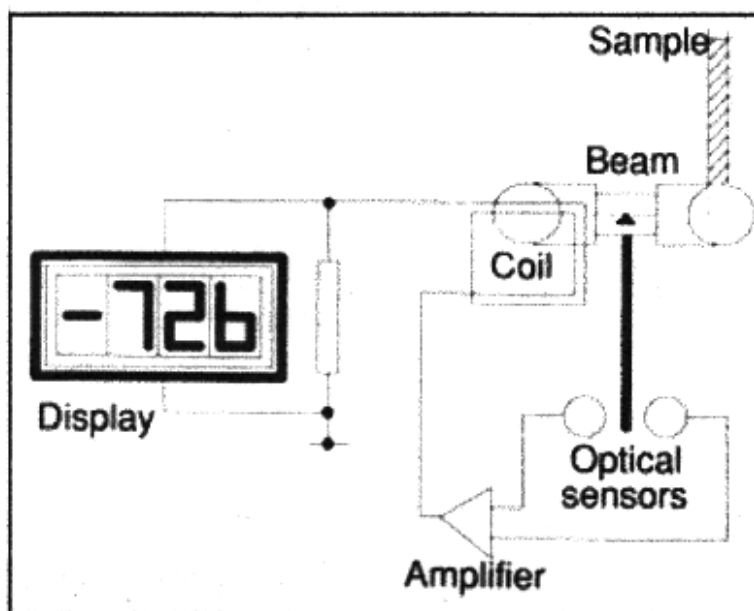


Figure 2-4: Schematic diagram of a magnetic susceptibility balance, taken from [89]

The derivation of the expression is based on the Gouy method, which is one of the most commonly used methods to determine the magnetic susceptibility. The difference to the Johnson Matthey balance is that the difference of force applied to the lever of the system is directly measured in terms of force, which is a function of $\delta_{(m)}$:

$$F = \delta_{(m)} \times g \quad \text{equation 2-23}$$

$$F = 0.5 \times \chi_v \times A \times H^2 \quad \text{equation 2-24}$$

χ_v = volume susceptibility of the sample, A = sample cross sectional area, $\delta_{(m)}$ = apparent change in mass on application of the magnetic field, H = field strength and g = acceleration due to gravity (9.81 m/s²). With

$$\chi_v = \chi_g \times d \quad \text{equation 2-25}$$

$$\text{and } A = \frac{m}{l \times d} \quad \text{equation 2-26}$$

we obtain the expression for χ_g :

$$\chi_g = \frac{2 \times g \times l \times \delta_{(m)}}{H^2 \times m} \quad \text{equation 2-27}$$

Where m = sample mass, d = sample density and l = sample length. If H is kept constant and with $c = \frac{2 \times g}{H^2}$ this can be written as:

$$\chi_g = \frac{c \times l \times \delta_{(m)}}{m} \quad \text{equation 2-28}$$

Since $\delta_{(m)}$ is directly proportional to the drop of voltage using the Johnson Matthey balance, this expression can be transformed into the final form [88]:

$$\chi_g = \frac{c \times l \times (R_{full} - R_0)}{m} \quad \text{equation 2-22}$$

2.5.3. The Evans NMR Method

Using the NMR method, one compares the resonance absorption frequency of a pure solvent with the frequency of the same solvent as a solution of the sample with a certain concentration. The frequency difference is dependent on the magnetic susceptibility of the sample. For this kind of experiment a thin tube that possesses a narrow tip at the bottom is filled with the pure solvent and placed into an NMR-tube. This NMR tube contains a solution of the sample with a certain concentration in g/ml within the same solvent that was added to the thin coaxial tube. Then these two tubes are placed into the magnetic field of the NMR-spectrometer. The resonance absorption signals are detected after one transient without locking the signal. Two absorption signals can be observed, one representing the pure solvent, the other one representing the solvent containing the sample. Due to the paramagnetism of the sample, the solution experiences a stronger magnetic field than the applied field. This causes the solution to absorb at a lower frequency than the pure solvent. The observed frequency difference Δf and χ_g are related by the following expression [90]:

$$\chi_g = \frac{3 \times \Delta f}{4 \times \pi \times f \times n} + \chi_{\text{solvent}} \quad \text{equation 2-30}$$

Where f = frequency of NMR-device, χ_{solvent} = diamagnetic susceptibility of solvent and n is the mass of sample in one mL solvent.

3. Experimentals

3.1. General Considerations

All synthetic experiments were carried out in an inert atmosphere using a combination of glovebox, high-vacuum and Schlenk techniques. HPLC grade solvents were dried by passage over alumina and then stored in line-pots from which they were vacuum transferred from sodium/benzophenone. Argon was purified by passage over an oxy tower BASF catalyst (Aldrich) and 4A molecular sieves. The deuterated solvents were dried over 4A molecular sieves and stored in the glovebox. HPLC grade tetrahydrofuran (Fisher) for the electrochemical measurements was used as received. Elemental analyses were determined by Desert Analytics (Tucson, AZ).

NMR spectra were recorded on an IBM NR-300 (300 MHz ^1H) and an Avance 500 (500 MHz ^1H , 125 MHz ^{13}C , 470 MHz ^{19}F , 202 MHz ^{31}P). All chemical shifts are reported in ppm and referenced to solvent.

All X-ray single crystal structures were determined by Dr. Brendan Twamley. The single crystal X-ray diffraction experiments for complex **3** and $\text{CrBr}_2(\text{THF})_2$ were performed on a Siemens SMART 1K diffractometer. The structure was solved with the software XS, Bruker SHELXTL v. 5.10 and refined by Full-matrix least-squares procedures. The single crystal X-ray diffraction experiments for complex **4b** and **5** were performed on a Bruker/Siemens SMART APEX diffractometer. The structures were solved with the software XS, Bruker SHELXTL v. 6.10 and refined by Full-matrix least-squares procedures. The absorption corrections of all complexes were performed with SADABS, an empirical absorption correction program, Saint+ 6.22, Bruker AXS Inc., Madison, WI, 2001.

Mass spectra were recorded by Dr. Gary Knerr using a JEOL JMS/AX 505 HA GC-MS spectrometer.

Cyclic voltammetric measurements were performed on a BAS CV50W Voltammetric Analyzer in a nitrogen filled glove box. Potentials were measured, without IR compensation, against a reference electrode consisting of a silver wire immersed in a solution of AgNO_3 (0.01 M) in acetonitrile, using a glassy carbon working electrode and a platinum wire as the counter electrode. Measurements were performed on THF solutions of the sample complex (< 1mM) containing 0.3 M $[\text{NBu}_4][\text{PF}_6]$ electrolyte. All potentials are referenced to the ferrocene (II/III) couple (E_p 200 mV), which was measured separately and prior to the sample measurements.

IR-spectra were obtained on an ATI Mattson Genesis Series FTIRTM Spectrophotometer and on a Bio Rad FT-IR Spectrometer FTS 175C.

UV-VIS spectra were obtained on a Hewlett Packard 8453 diode array spectrophotometer. The samples were measured as THF solutions of the complexes under nitrogen in sealed 1 cm quartz cuvettes.

NIR-spectra were obtained on a PERKIN-ELMER 330 spectrophotometer. The samples were measured as THF and CH_2Cl_2 solutions of the complexes under nitrogen in sealed 1 cm quartz cuvettes.

Magnetic susceptibilities were determined using two methods independently:

- The Johnson Matthey Magnetic Susceptibility Balance Type MSB, model MK I
- The Evans NMR method, using the IBM NR-300 (300 MHz ^1H) NMR spectrometer.

3.2. Preparation of the Starting Materials

(1,1'-trans-1,2-diphenylethano) chromocene carbonyl (**1a**) and (1,1'-tetramethyl-ethano) chromocene carbonyl (**1b**) were synthesized as previously described [33,37].

Ferrocenyliisocyanide was prepared in six steps starting from ferrocene. The first four steps were performed as described previously [91]. The preparation of ferrocenyliisocyanide from ferrocenylamine proceeded as a one pot reaction. The previously described synthesis [92] was slightly modified as described below

5.10 g (25.4 mmol) of ferrocenylamine was heated in a glass bomb with 85 mL ethylformate to 70 °C. After 70 h the ethylformate was removed and the blackish residue was dissolved in 110 mL methylene chloride. 10 mL diisopropylamine was added. The solution was cooled to 0 °C and 1.9 mL (25.4 mmol) phosphoryl chloride was added slowly. The reaction mixture was allowed to warm to ambient temperature and was stirred for another 16 hours. Then the mixture was cooled to 0 °C and water was added in order to destroy the excess of phosphoryl chloride. The organic layer was washed three times with water, dried with anhydrous sodium sulphate and evaporated. The residue was chromatographed on neutral alumina. Petroleum ether eluted the orange product. Orange crystals remained after evaporation of the petroleum ether. Yield: 3.50 g (65.4%).

Ferrocenyldiisocyanide was prepared in six steps as described previously [8,93,94].

1,4-phenylene diisocyanide was purchased from Aldrich. All other reagents were purchased from either Aldrich or Acros and used as received.

3.3. Preparation of all new Polynuclear *Ansa*-Chromocene isocyanide Complexes

3.3.1. {1,1'-(*trans*-1,2-diphenylethano) dicyclopentadienyl} (ferrocenylisocyanide) chromium(II) (**3**)

989 mg of **1a** (2.5 mmol) was added to a Double Schlenk vessel. 458 mg (2.2 mmol) of ferrocenylisocyanide was also added and 50 mL of THF was vacuum transferred into the reaction vessel. The solution was stirred and heated to a temperature of 40 °C. The reaction took place at reduced pressure, evolving carbon monoxide. After 20 minutes, the THF was removed. A reddish brown residue remained consisting of the desired product **3** and a paramagnetic species, formed as a byproduct. **3** was separated from this byproduct by extraction with ethyl ether. Ca. 300 mL of ethyl ether was vacuum transferred into the system and the product was extracted five times. After that, the combined ethyl ether extracts were concentrated to ca. 30 mL, causing the product to precipitate. The impurities dissolved in the remaining solvent were separated from the product by filtration. The product was then dried under vacuum. Single crystals were obtained by leaving a solution of **3** in benzene- d_6 under inert atmosphere. After the solvent was evaporated completely, a blackish crystalline substance remained. Yield: 670 mg (54%). $^1\text{H-NMR}$, (500 MHz, 25 °C, C_6D_6) δ 3.87 (m, 2H, $\text{Cp}_{\text{Cr-unit}}$), δ 3.90 (s, 2H, $[(\text{aryl})_2\text{C}_2\text{H}_2]$), δ 3.91 (m, 2H, $\text{Cp}_{\text{Fe-subst}}$), δ 4.17 (s, 5H, $\text{Cp}_{\text{Fe-unsubst}}$), δ 4.26 (m, 2H, $\text{Cp}_{\text{Cr-unit}}$), δ 4.42 (m, 1H, $\text{Cp}_{\text{Fe-subst}}$), δ 4.45 (m, 1H, $\text{Cp}_{\text{Fe-subst}}$), δ 4.54 (t, 2H, $\text{Cp}_{\text{Cr-unit}}$, $J=1.3$), δ 4.94 (t, 2H, $\text{Cp}_{\text{Cr-unit}}$, $J=1.5$), δ 7.00, 7.07 (m, 6H, aryl, $J=7.3$), δ 7.13 (m, 4H, aryl, $J=7.0$). $^{13}\text{C-NMR}$, (500 MHz, 25 °C, C_6D_6) δ 54.8 ($[(\text{aryl})_2\text{C}_2\text{H}_2]$), δ 64.0, 65.9, ($\text{Cp}_{\text{Fe-subst}}$), δ 69.7 ($\text{Cp}_{\text{Fe-unsubst}}$), δ 77.9, 78.6, 80.0, 82.0 ($\text{Cp}_{\text{Cr-unit}}$), δ 126.7, 127.5, 128.3, 142.4 (aryl), δ 274.0 (NC). IR (NaCl plates, Nujol): 1829 cm^{-1} ($\nu(\text{NC})$). Anal. Calcd. for $\text{C}_{35}\text{H}_{29}\text{CrFeN}$: C, 73.56; H, 5.10; N, 2.45. Found: C, 73.95; H, 5.03; N, 2.52. CV: ($E_a + E_c$)/2 $\text{Fe}^{2+/3+}$, 281 mV, $\text{Cr}^{2+/3+}$, -1153 mV, $E_a \text{Cr}^{3+/4+}$, 131 mV i_a/i_c : $\text{Cr}^{2+/3+} = 1.21$; i_a/i_c : $\text{Fe}^{2+/3+} = 0.83$.

3.3.2. Bis {1,1'-(*trans*-1,2-diphenylethano) dicyclopentadienyl} (1,1'-ferrocenyldiisocyanide) chromium(II) (**4a**)

1000 mg of **1a** (2.6 mmol) was added to a double Schlenk vessel. 304 mg (1.3 mmol) of ferrocenyldiisocyanide was also added and 50 mL of THF was vacuum transferred into the reaction vessel. The solution was stirred and warmed to 40 °C. The reaction took place at reduced pressure, evolving carbon monoxide. After 20 minutes, the THF was removed. A reddish brown residue remained consisting of the desired product **4a** and a paramagnetic species, formed as a byproduct. **4a** was separated from this byproduct by extraction with ethyl ether. Ca. 300 mL of ethyl ether was vacuum transferred into the system and the product was extracted five times. After that, the combined ethyl ether extracts were concentrated to ca. 30 mL, causing the product to precipitate. The impurities dissolved in the remaining solvent were separated from the product by filtration. The product was then dried under vacuum. Yield: 783 mg (63%). ¹H-NMR, (500 MHz, 25 °C, THF *d*₈) δ 3.86 (m, 4H, Cp_{Cr-unit}), δ 4.12 (m, 4H, Cp_{Fe-subst}), δ 4.20 (s, 4H, [(aryl)₂C₂H₂]), δ 4.27 (m 4H, Cp_{Cr-unit}), δ 4.38 (m, 1H, Cp_{Fe-subst}), δ 4.41 (m, 2H, Cp_{Fe-subst}), δ 4.43 (m, 1H, Cp_{Fe-subst}) [(70 °C) δ 4.37 (m, 1H, Cp_{Fe-subst}), δ 4.39 (m, 1H, Cp_{Fe-subst}), δ 4.40 (m, 1H, Cp_{Fe-subst}) δ 4.41 (m, 1H, Cp_{Fe-subst})], δ 4.75 (m, 4H, Cp_{Cr-unit}), δ 5.30 (m, 4H, Cp_{Cr-unit}), δ 7.08, 7.16, 7.28 (m, 20H, aryl). ¹³C-NMR, (500 MHz, 25 °C, THF *d*₈) δ 55.3 ((aryl)₂C₂H₂), δ 65.2, 65.3, 65.4, 67.0 (Cp_{Fe-subst}), δ 78.1, 79.1, 80.5, 82.5, 82.6 (Cp_{Cr-unit}), δ 127.2, 128.5, 128.9, 143.7 (aryl), δ 276.2 (NC). IR (NaCl plates, Nujol): 1763 cm⁻¹ (ν(NC)). Anal. Calcd. for C₆₀H₄₈Cr₂FeN₂: C, 75.31; H, 5.06; N, 2.93. Found: C, 69.03 ; H, 4.71 ; N, 2.71. CV: (E_a + E_c)/2 Fe^{2+/3+}, 589 mV, Cr^{2+/3+}, -1152 mV, E_a Cr^{3+/4+}, 33 mV, i_a/i_c: Cr^{2+/3+} = 0.99.

3.3.3. Bis {1,1'-(tetramethylethano) dicyclopentadienyl} (1,1'-ferrocenyldiisocyanide) chromium(II) (4b)

1000 mg of **1b** (3.4 mmol) was added to a double Schlenk vessel. 403 mg (1.7 mmol) of ferrocenyldiisocyanide was also added and 50 mL of THF was vacuum transferred into the reaction vessel. The solution was stirred and warmed to 40 °C. The reaction took place at reduced pressure, evolving carbon monoxide. After 20 minutes, 2/3 of the THF was removed and ca. 60 mL of hexane was vacuum transferred into the vessel. The reddish brown product was crystallized out of a 20:80 THF/hexane mixture at -78 °C. Single crystals were obtained by leaving a solution of **4b** in d_6 -benzene under inert atmosphere. After the solvent evaporated completely a blackish crystalline substance remained. Yield: 640 mg (49%). $^1\text{H-NMR}$, (500 MHz, 25 °C, THF d_8) δ 1.19 (s, 24H, $\text{C}_2(\text{CH}_3)_4$), δ 3.92 (m, 8H, $\text{Cp}_{\text{Cr-unit}}$), δ 4.04 (m, 4H, $\text{Cp}_{\text{Fe-subst}}$) δ 4.30 (m, 4H, $\text{Cp}_{\text{Fe-subst}}$), δ 4.76 (m, 8H, $\text{Cp}_{\text{Cr-unit}}$). $^{13}\text{C-NMR}$, (500 MHz, 25 °C, C_6D_6) δ 27.5 ($\text{C}_2(\text{CH}_3)_4$), δ 44.5 ($\text{C}_2(\text{CH}_3)_4$), δ 65.2, 66.8, ($\text{Cp}_{\text{Fe-subst}}$), δ 76.1, 80.8, ($\text{Cp}_{\text{Cr-unit}}$), δ 278.6 (NC). IR (NaCl plates, Nujol): 1751 cm^{-1} (v(NC)). Anal. Calcd. for $\text{C}_{50}\text{H}_{54}\text{Cr}_2\text{FeN}_2$: C, 69.1; H, 6.37; N, 3.63. Found: C, 68.72; H, 6.21; N, 3.49. CV: ($E_a + E_c$)/2 $\text{Fe}^{2+/3+}$, 574 mV, $\text{Cr}^{2+/3+}$, -1149 mV, E_a $\text{Cr}^{3+/4+}$, 61 mV, i_a/i_c : $\text{Cr}^{2+/3+} = 1.0$; i_a/i_c : $\text{Fe}^{2+/3+} = 1.18$.

3.3.4. Bis {1,1'-(tetramethylethano) dicyclopentadienyl} (1,4-phenylene diisocyanide) chromium(II) (5)

1345 mg of **1b** (4.6 mmol) was added to a Double Schlenk vessel. 295 mg (2.3 mmol) of 1,4-phenylene diisocyanide was also added and 50 mL of THF was vacuum transferred into the reaction vessel. The solution was stirred and warmed to 40 °C. The reaction took place at reduced pressure, evolving carbon monoxide. After 20 minutes, half of the THF was removed and the deep red product was crystallized out of the remaining THF at -78 °C. Single crystals were obtained by leaving a solution of **5** in a mixture of THF and d_6 -benzene under inert atmosphere. After half of the solvent

evaporated, a dark crystalline precipitate had formed. The solvent mixture was decanted and mineral oil was poured over the crystals. Yield: 985 mg (65%). $^1\text{H-NMR}$, (500 MHz, 25 °C, C_6D_6) δ 0.95 (s, 24H, $\text{C}_2(\text{CH}_3)_4$), δ 3.99 (m, 8H, $\text{Cp}_{\text{Cr-unit}}$), δ 4.57 (m, 8H, $\text{Cp}_{\text{Cr-unit}}$), δ 7.53 (s, 4H, phenyl). $^{13}\text{C-NMR}$, (500 MHz, 25 °C, C_6D_6) δ 27.4 ($\text{C}_2(\text{CH}_3)_4$), δ 44.5 ($\text{C}_2(\text{CH}_3)_4$), δ 76.2, 80.6, ($\text{Cp}_{\text{Cr-unit}}$), δ 124.7, 140.4, (phenyl), δ 278.3 (NC). IR (NaCl plates, Nujol): 1766 cm^{-1} (v(NC)). Anal. Calcd. for $\text{C}_{40}\text{H}_{44}\text{Cr}_2\text{N}_2$: C, 73.15; H, 6.75; N, 4.27. Found: C, 70.36; H, 6.37; N, 3.81. CV: ($E_a + E_c$)/2 $\text{Cr}^{2+/3+}$, -1096 mV, $E_a \text{Cr}^{3+/4+}$, 163 mV, $i_a/i_c: \text{Cr}^{2+/3+} = 0.96$.

3.4. Chemical Oxidation of Heteronuclear Complexes

3.4.1. Oxidation of {1,1'-(*trans*-1,2-diphenylethano) dicyclopentadienyl} (ferrocenylisocyanide) chromium(II)

800 mg of **1a** (2.1 mmol) was added to a Double-Schlenk vessel. 400 mg (1.9 mmol) of ferrocenylisocyanide was also added and 50 mL of THF was vacuum transferred into the reaction vessel. The solution was stirred and heated to a temperature of 40 °C. The reaction took place at reduced pressure, evolving carbon monoxide. After 20 min., 626 mg (1.9 mmol) of ferrocenium hexafluorophosphate was added at 0 °C. This mixture was stirred for 30 min. at 0 °C under atmospheric pressure. The solution was cooled to -78 °C forming a brown paramagnetic precipitate of **[3]⁺ PF₆⁻**. The brown product was collected on the filter of the Double Schlenk vessel. Yield: 909 mg (68%). $^1\text{H-NMR}$, (300 MHz, 25 °C, acetone- d_6) δ 1.78 (m, THF), δ 3.27 (broad, $\text{Cp}_{\text{Fe-subst}}$), δ 3.49 (m, THF), δ 4.13 (broad, $\text{Cp}_{\text{Fe-unsubst}}$), δ 4.76 (broad, $\text{Cp}_{\text{Fe-subst}}$), δ 7.08 (broad, aryl), δ 7.88 (broad, aryl). $^{31}\text{P-NMR}$, (202 MHz, 25 °C, acetone- d_6) δ -142.7 (hept., $J=707$). $^{19}\text{F-NMR}$, (470 MHz, 25 °C, acetone- d_6) δ -69.85 (d, $J=707$). IR (NaCl plates, Nujol) : 2118 cm^{-1} (v(NC)). Anal. Calcd. for $\text{C}_{35}\text{H}_{29}\text{CrFeNPF}_6$: C, 59.06; H, 4.42; N, 1.86.

Found: C, 59.12; H, 4.35; N, 1.66. CV: $(E_a + E_c)/2$ Fe^{2+/3+}, 278 mV, Cr^{2+/3+}, -1143 mV, E_a Cr^{3+/4+}, 6 mV, i_a/i_c : Cr^{2+/3+} = 1.01; i_a/i_c : Fe^{2+/3+} = 0.87. $\mu_{\text{eff}} = 1.86$ BM.

3.4.2. Oxidation of Bis {1,1'-(*trans*-1,2-diphenylethano) dicyclopentadienyl} (1,1'-ferrocenyldiisocyanide) chromium(II)

901 mg of **1a** (2.3 mmol) was added to a Double Schlenk system. 274 mg (1.16 mmol) of ferrocenyldiisocyanide was also added and 50 mL of THF was vacuum transferred into the reaction vessel. The solution was stirred and warmed to 40 °C. The reaction took place at reduced pressure, evolving carbon monoxide. After 20 min., 768 mg (2.3 mmol) of ferrocenyl hexafluorophosphate was added at 0 °C. This mixture was stirred for 30 min. at 0 °C under atmospheric pressure. The solution was cooled to -78 °C forming a brown paramagnetic precipitate of **[4a]²⁺(PF₆⁻)₂**. The brown product was collected on the filter of the Double Schlenk vessel. Yield: 946 mg (65%). ¹H-NMR, (300 MHz, 25 °C, acetone-*d*₆) δ 3.13 (broad, Cp_{Fe-subst}), δ 4.96 (broad, Cp_{Fe-subst}), δ 7.07 (broad, aryl), δ 7.37 (broad, aryl), δ 8.03 (broad, aryl). ³¹P-NMR, (202 MHz, 25 °C, d₆-acetone) δ -142.2 hept., J=707). ¹⁹F-NMR, (470 MHz, 25 °C, acetone-*d*₆) δ -69.83 (d, J=709). IR (NaCl plates, Nujol): two bands 2113 cm⁻¹, 2137 cm⁻¹ ν ((NC)). Anal. Calcd. for C₆₀H₄₈Cr₂FeN₂P₂F₁₂: C, 57.80; H, 3.88; N, 2.25. Found: C, 54.98; H, 3.84; N, 2.21. CV: $(E_a + E_c)/2$ Fe^{2+/3+}, 574 mV, Cr^{2+/3+}, -1136 mV, E_a Cr^{3+/4+}, -20 mV, i_a/i_c : Cr^{2+/3+} = 1.16; i_a/i_c : Fe^{2+/3+} = 1.04. $\mu_{\text{eff}} = 2.52$ BM (1.78 BM per Cr atom).

3.5. Determination of the Effective Magnetic Moments

3.5.1. Johnson Matthey Magnetic Susceptibility Balance

A sample of $[3]^+PF_6^-$ was ground to a very fine and homogeneous powder that was filled into the sample tube. The height of the sample was 2.15 cm and the weight was determined to be 111 mg. The calibration constant of the balance was declared as $c = 1.071$. The value R was determined to be 100. Using equations 2-22 and 2-16 to elucidate χ_M , derived in 2.5., resulted in $\chi_M = 1.486 \times 10^{-3}$ cgs/mol:

$$\chi_g = \frac{c \times l \times R}{m \times 10^9}; \quad \chi_g = \frac{1.071 \times 2.15 \times 100}{111g} \times 10^{-6} \text{ cgs}$$

$$\chi_g = \frac{230.265}{111g} \times 10^{-6} \text{ cgs}; \quad \chi_g = 2.075 \times 10^{-6} \text{ cgs/g}$$

With equation 2-16 χ_g was converted into χ_M :

$$\chi_M = \chi_g \times M; \quad \chi_M = 2.075 \times 10^{-6} \text{ cgs/g} \times 716.12g/mol$$

$$\chi_M = 1.486 \times 10^{-3} \text{ cgs/mol}$$

3.5.2. Evans Method using the NMR Device

A solution of $[3]^+ PF_6^-$ in DMSO was prepared with a concentration $n = 0.012$ g/mL. A portion of this solution was filled into an NMR tube. As described in 2.5.2, a coaxial tube containing pure DMSO was placed into the solution inside the NMR tube. The NMR spectrum of this arrangement was determined with the 300 MHz device, taking one scan without locking the signal at room temperature. The spectrum showed the peak of the pure solvent as well as the one of the solution separated by 50.623 Hz. The magnetic susceptibility of the solvent (DMSO) is published as -0.66×10^{-6} cgs [95]. Equations 2-30 and 2-16 derived in 2.5. delivered a value of 1.932×10^{-3} cgs/mol for $[3]^+ PF_6^-$:

$$\chi_g = \frac{3 \times \Delta f}{4 \times \pi \times f \times n} + \chi_{solvent}; \quad \chi_g = \frac{3 \times 50.623 \text{ Hz}}{4 \times \pi \times 300 \text{ MHz} \times 0.012 \text{ g/mL}} + \chi_{solvent}$$

$$\chi_g = \frac{151.896}{45.239} \times 10^{-6} \text{ cgs/g} + -0.66 \times 10^{-6} \text{ cgs/g}$$

$$\chi_g = 3.358 \times 10^{-6} \text{ cgs/g} - 0.66 \times 10^{-6} \text{ cgs/g}; \quad \chi_g = 2.698 \times 10^{-6} \text{ cgs/g}$$

Equation 2-16 again delivers the value for χ_M :

$$\chi_M = \chi_g \times M; \quad \chi_M = 2.698 \times 10^{-6} \text{ cgs/g} \times 716.12 \text{ g/mol}$$

$$\chi_M = 1.932 \times 10^{-3} \text{ cgs/mol}$$

3.5.3. Correction Values

Since the other fragments of the molecules besides the metal centers contribute small values of diamagnetic susceptibility, the experimentally measured values for χ_M have to be adjusted by adding these correction values of the molecule fragments. The values of the specific molecule fragments can be seen in Table 3-1.

Table 3-1: Diamagnetic Correction Factors [96]:

Fragment	χ_M (in cgs/mol)
$(C_6H_5)_2C_2H_2(Cp)_2$	-2.14×10^{-4}
CN	-10.35×10^{-6}
Fc [3]	-1.25×10^{-4}

Adding these values together results in a correction factor of -0.349×10^{-3} cgs/mol for $[3]^+ PF_6^-$ and -0.573×10^{-3} cgs/mol for $4a^{2+}(PF_6)_2^-$. If we take $\chi_M = 1.932 \times 10^{-3}$ cgs/mol for $[3]^+ PF_6^-$ as calculated above and add the correction value, we obtain 1.583×10^{-3} cgs/mol as $\chi_{Mcorr.}$. To determine the effective magnetic moment, we have to use equation 2-21, derived in 2.5.1:

$$\mu_{eff} = 2.84 \times \sqrt{(1.583 \times 10^{-3} \text{ cgs/mol} \times 293.13K)} ; \mu_{eff} = 1.93BM$$

4. Results

4.1. Electrochemistry of *Ansa*-Chromocene Complexes

The electrochemical behavior of a variety of *ansa*-chromocene complexes was examined, using cyclic voltammetry in order to elucidate the accessibility of the 3+ and 4+ oxidation states at the Cr metal centers [37]. We reexamined the parent complex chromocene [97] and Brintzinger's (tetramethyl-ethano) chromocene carbonyl complex **1b** [98]. This enabled us to compare their values with the complexes made in the Shapiro work group under identical experimental conditions.

The experiments revealed that all *ansa*-chromocene complexes that were investigated can be reversibly oxidized to the Cr³⁺ and reduced to the Cr²⁺ oxidation state electrochemically. We found that the formal redox potential of the Cr^{2+/3+} couple is somewhat influenced by the nature of the transannular bridge and that the ligand complexed to the metal center profoundly influences the redox potential as can be seen in Table 4-1.

Table 4-1: Redox Potentials of selected *ansa*-Chromocene Complexes:

complex	L	(E _a + E _c)/2
Cp ₂ Cr		-1103 mV
1a	CO	-948 mV
1b	CO	-882 mV
2a	CN-t-Bu	-1154 mV
2b	CN-t-Bu	-1238 mV

Apparently the carbonyl ligand causes a shift of the formal redox potential to more positive values compared to the chromocene parent compound. However, the

isocyanide analogues show the opposite trend, resulting in a shift to more negative values. Thus, the electron donor ligand that is complexed to the metal center directly influences the redox potential of the corresponding complex. Figure 4-1 shows the overlaid cyclic voltammograms of Brintzinger's carbonyl complex **1b** and the *tert*-butyl isocyanide analogue **2b**. These results confirm that isocyanide ligands are better σ electron donors than the isoelectronic carbonyl analogues [99].

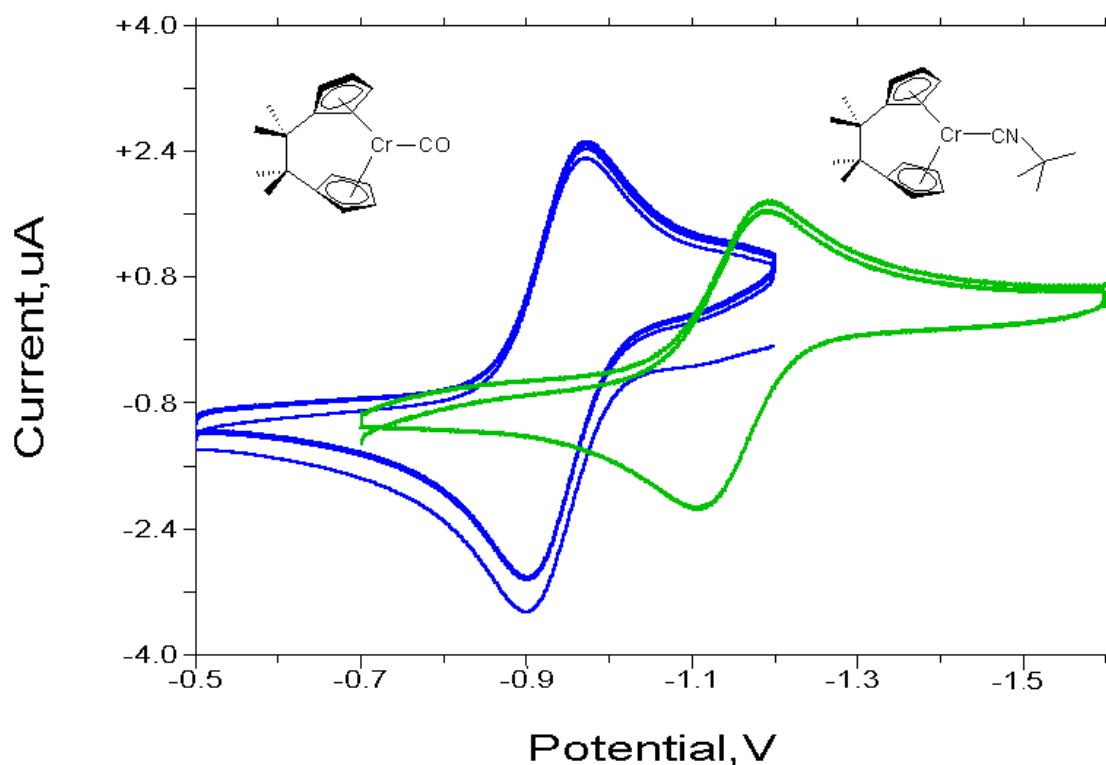


Figure 4-1: Redox potentials of the carbonyl and the isocyanide species

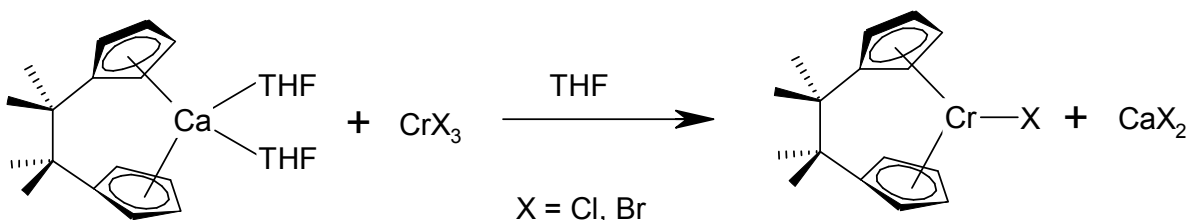
In order to determine the availability of additional oxidation states, these complexes were examined at anodic and cathodic potentials beyond the values for the $\text{Cr}^{2+/3+}$ couples. In addition to the reversible $\text{Cr}^{2+/3+}$ redox system, an electrochemically irreversible oxidation peak can be observed for most *ansa*-chromocenes that is attributable to the $\text{Cr}^{3+/4+}$ couple. However, the return wave due to the reduction of Cr^{4+} to Cr^{3+} can be barely observed for some of the complexes and is completely absent

for other ones. Apparently the electrochemical electron transfer for the reduction of the Cr^{4+} species proceeds so slowly that no clean redox peak system can be observed in the CV. This irreversibility might be attributable to the complexation of the Cr^{4+} by the THF solvent or by the electrolyte anion. Most of these complexes also show a weak irreversible cathodic peak at ca. -2200 mV that is attributed to the one-electron reduction of the neutral species to the corresponding monoanions.

4.2. Generation of *ansa*-Chromocene(III) halide Complexes

Several attempts were undertaken to obtain *ansa*-chromocene(III) halide complexes. The resulting compounds were supposed to enable us to synthesize a variety of interesting new *ansa*-chromocene(III) complexes by metathesis reactions.

In the first attempt tetramethylethano-bridged calcocene was reacted with chromium(III) bromide. THF was used as solvent and the reaction took place at room temperature under vigorous stirring over 24 h. After the THF was removed, the green product was dissolved in toluene and separated from the calcium bromide byproduct by filtration. The product was obtained as a green paramagnetic powder.

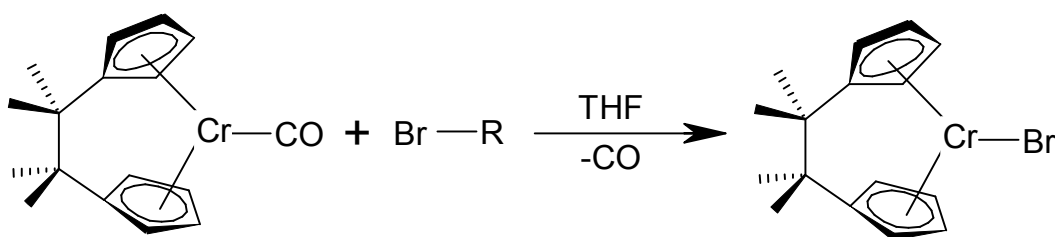


Scheme 4-1: Synthesis of *ansa*-chromocene(III) halide complexes

One annoyance that occurred repeatedly after the workup was the coprecipitation of white solid with the green product. This turned out to be additional calcium bromide

that was not removed entirely due to its coordination to the product. The identification of coordinated THF in the product by ^1H NMR spectroscopy also suggested the presence of calcium in the product. It appeared to be impossible to obtain the *ansa*-chromocene(III) bromide as pure material. Efforts were made to remove the THF by heating the product under vacuum and with repeated recrystallizations.

Analogous *ansa*-samarocene and *ansa*-ytterbiocene chlorides were obtained previously by reacting the corresponding *ansa*-metallocene with *tert*-butyl chloride [100]. This encouraged us to perform similar reactions with *ansa*-chromocene species. We decided to react the *ansa*-chromocene(II) carbonyl complex with alkyl- and allyl bromides. The advantage of this procedure was that only volatile organic compounds would be generated as byproducts. This was supposed to simplify the work-up tremendously.



Scheme 4-2: Synthesis of *ansa*-chromocene(III) bromide complexes by reaction of the *ansa*-chromocene carbonyl complexes with organo-bromide species as starting materials

In the first experiment, tetramethylethano-bridged chromocene carbonyl was placed in a glass bomb and dissolved in THF. One equivalent of 1-bromo-2-methyl propane was added and this mixture was kept at a temperature of 90 °C for four days. The NMR spectrum of the reddish brown solution showed that a paramagnetic product was generated. The IR spectrum showed that the carbonyl ligand was not present anymore. The volatile organic compound that was formed as byproduct was distilled into a separate NMR tube and identified by ^1H NMR spectroscopy and mass spectroscopy. Both experiments revealed that isobutene was formed as byproduct.

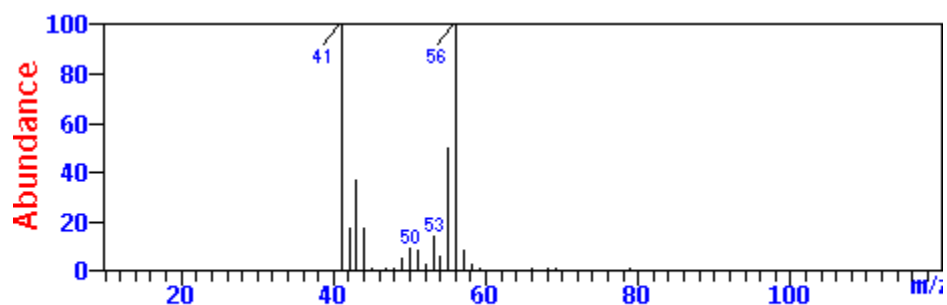


Figure 4-2: Mass spectrum of the volatile byproduct

The mass spectrum of the volatiles also showed that the free ligand of the *ansa*-chromocene with a mass of 214 was regenerated during the reaction:

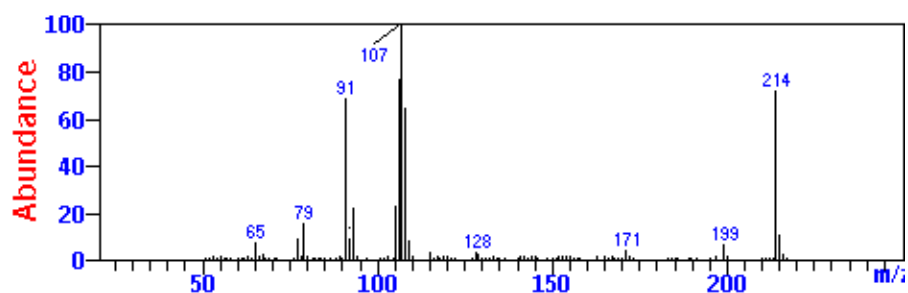


Figure 4-3: Mass spectrum of the paramagnetic product

A single crystal of the paramagnetic species was obtained and the crystal structure was elucidated by an X-Ray diffraction experiment. This procedure revealed that chromium(II) bromide was formed as a solvated species with two THF molecules coordinated to the Cr metal centers [101].

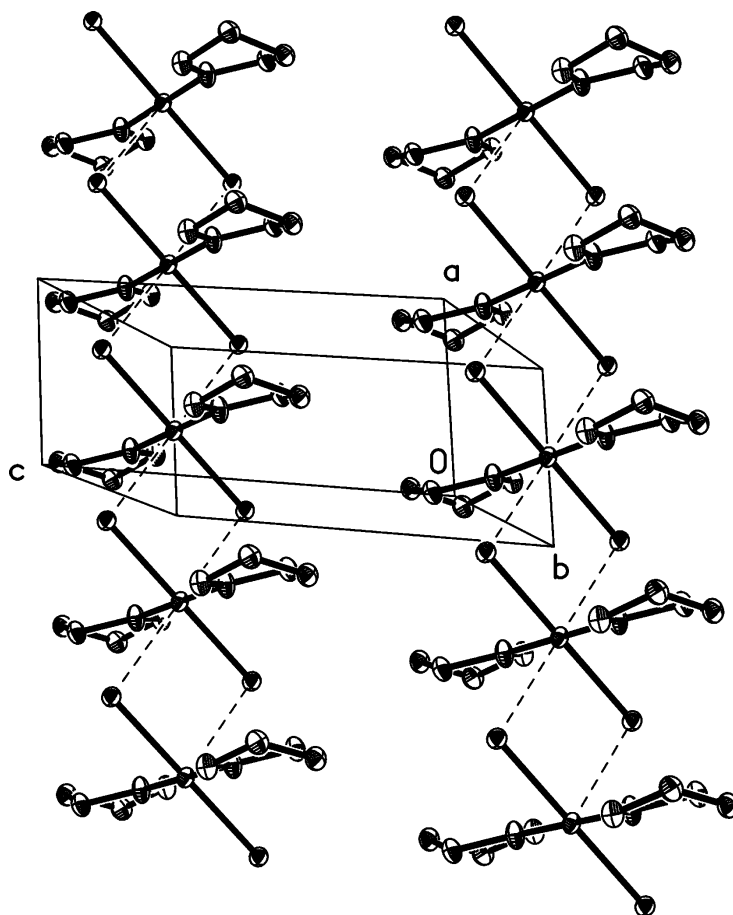
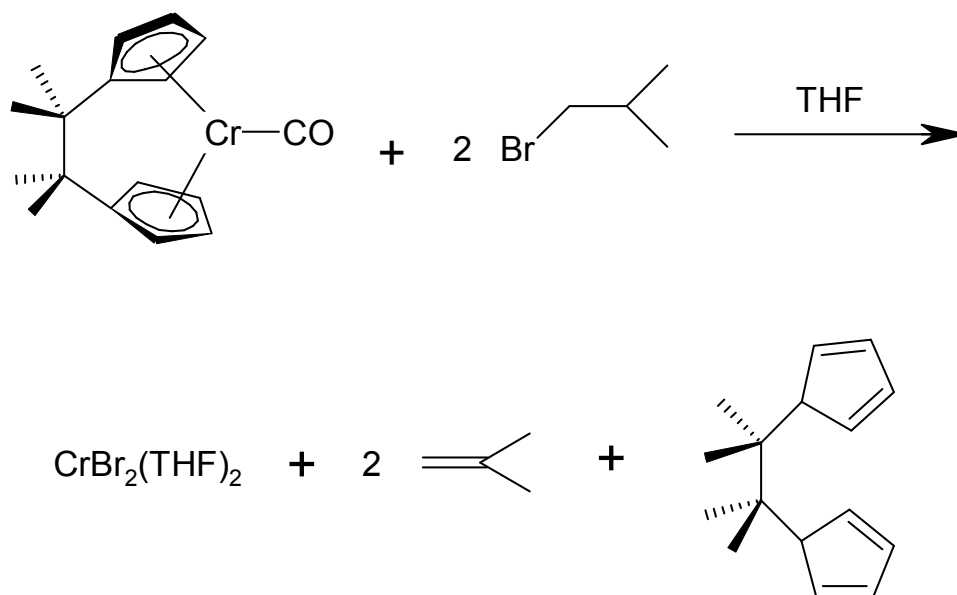


Figure 4-4: Crystal packing diagram of $\text{CrBr}_2(\text{THF})_2$

The Cr-O distance was found to be 2.072 (3) Å and the Cr-Br distance is 2.5825 (5) Å. The Cr atom lies in the center of inversion. The THF molecules are coordinated orthogonally to the Cr-Br bonds, exhibiting an angle of 90.009 (8)°. The vacant sites exhibit intermolecular $\text{Cr} \cdots \text{Br}$ interactions of 2.9874 (5) Å that are almost orthogonal to the Cr-O bonds. This extends the system into a linear chain along the {100} direction. Figure 4-4 shows the packing diagram of this structure with the staggered propagation along the {100} direction.

These results suggest that a β elimination takes place at the 1-bromo-2-methyl propane generating isobutene. Two bromine atoms replace the carbonyl ligand at the chromium metal center under ring loss. This results in the formation of chromium(II) bromide and the regeneration of the neutral tetramethylethano-bridged di-cyclopentadiene ligand:



Scheme 4-3: Formation of solvated CrBr_2 , isobutene and regeneration of the neutral tetramethyl ethane di-cyclopentadienyl ligand

The reaction was performed again using *tert*-butyl bromide instead of the 1-bromo-2-methyl propane. This reaction also yielded a paramagnetic product and the generation of isobutene could be observed as well. It seems that the same mechanism took place as proposed for the reaction before. Presumably the reaction of *ansa*-chromocene carbonyl complexes with any alkyl halide that can undergo a β H abstraction, in general, leads to the β elimination product of the alkyl halide and chromium(II) bromide with concurrent ring loss.

Another experiment was performed using allyl bromide as the halogen source. This generated a paramagnetic product whose IR spectrum showed that there was still CO present as ligand at the metal center. The NMR spectrum of the volatile organic compound indicates an alkane. The mass spectrum shows fragments with the masses 100 and 98 that could not be assigned. The products were not further characterized. All these attempts to produce *ansa*-chromocene halide complexes in pure form and characterize the products were unsuccessful. We decided then to focus on the synthesis of diamagnetic *ansa*-chromocene isocyanide species.

4.3. Synthesis, Physical and Electronic Properties of Heteronuclear and Homobinuclear *Ansa*-Chromocene isocyanide Complexes

4.3.1. Synthesis of Ferrocenyliisocyanide Derivatives

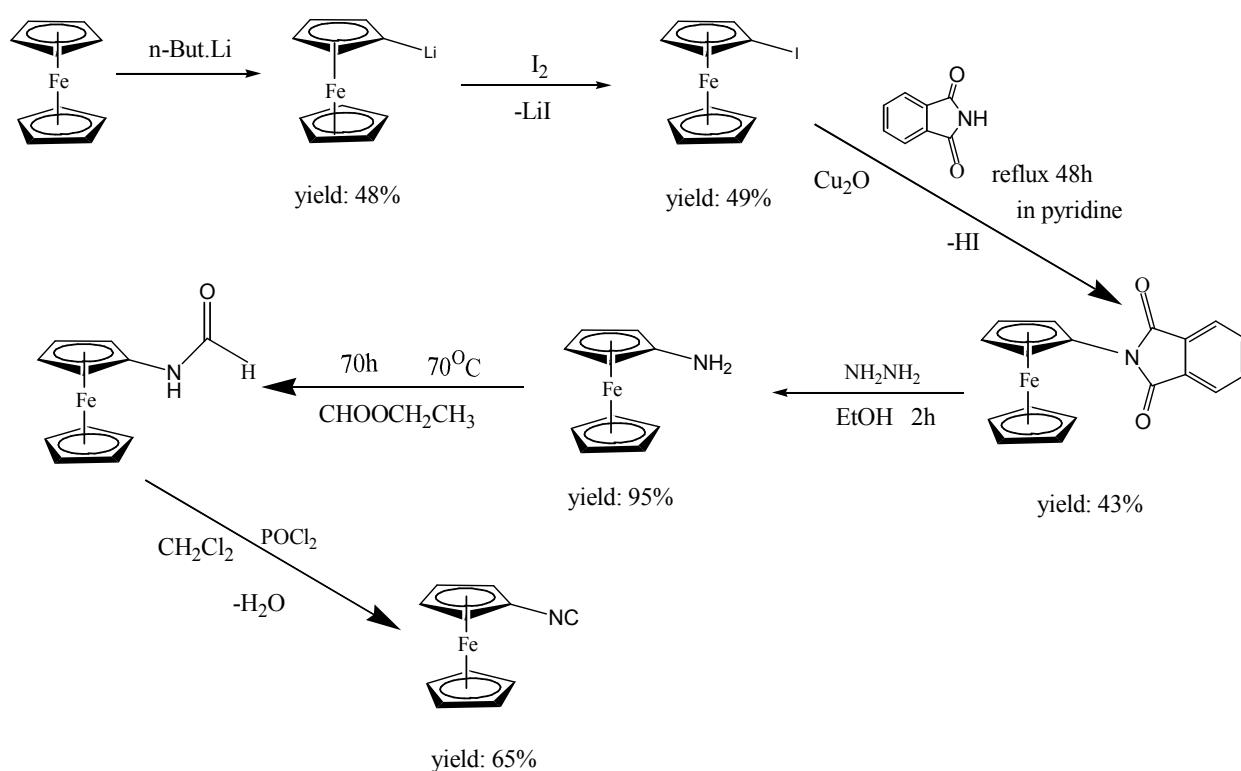
4.3.1.1. Synthesis of Ferrocenyliisocyanide

Ferrocenyliisocyanide was prepared in six steps starting from ferrocene [91,92]. The synthesis of ferrocenyliisocyanide from ferrocenylamine following the procedure previously described in the literature turned out to be very difficult and not reproducible [92]. As described, a solution of ferrocenylamine in ethyl formate was refluxed. The product N-formylferrocenylamine was supposed to form in low yields. The reaction was monitored by TLC and $^1\text{H-NMR}$ experiments. According to the description, after 5 h, ferrocene would be recovered from the reaction. At that time the experiment was supposed to be stopped because the yield of N-formylferrocenylamine would decrease. However, the actual experiment did not produce any desired product at all. Therefore the reaction conditions were changed slightly, resulting in the production of N-formylferrocenylamine in good yields.

The ferrocenylamine was treated with ethyl formate in a glass bomb at 70 °C. The generation of N-formylferrocenylamine was monitored by $^1\text{H-NMR}$ spectroscopy. After 70 h all ferrocenylamine was converted to N-formylferrocenylamine and the experiment was terminated. A black material was obtained in 76% crude yield that was very difficult to clean. Rather than cleaning this intermediate, it was further converted in the same vessel .

In the one pot synthesis, ferrocenylamine was heated in a sealed glass vessel with ethyl formate to 70 °C. After 70 h, the ethyl formate was removed and the blackish residue was treated with diisopropylamine. Phosphoryl chloride was employed to dehydrate the N-formylferrocenylamine. The yield of product from this one pot reaction was 65.4%.

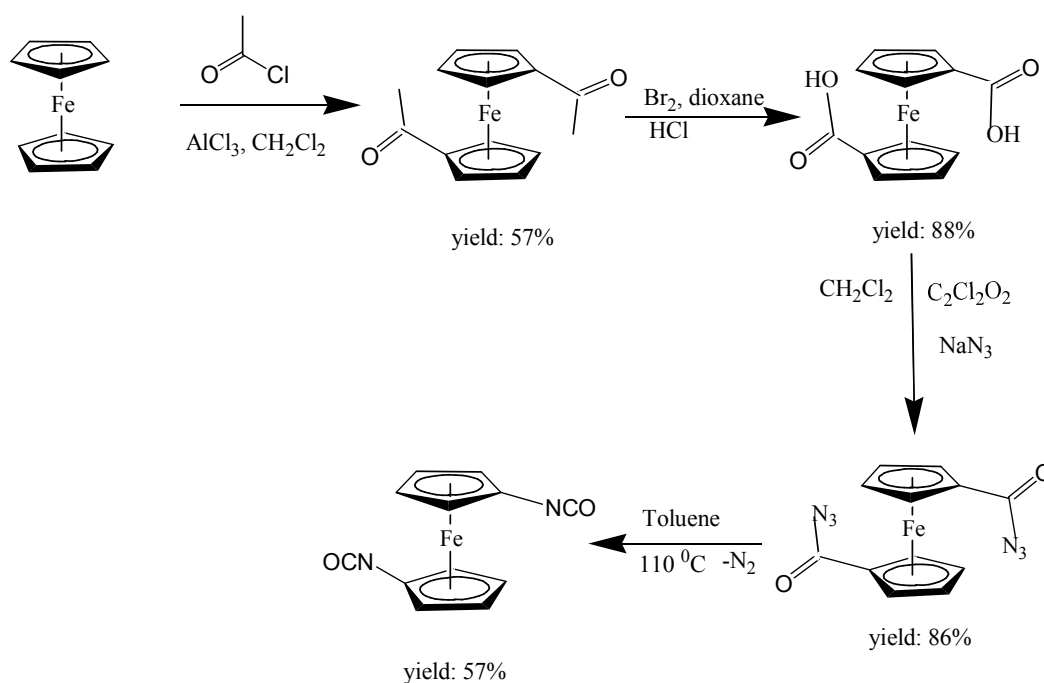
Scheme 4-4 provides an overview of the six synthetic steps to produce ferrocenylisocyanide. Most of these steps generated the products in moderate yields. Only the fourth step generated ferrocenylamine in a very high yield of 95%. To obtain enough starting material for further synthetic reactions, this procedure had to be repeated several times and ca. 40g of ferrocene was employed as starting material each time.



Scheme 4-4: Six step synthesis of ferrocenylisocyanide starting from ferrocene

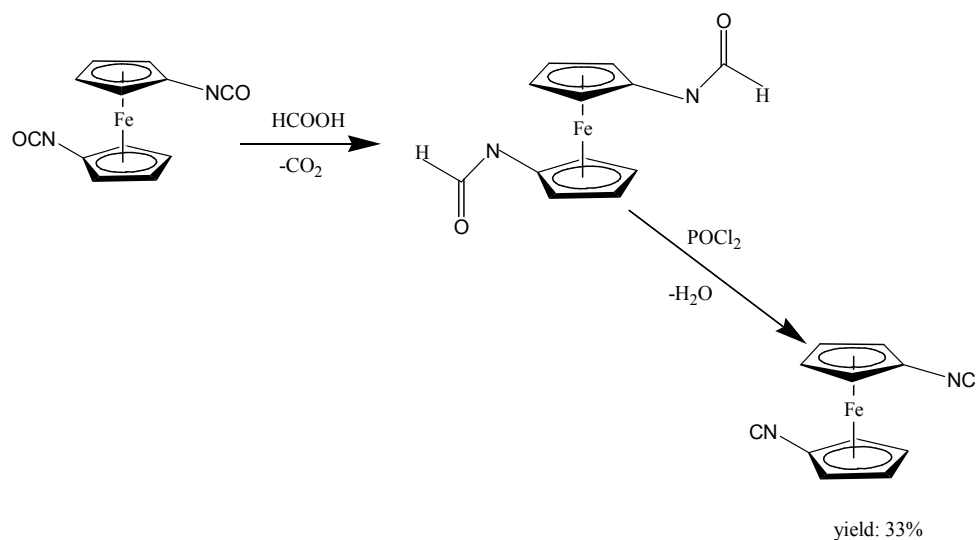
4.3.1.2. Synthesis of Ferrocenyldiisocyanide:

Ferrocenyldiisocyanide was also prepared in six steps starting from ferrocene [8,93,94]. Scheme 4-5 shows that the products of the first four steps can be produced in good yields:



Scheme 4-5: First four steps in the synthesis of ferrocenyldiisocyanide, producing the intermediates in good yields

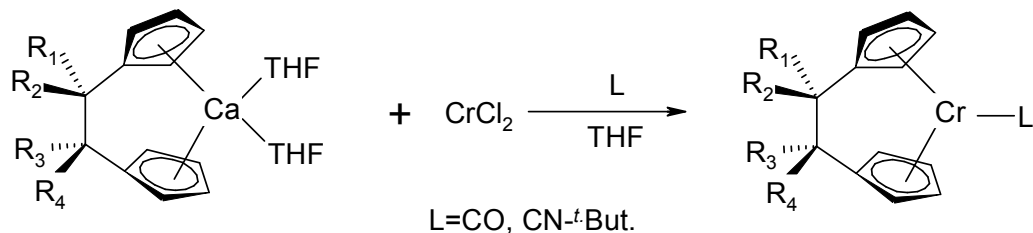
However the last two steps, which were also performed as a one pot synthesis from ferrocenyldiisocyanate, produced very low yields (Scheme 4-6). Therefore, this procedure also had to be repeated several times and ca. 30 g of ferrocene was used as starting material each time.



Scheme 4-6: Last two synthetic steps, producing ferrocenyldiisocyanide in low yields

4.3.2. New Synthetic Route to *Ansa*-Chromocene isocyanides

Complexes **3**, **4a**, **4b** and **5** were synthesized following a new route to obtain *ansa*-chromocene isocyanide adducts in good yields. The first attempts to synthesize the heterobinuclear complex **3** were made by employing the previously reported route to obtain 18 electron *ansa*-chromocene complexes [33]. The reaction of the *ansa*-calcocene with chromium(II) chloride in the presence of the ligand (L) results in the generation of the corresponding diamagnetic neutral 18 electron *ansa*-chromocene (II) species:



1a: R₁= R₄ = Ph; R₂= R₃ = H; L = CO

2a: R₁= R₄ = Ph; R₂= R₃ = H; L = CN-^tBut.

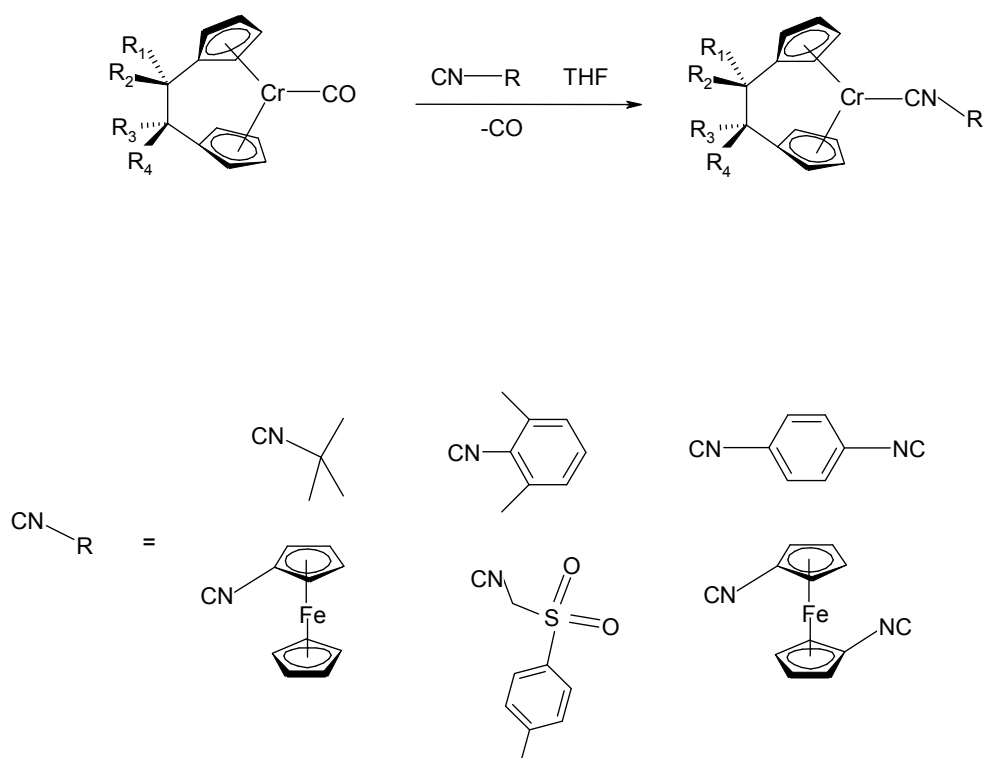
1b: R₁ = R₂= R₃= R₄= Me; L = CO

2b: R₁ = R₂= R₃= R₄= Me; L = CN-^tBut.

Scheme 4-7: Conventional synthetic approach to *ansa*-chromocene derivatives

Carbonyl ligands as well as isocyanide derivatives fulfill the requirement of being neutral two electron donors. This is essential to obtain the desired neutral 18 electron *ansa*-chromocenes. As can be seen in Scheme 4-7, the synthesis is successful with the carbonyl ligand if the reaction is performed under one atmosphere of carbon monoxide. Also the formation of the *tert*-butyl isocyanide adduct is accomplished with a yield of 87% [37]. However, using the same reaction conditions and adding ferrocenylisocyanide as the two electron donor ligand did not result in the formation of the desired complex **3**. Only paramagnetic reaction products could be observed, which were not further characterized. Apparently this synthetic route is not reliable for the formation of every *ansa*-chromocene isocyanide species.

Earlier attempts in the Shapiro group to synthesize the methylisocyanide and other isocyanide complexes also failed or resulted in the formation of products in very low yields. Substitution reactions of the carbonyl ligand in organometallic transition metal complexes had been subject to early studies in organometallic chemistry [102,103].



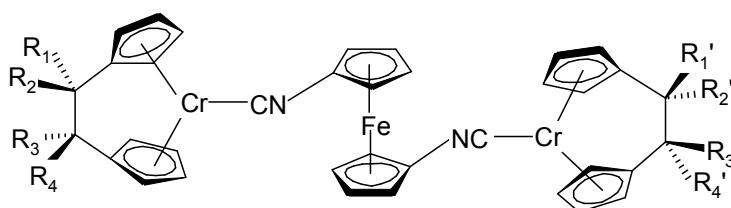
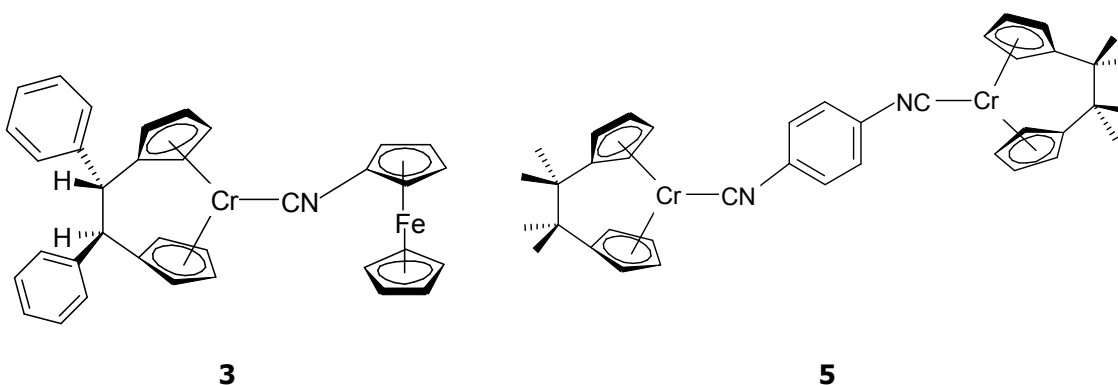
Scheme 4-8: Synthetic approach to new *ansa*-chromocene isocyanides in the Shapiro group

It has been shown that substitution reactions replacing the carbonyl ligand can provide a direct route to organometallic compounds containing other ligands [104]. The Shapiro group gained access to a variety of neutral 18 electron *ansa*-chromocene isocyanide adducts by replacing the carbonyl ligands of *ansa*-chromocene complexes as can be seen in Scheme 4-8.

4.3.3. Synthesis of Neutral Polynuclear *Ansa*-Chromocene isocyanides

Complexes **3**, **4a**, **4b** and **5** were synthesized following this new approach. The *ansa*-chromocene carbonyl species was used as a precursor and the carbonyl ligand was substituted by the isocyanide ligand. All reactions took place under nearly the same conditions. The *ansa*-chromocene carbonyl species and the respective isocyanide derivative were dissolved in THF under vacuum. The mixtures were warmed to approximately 40 °C and the evolution of carbon monoxide was observed. After the gas evolution was finished, the solutions were stirred for another 20 minutes. The products were worked up differently and the product yields were between 50 and 65%. These yields are markedly improved when compared with the former method.

All products were characterized by elemental analysis. The measured values for C, H and N agree very well with the calculated ones in complexes **3** and **4b**. Complexes **4a** and **5**, however, show some differences in the values for carbon. The measured value for C in **4a** is 6% lower than the calculated one and **5** exhibits a value for C that is 3% lower than in theory. Since both species were fully characterized by NMR and **5** additionally by X-ray crystallography, we attribute these deviations to incomplete combustion during the analyses. We observed such difficulties before with other *ansa*-chromocene complexes. Thus, this seems to be a commonly occurring problem with these kinds of transition metal complexes.



4a: $R_1 = R_4 = R_1' = R_4' = \text{Ph}$; $R_2 = R_3 = R_2' = R_3' = \text{H}$

4b: $R_1 = R_2 = R_3 = R_4 = R_1' = R_2' = R_3' = R_4' = \text{Me}$

4.3.4. Characterization with NMR- and IR-Spectroscopy

Characteristic for the ^1H -NMR spectra of complexes **3** and **4a** are four resonance signals within the region between 3 and 5 ppm representing the protons of the *ansa*-chromocene Cp rings. For **3**, two of these signals can be recognized as distinct pseudo triplets at 4.54 and 4.94 ppm. A sharp single resonance belonging to the benzylic protons of the diphenylethanediyl bridge is found at ca. 4 ppm for both species. Complex **3** exhibits one signal representing two protons that belong to the substituted Cp ring of the ferrocenyl unit at ca. 3.9 ppm. The other two protons of this Cp ring appear as two signals at ca. 4.4 ppm. The protons of the unsubstituted Cp ring appear as a single resonance signal at 4.17 ppm. The spectrum of **4a** shows one resonance signal for four protons at ca. 4.1 ppm and another three signals between 4.2 and 4.7 ppm, representing together four protons, all belonging to the ferrocenyl Cp rings. The

latter three signals are actually four signals; at room temperature two of them are overlaid and seem to exist as one signal. As Figure 4-5 shows, raising the temperature up to 70 °C causes a separation of these three signals into four signals, each representing one proton of the ferrocenyl unit.

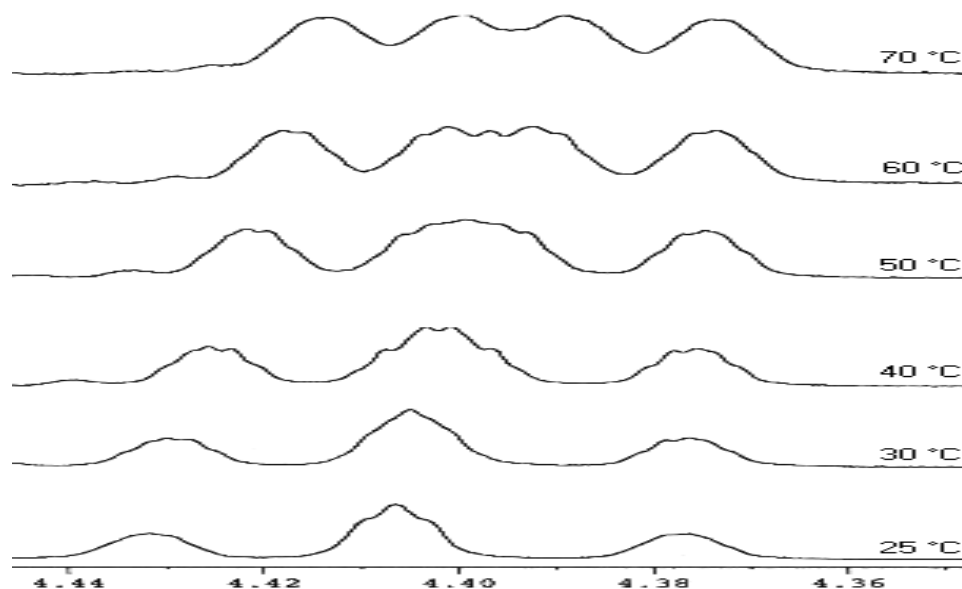


Figure 4-5: Separation of ^1H absorption signals in **4a** with increasing temperature

The pattern of resonance signals belonging to the *ansa*-chromocene Cp rings is quite similar to that one of **3**.

HMQC as well as COSY experiments were performed to make definitive ^1H and ^{13}C assignments for these two complexes.

The HMQC spectrum for **3**, shown in Figure 4-6, reveals that the ^{13}C resonances of the substituted ferrocenyl unit at 64.0 and 65.9 ppm are correlated to the ^1H -resonance for the two protons at 3.91 ppm as well as the signals at 4.42 and 4.45 ppm, each representing one proton. It also enables us to assign the signal at 3.90 ppm to the two protons of the transannular bridge, whose ^{13}C signal appears at 54.8 ppm. The proton signals at 3.87, 4.26, 4.54, and 4.94 ppm can be assigned to the four carbon signals at 77.9, 78.6, 80.0 and 82.0 ppm that belong to the *ansa*-chromocene Cp rings.

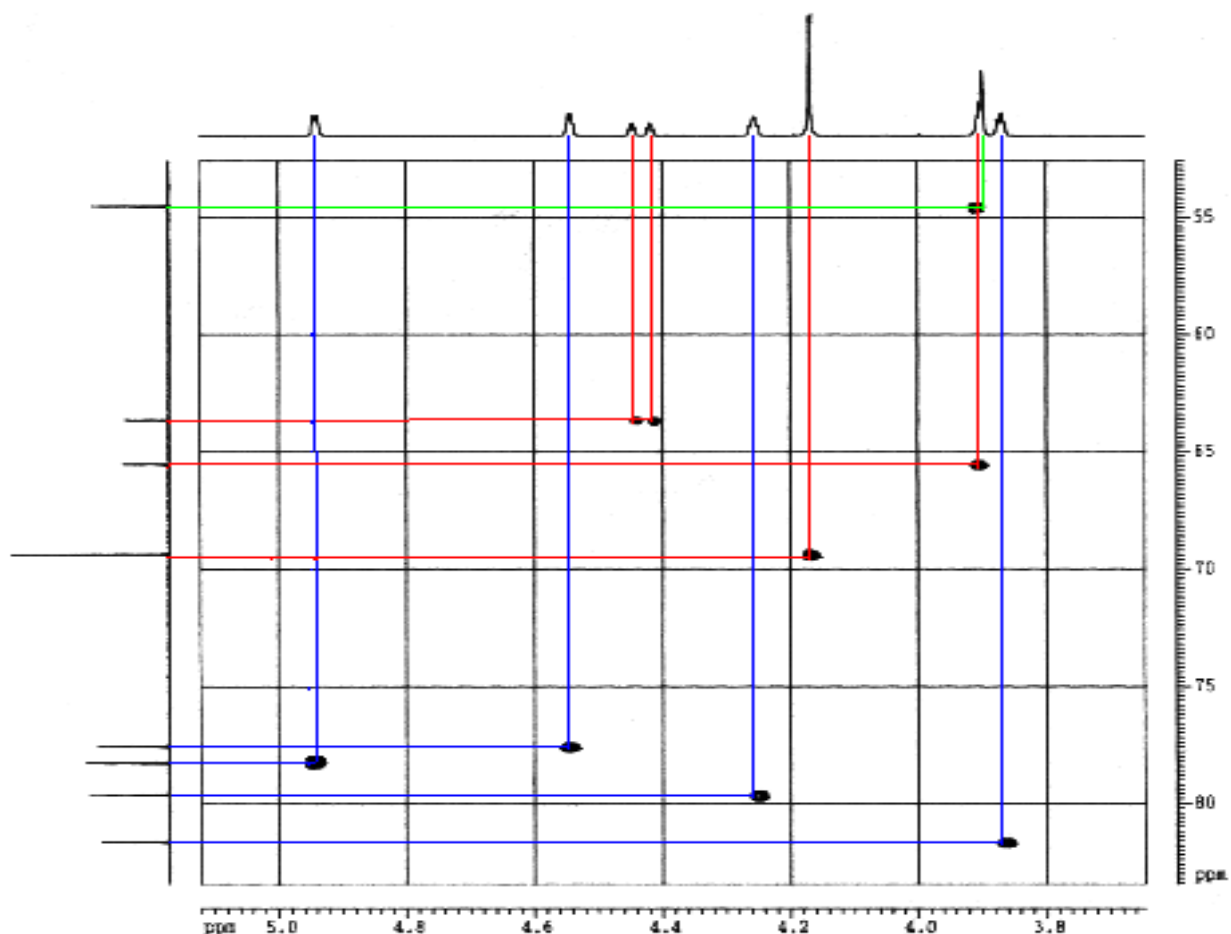


Figure 4-6: ^1H - ^{13}C correlation of **3**, red lines correspond to the ferrocenyl unit, blue lines to the *ansa*-chromocene group and green lines to the transannular bridge

The COSY experiment for **3** confirms that these protons indeed belong to the Cp rings of the *ansa*-chromocene unit. All of them spin couple with each other as can be seen in Figure 4-7 (blue lines). Also, the signals at 3.91, 4.42 and 4.45 ppm spin couple with each other (red lines). Thus, they belong to the ferrocenyl Cp rings. The two α protons of the substituted Cp ring experience inequivalent electronic environments because if free rotation about the Cp-NC bond is absent, the isocyanide ligand is no longer axially symmetric due to the sp^2 hybridization of the nitrogen. Another reason could be that, in solution, the ferrocenyl unit is tilted out of the horizontal plane with respect to the *ansa*-chromocene unit. A twisted ferrocenyl C-N bond would leave the α protons in different environments.

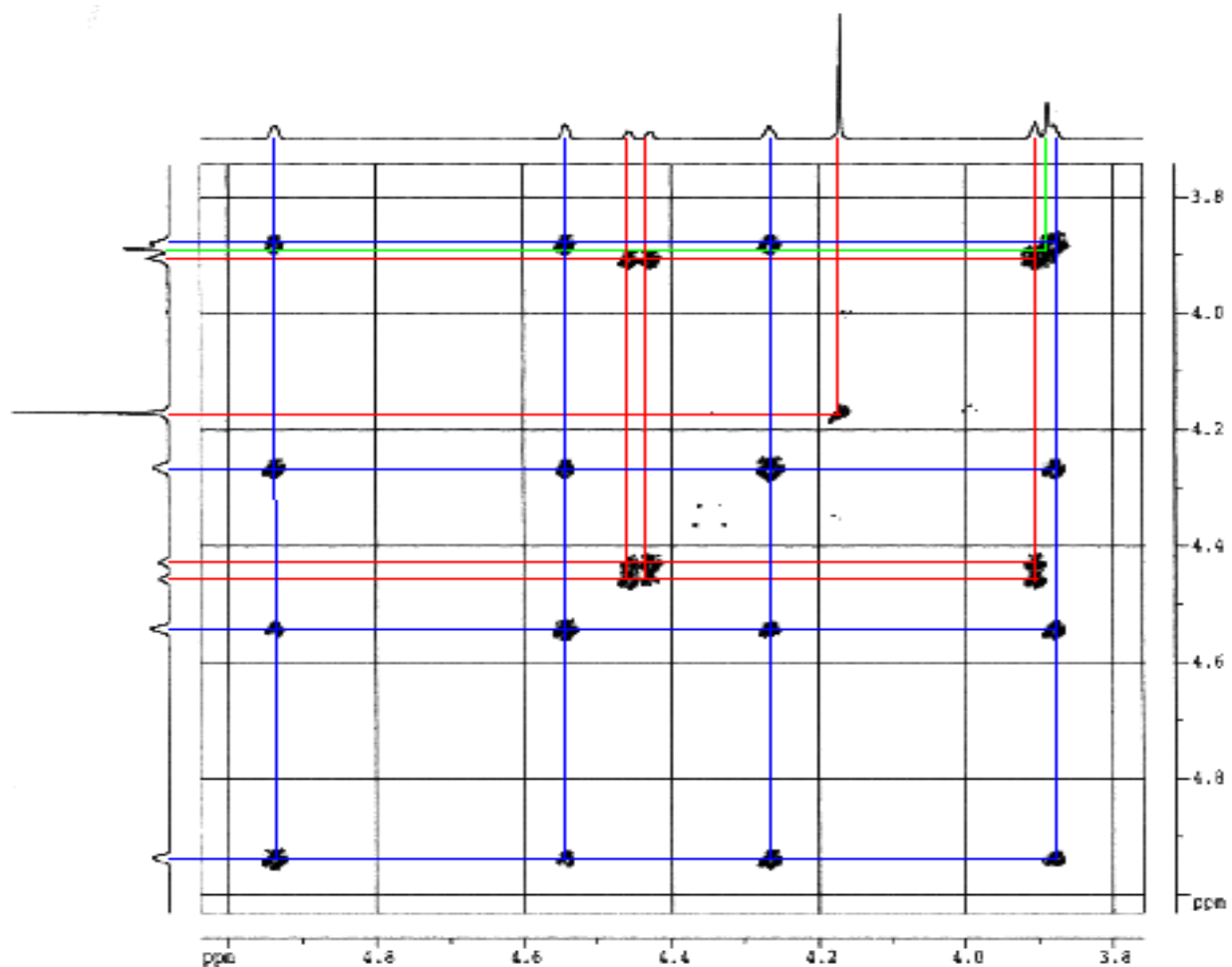


Figure 4-7: COSY experiment of **3**, red lines correspond to the ferrocenyl unit, blue lines to the *ansa*-chromocene group and green lines to the transannular bridge

The HMQC experiment of **4a** (Figure 4-8) shows, that the ^1H signal at 4.12 ppm is correlated to the ^{13}C signal at 67 ppm (hidden under the strong solvent THF signal). The ^1H signals at 4.38, 4.40 and 4.41 ppm are related to the three ^{13}C signals at ca. 65 ppm. All these signals belong to the substituted ferrocenyl Cp rings (red lines). The proton signals at 3.86, 4.27, 4.75 and 5.30 ppm are correlated to the ^{13}C signals at ca. 80 ppm that reflect the carbon atoms of the *ansa*-chromocene Cp rings (blue lines). The resonance at 4.19 ppm, reflecting the two protons of the transannular bridge is correlated to the ^{13}C signal at 55.3 ppm (green line).

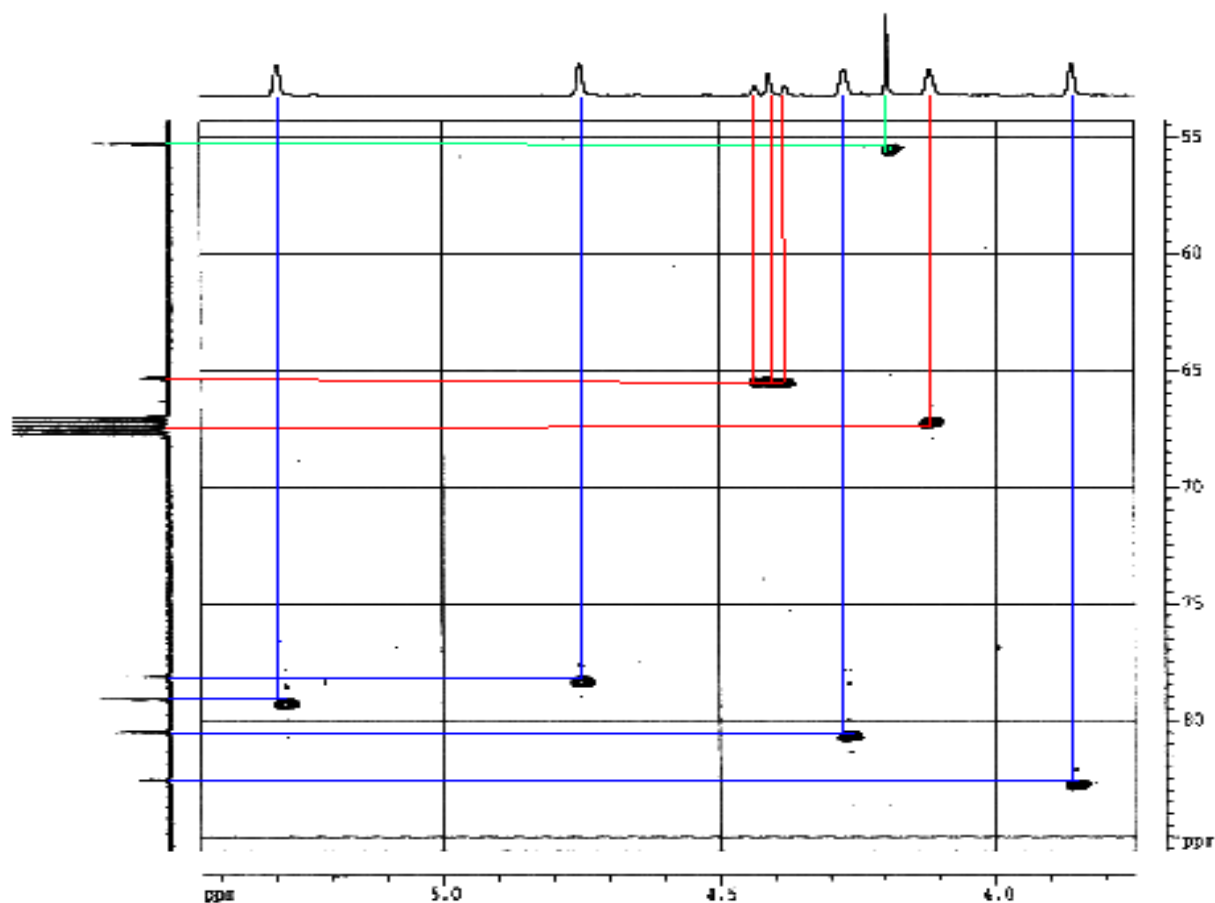


Figure 4-8: ^1H - ^{13}C correlation of **4a**, red lines correspond to the ferrocenyl unit, blue lines to the *ansa*-chromocene groups and green lines to the transannular bridges

The COSY experiment, shown in Figure 4-9, indicates that only the protons represented by the signals at 4.38 and 4.43 ppm spin couple with each other as well as with the one represented by the signal at 4.12 ppm. Analogous spin coupling can be observed between the protons belonging to the signals at 4.40 ppm as well as with the one reflected by the signal at 4.12 ppm (red lines). That we can observe four different signals (70 °C) for the four protons of the ferrocenyl Cp rings next to the isocyanide groups is attributable to the fact that the chromocene units are chiral and the racemic mixture of R and S enantiomers can combine with the ferrocenyl diisocyanide in combinations of RR, RS, SR, and SS. Thus, two of the α proton signals arise from the indistinguishable RR and SS combinations, and an additional two signals arise from the indistinguishable RS and SR combinations.

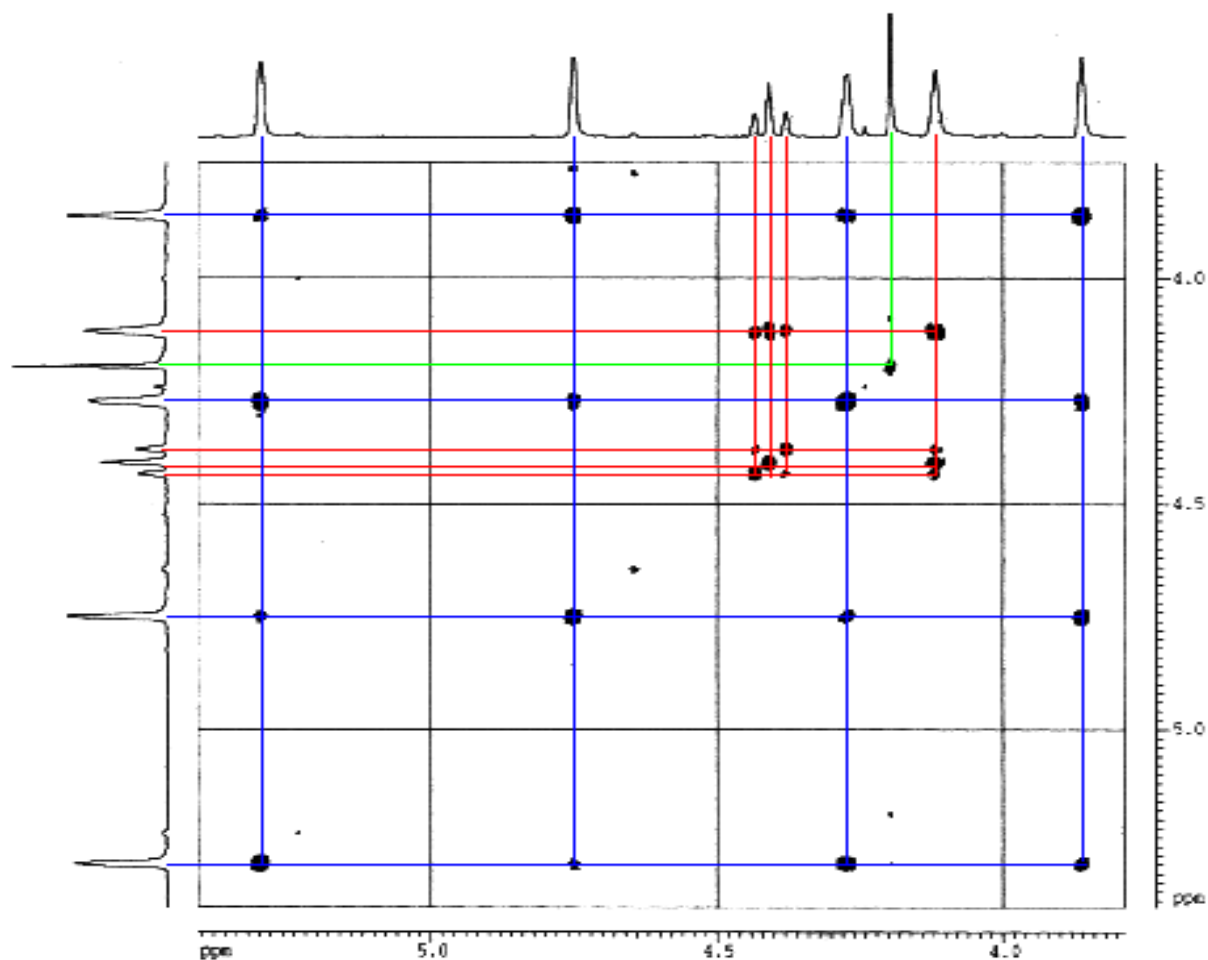


Figure 4-9: COSY experiment of **4a**, red lines correspond to the ferrocenyl unit, blue lines to the *ansa*-chromocene groups and green lines to the transannular bridges

Overall, we observe two sets of two different protons. Each set results from two inequivalent groups of stereoisomers and no spin coupling can be observed between the inner signals and the outer signals.

The protons resonating at 3.86, 4.27, 4.75 and 5.30 ppm all spin couple with each other. This confirms that they are all part of the *ansa*-chromocene Cp rings (blue lines).

The spectra for complexes **4b** and **5** are much simpler; both spectra show a single resonance signal at ca. 1 ppm representing the 24 protons of the methyl groups that belong to the tetramethylethanediy bridge. Also, two signals between 3.9 and 4.8 ppm can be observed representing the protons of the *ansa*-chromocene Cp rings. Complex

4b shows two signals between 4.0 and 4.4 ppm reflecting the protons of the substituted ferrocenyl Cp rings. Complex **5** exhibits one resonance signal at 7.5 ppm that reflects the four protons of the 1,4-phenylene diisocyanide bridge.

The ^{13}C resonance signals of the isocyanide carbon atoms appear at 274.05 ppm for **3**, 276.18 ppm for **4a**, 278.57 ppm for **4b** and 278.26 ppm for **5**.

All complexes show a significant shift of their $\nu(\text{NC})$ IR absorption bands to lower energies compared to free ferrocenylisocyanide, ferrocenyldiisocyanide and 1,4-phenylene diisocyanide. This is due to the fact that the sp character of the NC bonds in the free isocyanide species decreases and the NC bonds in the new isocyanide bridged species assume more sp^2 character. Thus, the NC bonds in these new complexes are significantly weaker than in their parent compounds. The attempts to obtain single crystals of all complexes were only successful for **3**, **4b**, and **5**.

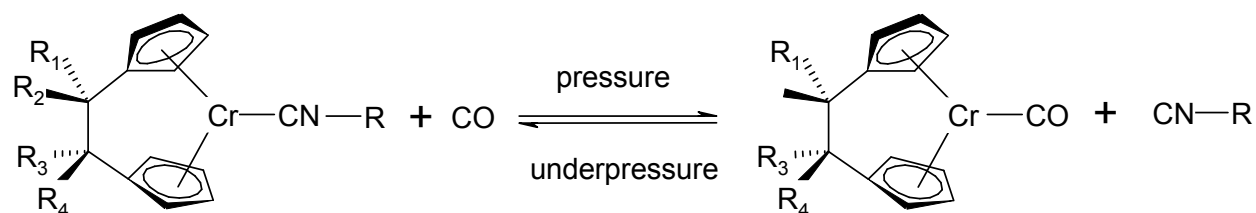
Another interesting observation is that all complexes incorporating a ferrocene unit (**3**, **4a**, **4b**) show a remarkable stability against light and heat. Unlike their counterparts that do not possess a ferrocene unit, they do not decompose under photolysis and they are stable up to a temperature of 80 °C. The *tert*-butyl isocyanide species, for instance, decomposes if photolysed or thermolysed. In both cases the formation of isobutene and a paramagnetic species can be observed. **3**, **4a** and **4b** are also stable in solvents like acetone or DMSO.

However, like all other *ansa*-chromocene(II) complexes, they are highly air sensitive. Upon exposure to air, they decompose, forming paramagnetic species and regenerating the free ferrocenylisocyanide ligands. These compounds react with acetonitrile and halogenated solvents, such as methylene chloride or chloroform, to form paramagnetic species.

4.3.5. Ligand Exchange with CO

Complex **3** undergoes ligand exchange with CO in the presence of an atmosphere of carbon monoxide. This suggests that all *ansa*-chromocene isocyanide adducts can reversibly exchange ligands with CO because this behavior has already been observed before for all *tert*-butyl isocyanide analogues [37]. It is still uncertain and has yet to be determined which kind of substitution mechanism takes place. In general, most 18 electron organometallic complexes exchange ligands by a dissociative mechanism pathway in order to avoid 20 electron intermediates [9]. However, they can also proceed by an associative mechanism if a poly-hapto ligand is present that can adopt a lower hapticity coordination [105]. In the case of sterically bulky ligands, as it applies to the complexes described herein, the former appears to be more likely. However, since the *ansa*-chromocene species can also undergo ring slippage to η^3 -intermediates, the latter cannot be excluded.

The ligand substitution reaction was performed at room temperature with a small sample of **3** dissolved in THF- d_8 in a sealed NMR-tube under an overpressure of carbon monoxide. According to the ^1H -NMR spectrum, the ferrocenyliisocyanide was replaced stoichiometrically by CO and the corresponding *ansa*-chromocene carbonyl complex was regenerated. Thus, the substitution of isocyanide with CO is reversible (Scheme 4-9).



Scheme 4-9: Ligand exchange controlled by the pressure

4.3.6. Electrochemistry and X-Ray Single Crystal Structures

The cyclic voltammogram for complex **3** shows two electrochemically reversible redox systems at 281 mV representing the $\text{Fe}^{2+/3+}$ couple and at -1153 mV representing the $\text{Cr}^{2+/3+}$ couple. As could be observed for other *ansa*-chromocene complexes, at 131 mV an electrochemically irreversible oxidation peak is present that is attributed to the $\text{Cr}^{3+/4+}$ couple (Figure 4-10). The redox potential for ferrocenylisocyanide appears at 186 mV. The potential of the $\text{Fe}^{2+/3+}$ couple experienced a shift to ca. 100 mV more positive values in $\mathbf{3}^{2+}$. Thus, the ferrocene unit in $\mathbf{3}^{2+}$ is harder to oxidize than it is in free ferrocenylisocyanide. The Cr^{4+} moiety on the ferrocenylisocyanide effectively withdraws electron density from the ferrocene unit.

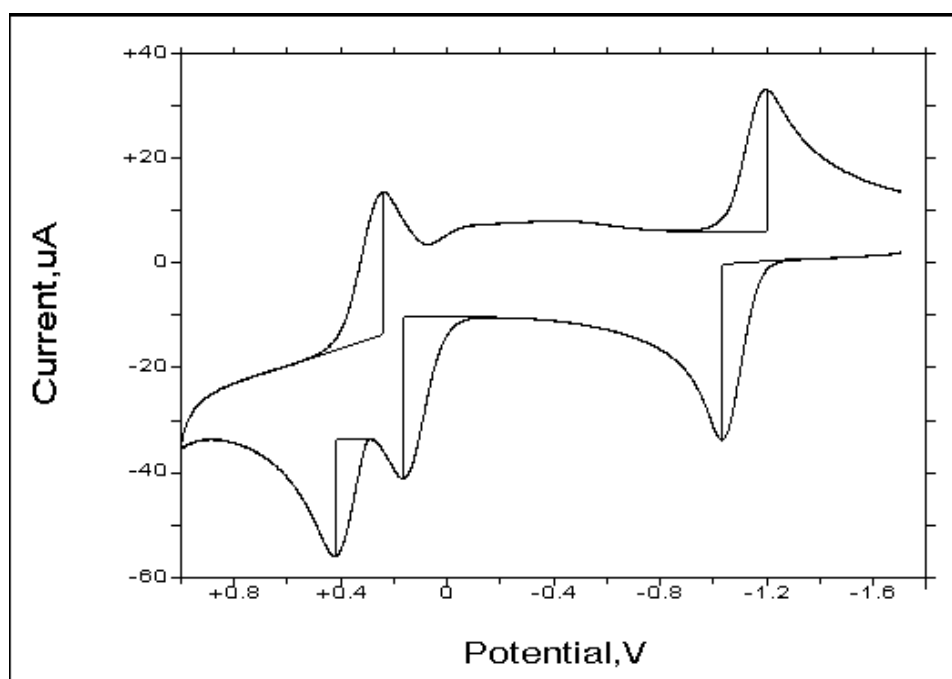


Figure 4-10: CV of **3** with a scan rate of 250 mV/s

For complex **2b** [33], for instance, a similar $\text{Cr}^{2+/3+}$ redox potential of -1154 mV was observed. The fact that both complexes possess quite similar IR absorption frequencies at 1829 cm^{-1} for **3**, and 1835 cm^{-1} for **2b**, indicates that the *tert*-butyl group and the ferrocene unit of these complexes behave quite similar in respect to their electron donating properties. One would expect both complexes to exhibit quite similar values

for their bond distances and the C-N-C bond angles. This can indeed be confirmed by comparison of the single crystal X-ray structure data. Both complexes possess similar C-N-C bond angles as can be seen in Table 4-2. The Cr-C bond distances are very close to 1.88 Å and the N-C bond distances are close to 1.21 Å. These values suggest that the nitrogen atoms exhibit significant sp^2 character.

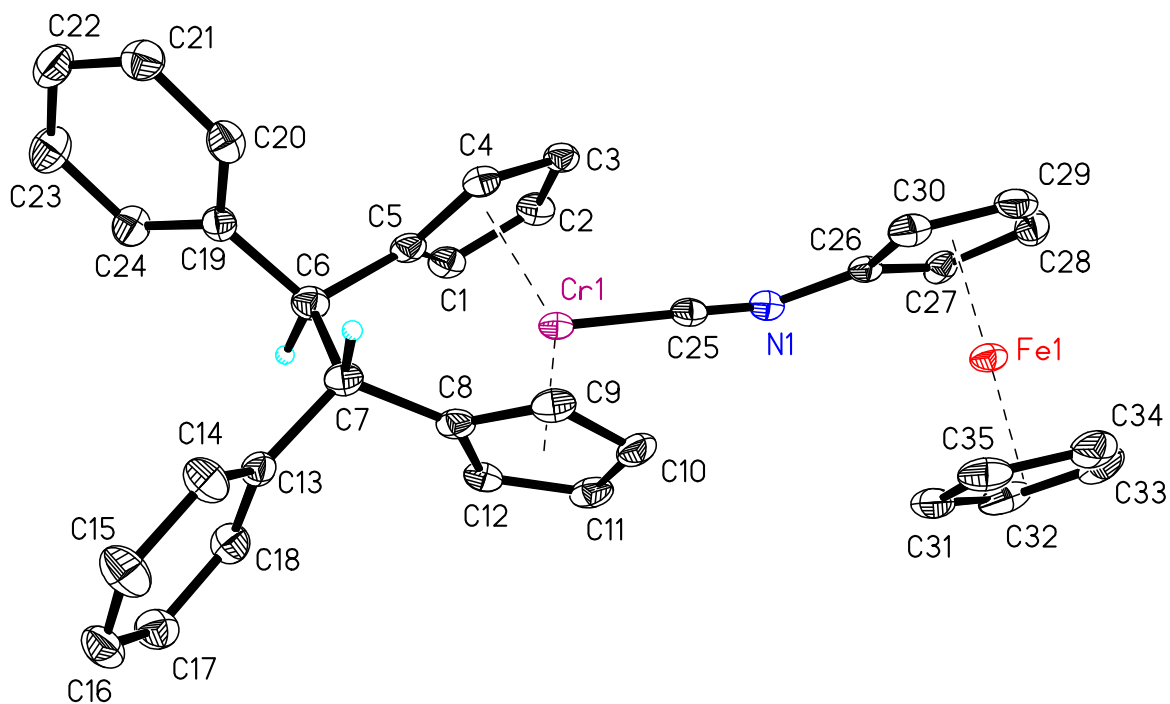


Figure 4-11: Single crystal X-ray structure of **3**

Table 4-2: Comparison of selected single crystal X-ray structure data of **3** and **2b**:

Complex 3		Complex 2b	
C(25)-N(1)-C(26):	134.4 (4) ^o	C(17)-N(1)-C(18):	131.1 (3) ^o
N(1)-C(25)-Cr(1):	173.9 (3) ^o	N(1)-C(17)-Cr(1):	177.0 (3) ^o
N(1)-C(26):	1.411 (5) Å	N(1)-C(18):	1.482 (4) Å
N(1)-C(25):	1.205 (5) Å	N(1)-C(17):	1.214 (4) Å
Cr(1)-C(25):	1.879 (4) Å	Cr(1)-C(17):	1.873 (3) Å
Cp>Cp	40.0(4) ^o	Cp>Cp	40.2 ^o

Complexes **4a** and **4b** possess two *ansa*-chromocene units linked to each other by a ferrocenyldiisocyanide unit. The cyclic voltammograms of these two species exhibit the same features: two electrochemically reversible redox systems at 589 (**4a**), 574 (**4b**) mV representing the Fe^{+2/+3} couple and at -1152 (**4a**), -1149 (**4b**) mV representing the Cr^{+2/+3} couple. At 33 mV (**4a**) and 61 mV (**4b**) the same electrochemically irreversible oxidation peak can be observed as for **3**.

Since **4a** and **4b** contain two *ansa*-chromocene units that are linked over a ferrocenyldiisocyanide bridge one would expect that these molecules could form a mixed valence species by oxidation of one of the chromium centers and not the other. In this case, the CVs should exhibit two reversible redox systems for the Cr^{+2/+3} couples that are separated from each other. However, this was not observed. As Figure 4-12 shows, both redox couples appear at the same potentials of -1152 mV, (**4a**) and -1149 mV (**4b**). Thus, according to the electrochemical experiment, it seems to be impossible to oxidize specifically one chromium metal center to the Cr³⁺ species. In fact, this observation could be established in a chemical oxidation experiment, as will be described later. Unlike in **3**²⁺ the oxidation potentials of the ferrocenyl units in **4a**⁴⁺

(589 mV) and $\mathbf{4b}^{4+}$ (615 mV) are shifted to slightly more negative values compared with the oxidation potential of the free ferrocenyldiisocyanide (639 mV).

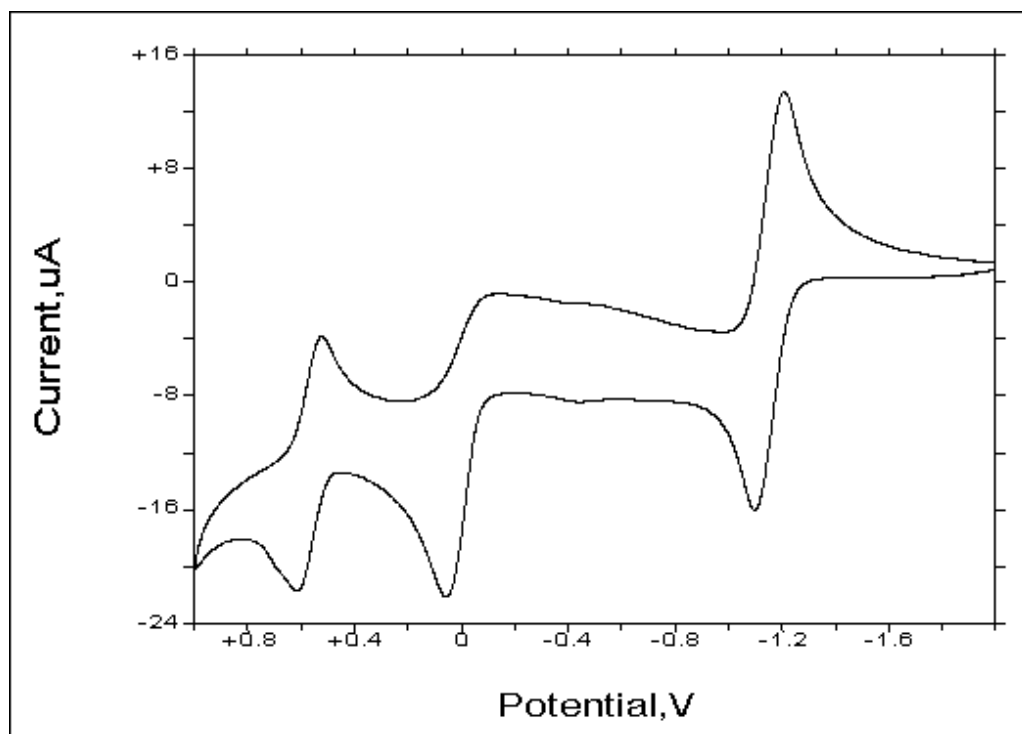


Figure 4-12: CV of **4b** with a scan rate of 25 mV/s

That implies that in the case of these trimetallic complexes the ferrocenyl unit is richer in electron density than the ferrocenyldiisocyanide, even with two Cr^{4+} moieties attached to it.

Complexes **4a** and **4b** exhibit a significantly lower IR absorption energy band at 1763 cm^{-1} and 1751 cm^{-1} . This implies that the N-C bonds in both complexes are weaker than the one in **3**. The IR absorption band of the free ferrocenyldiisocyanide appears at 2114 cm^{-1} . This is insignificantly weaker than the one of the ferrocenylisocyanide at 2121 cm^{-1} .

Regarding the X-ray single crystal structure of **4b** in Figure 4-13, it turns out to be very interesting to compare the bond angles as well as the bond distances of **4b** with the ones of **3** and **2b**. This reveals that **4b** exhibits nearly the same bond distances like **3**

and **2b**. The only significant difference in respect to the other two complexes are the ca. 5-8° smaller C-N-C bond angles.

Another interesting effect is the arrangement of the metallocene units in **4b**. The most sterically effective arrangement would be an arrangement of the *ansa*-chromocene units as far apart from each other as possible. That would require a staggered formation of the ferrocenyl Cp rings. However, these groups are very close to each other and the Cp rings of the ferrocenyl unit are in the eclipsed formation.

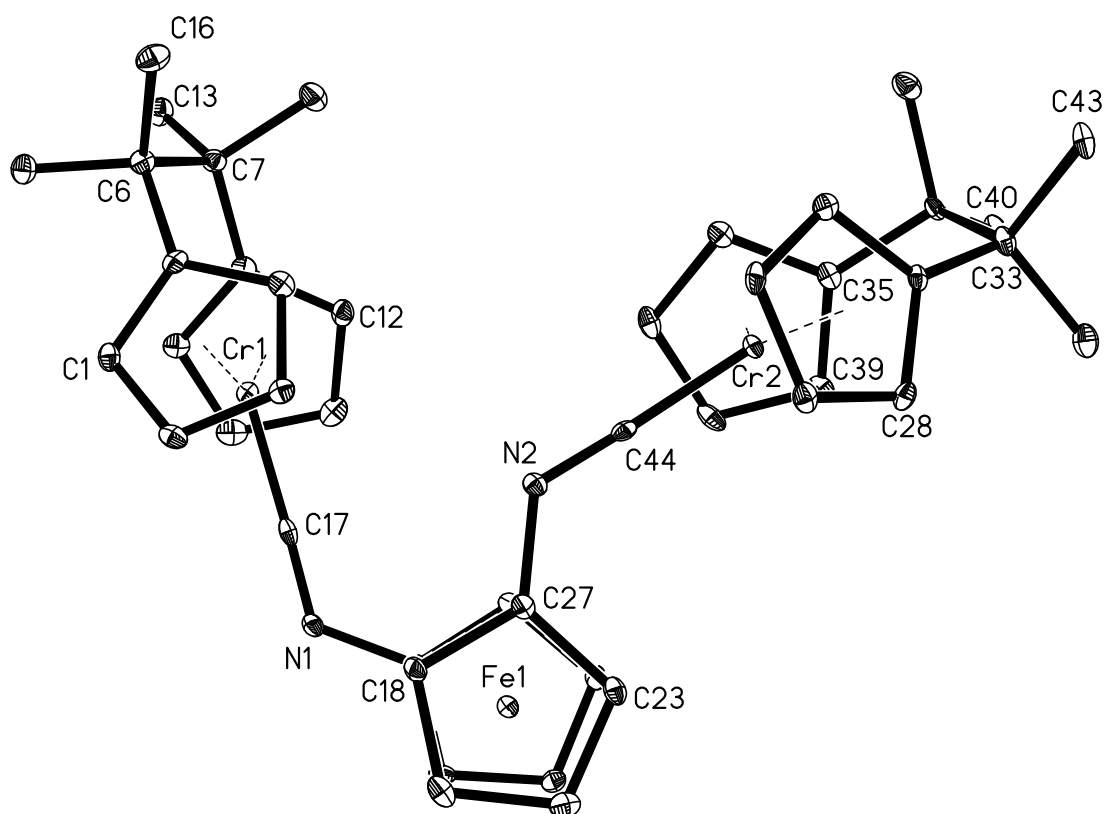
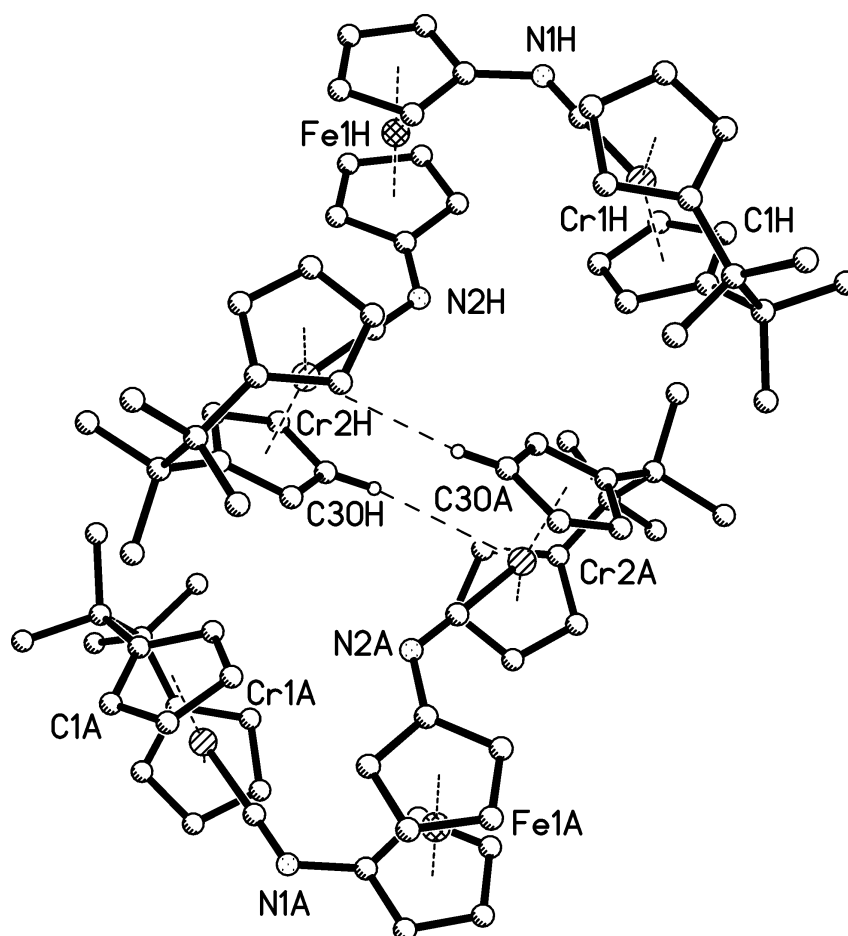


Figure 4-13: Single crystal X-ray structure of **4b**

Table 4-3: Selected X-ray structure data of **4b**:

C(17)-N(1)	1.230(4) Å	C(27)-N(2)	1.409(4) Å
C(17)-Cr(1)	1.852(4) Å	C(44)-N(2)	1.224(4) Å
C(18)-N(1)	1.415(4) Å	C(44)-Cr(2)	1.862(4) Å
C(17)-N(1)-C(18)	125.8(3)°	C(44)-N(2)-C(27)	126.4(3)°
N(1)-C(17)-Cr(1)	178.3(3)°	N(2)-C(44)-Cr(2)	177.6(3)°
Cp>Cp	39.1(3)°	Cp>Cp	39.9(3)°

The crystal packing in the solid state (Figure 4-14) shows weak intermolecular C-H \cdots Cr hydrogen bonds, with the Cr metal centers acting as the acceptors.

**Figure 4-14:** Arrangement of two molecules **4b**, exhibiting intermolecular C-H \cdots Cr bonds

The distances are ca. 3.033(5) Å, with a C-H \cdots Cr angle of 149.8(5)°. These intermolecular hydrogen bonding interactions may be partly responsible for the arrangement of the chromocene units in each molecule. In solution, however, it is likely that rotation of the ferrocene Cp rings occurs.

In benzene- d_6 , for instance, the two $^1\text{H-NMR}$ resonance signals of the substituted ferrocenyl Cp systems appear as very broad unresolved signals at 4.23 and 4.65 ppm. In THF- d_8 , however, these two resonance signals appear as sharp peaks at 4.06 and 4.32 ppm. The behavior in acetone- d_6 is similar to that in C_6D_6 . In toluene- d_8 , however, the signals appear again as sharp peaks. Thus, what is observed here are extremely weak interactions that presumably play a significant role in the crystal packing though.

An experiment was performed to synthesize an *ansa*-chromocene ferrocenyl diisocyanide species in which just one *ansa*-chromocene unit would be connected to one of the two isocyanide groups. It was hoped that more conclusions could be drawn from the electrochemical and spectroscopic data of this derivative.

A similar experiment performed by Lentz and co-workers with diisocyanomethane and hexacarbonyl chromium generated a mixture of both possible adducts [106]. They combined hexacarbonyl chromium with two equivalents of isocyanomethane. The workup resulted in 12.7% of the diisocyanomethane bis(pentacarbonyl chromium) and 64.2% of the diisocyno pentacarbonyl chromium.

However, when ferrocenyldiisocyanide and one equivalent of **1b** were reacted, only half an equivalent of the ferrocenyl diisocyanide was used up to form complex **4b**.

In the homo binuclear complex **5** two *ansa*-chromocene units are linked with each other by a 1,4-phenylene diisocyanide bridge. The CV of this molecule, shown in Figure 4-15, exhibits a reversible redox system at -1096 mV representing the $\text{Cr}^{2+/3+}$ couple. The oxidation peak to the Cr^{4+} species can be observed at 163 mV.

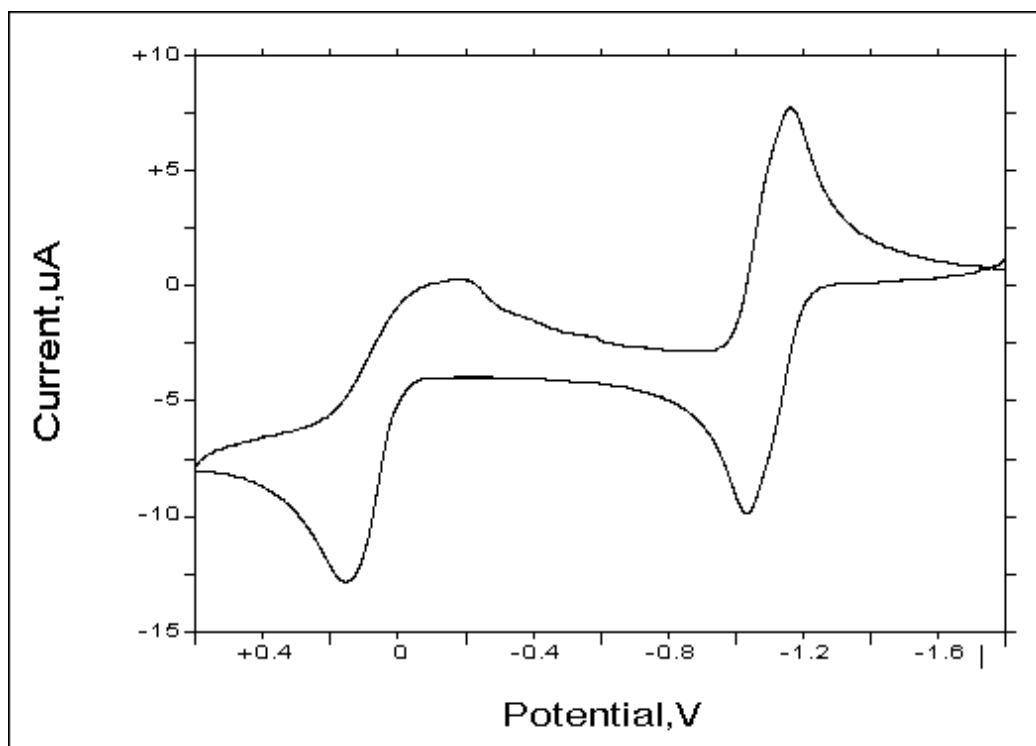


Figure 4-15: CV of **5** with a scan rate of 25 mV/s

The IR absorption band of **5** appears at 1766 cm^{-1} . The X-ray single crystal structure, shown in Figure 4-16, reveals that the C-N-C bond angles of 128.6° fit in-between the ones of **3** and **4b**.

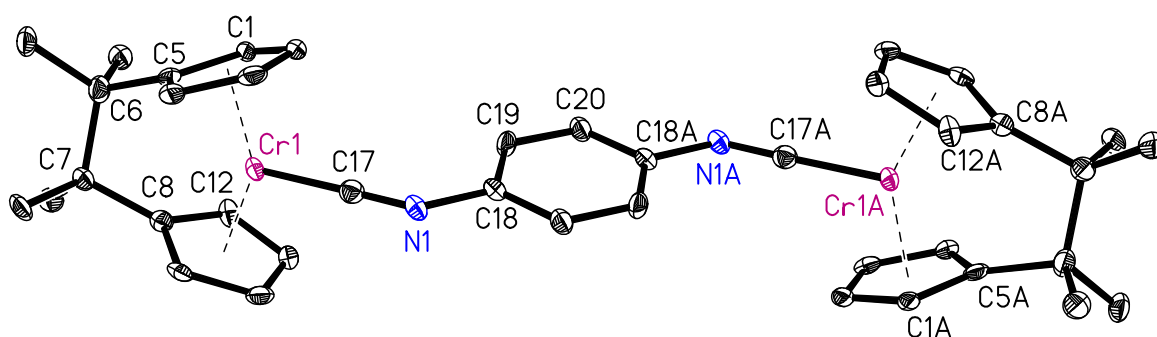


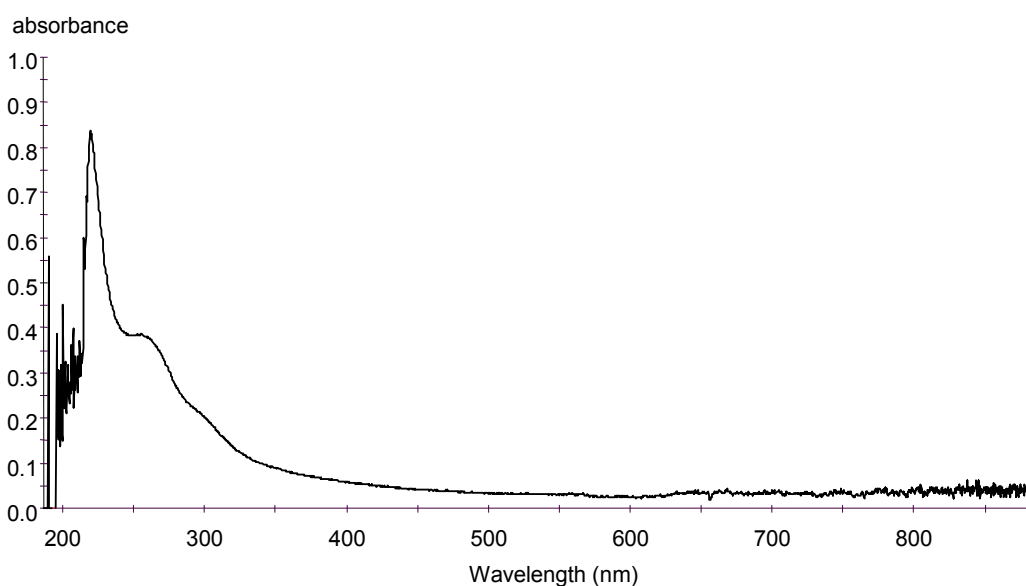
Figure 4-16: Single crystal X-ray structure of **5**

Table 4-4: Selected X-ray structure data of **5**:

C(17)-N(1)	1.232(6) Å	C(17)-N(1)-C(18)	128.6(5)°
C(17)-Cr(1)	1.861(5) Å	N(1)-C(17)-Cr(1)	177.2(5)°
C(18)-N(1)	1.427(6) Å	Cp>Cp	39.0(4)°

4.3.7. UV-VIS Spectroscopy

The UV-VIS spectra of **3**, **4a**, **4b** and **5** do not show any significant differences among these complexes or any features within the visible region. They all show the same features, exhibiting a very strong ligand-to-metal charge transfer absorbance at 235 nm. Another shoulder can be seen at 260 nm. The absorbance intensity decreases continuously with increasing wavelength until it stays at insignificantly low values from ca. 500 nm on. This absorption behaviour between 300 and 500 nm causes the deep red/brown color of all complexes. Figure 4-17 shows the UV-VIS spectrum of complex **3** but can be regarded as representative for all of the polynuclear *ansa*-chromocene complexes.

**Fig. 4-17** UV VIS spectrum of complex **3** as a solution of ca. 40 ppm in THF

4.4. Chemical Oxidation of Heteronuclear *Ansa*-Chromocene isocyanide Complexes

4.4.1. Oxidation of **3** and **4a** with the Ferrocenylium Cation as well as Benzoquinone

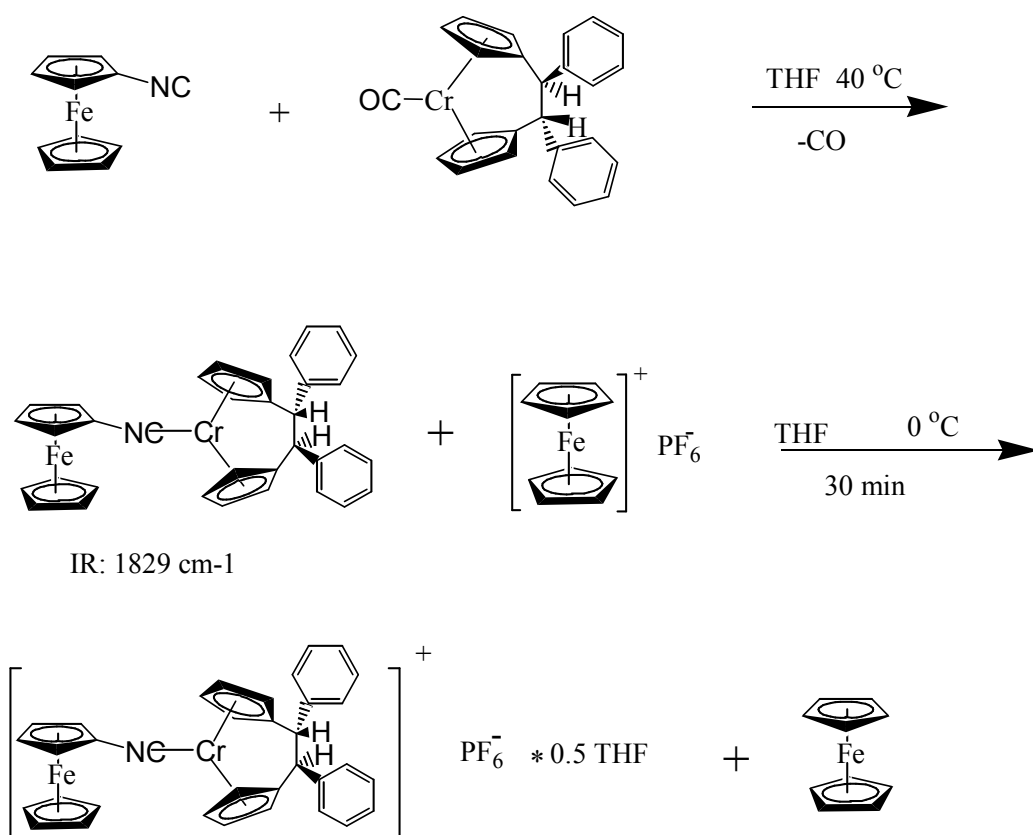
To examine if these complexes could be converted to mixed valence species, chemical oxidation reactions with complexes **3** and **4a** were performed. The idea was to oxidize one metal center of **3** and one or two metal centers of **4a**. This could lead to the formation of complexes that exhibit the desired mixed valence behavior. As demonstrated with the Creutz Taube ion this would result in the delocalization of the positive charge over the whole molecules [38,47]. Hence, it would be harder to oxidize the other metal centers because they would provide less electron density than the neutral parent complex. Mixed valence species like these, in general, exhibit a broad metal to metal charge transfer absorption band within the NIR region between 800 and 1800 nm.

In order to perform chemical oxidation reactions with organometallic complexes, there exists a variety of redox agents to choose from [107]. We decided to use ferrocenyl hexafluorophosphate (FcPF₆) as the oxidizing agent. The ferrocinium ion is a mild one-electron oxidant with a redox potential of 0 mV (vs. Fc), which is sufficiently high for these purposes. It is usually regarded as an outer-sphere reagent [108] and is commercially available. Long and co-workers performed the synthesis of heterobimetallic bis(acetylide) ferrocene complexes incorporating a ruthenium metal center [59]. They described the generation of the corresponding mixed valence counterparts by oxidizing the neutral molecules with FcPF₆. The oxidations of **3** and **4a** were performed as a modified version of the reaction described by Long.

Complex **3** was mixed with an equimolar amount of FcPF₆ and **4a** was mixed with two equivalents of FcPF₆. The reactions took place at 0 °C in a double Schlenk vessel using

THF as solvent. The products were precipitated out of the solution at $-78\text{ }^{\circ}\text{C}$ and separated from the supernatant by filtration. The remaining brown solids were washed with hexane to remove the generated ferrocene. The yields of the cationic products were around 50% starting from the neutral counterparts.

In order to increase the isolated yields of the oxidized complexes without wasting starting materials, the procedure was modified to a one pot synthesis. These reactions started with the ferrocenylisocyanide ligands and the *ansa*-chromocene carbonyl complexes. The overall yields improved to 65% ($\mathbf{4a}^{2+}$) and 68% ($\mathbf{3}^+$). The neutral complexes $\mathbf{3}$ and $\mathbf{4a}$ were generated as precursors *in situ* following the earlier described procedures. Then, instead of isolating the neutral products, the solutions were cooled to $0\text{ }^{\circ}\text{C}$ and the oxidant FcPF_6 was added slowly from a solid material dispenser. The solutions were stirred for another half an hour. The products were worked up as described above.



Scheme 4-9: One pot synthesis of $\mathbf{3}^+$

The cation **3**⁺ coordinates half an equivalent of THF. The one pot synthesis of **4a**²⁺ proceeded the same way as for **3**⁺ except that two equivalents of FcPF₆ were added as the oxidant. Each of the ionic species **3**⁺PF₆⁻ and **4a**²⁺(PF₆)⁻₂ consists of a brown, microcrystalline, paramagnetic powder.

The ¹H-NMR spectra look almost identical. Very broad resonance signals can be observed for the phenyl groups and the substituted ferrocenyl Cp rings. In the spectra for **3**⁺PF₆⁻ one more signal appears, representing the unsubstituted ferrocenyl Cp ring. All other resonance signals cannot be observed because the corresponding protons are too close to the paramagnetic metal centers. The ³¹P-NMR-spectra show a well resolved heptet resonance signal at -142 ppm and the ¹⁹F-NMR-spectra show a well resolved doublet resonance signal at -70 ppm representing the PF₆⁻ anions.

Besides NMR-spectroscopy, these complexes were characterized with IR-, UV-VIS-NIR spectroscopy, elemental analyses, and their effective magnetic moments were determined as well. The electrochemical behavior of these ionic complexes was similar to their neutral counterparts. All results indicate that the expected oxidation products were formed successfully. First of all, a stoichiometric amount of ferrocene, produced as byproduct, indicates that all the oxidant FcPF₆ was used up and reduced to ferrocene. Therefore, all of the neutral complexes must have been converted into corresponding oxidized species.

This fact alone, however, cannot be regarded as evidence for the successful oxidation. These molecules could have suffered oxidation at other parts of their scaffolds, or the destruction of their molecular structure. However the CVs look very similar to the corresponding CVs of the neutral species **3** and **4a**. The values of the redox potentials for the Fe^{2+/3+} and Cr^{2+/3+} couples do not show any significant differences. These results provide good evidence for the fact that the molecules did not suffer any structural changes apart from the change in their overall oxidation state.

The IR absorption bands also support the generation of the desired ionic products. Upon oxidation the CN stretch of **3** shifted to a high energy value of 2118 cm^{-1} , and $\mathbf{4a}^{2+}(\text{PF}_6)^{-}_2$ possesses two overlapping bands at 2113 cm^{-1} and 2137 cm^{-1} . Thus, the isocyanide groups of the cationic species possess much stronger bonds between the N and the C atoms. These values are very close to the ones of the free isocyanide species at 2121 cm^{-1} for the mono- and 2114 cm^{-1} for the di-isocyanide. Nevertheless, the possibility that the parent compounds ferrocenyl-isocyanide and -diisocyanide were generated during the oxidations can be ruled out from the following observations.

These oxidized complexes are not soluble in benzene or diethyl ether at all, and they are just slightly soluble in THF. Unlike their neutral parent complexes, $\mathbf{3}^+\text{PF}_6^-$ and $\mathbf{4a}^{2+}(\text{PF}_6)^{-}_2$ are stable in methylene chloride. Unfortunately, efforts to grow X-ray quality single crystals of the ionic species were unsuccessful.

Santi and Ceccon used p-benzoquinone and ammonium hexafluorophosphate to generate the cationic species of heterobimetallic ferrocenyl indenyl rhodium complexes that exhibit mixed valence properties [109]. This reaction was slightly modified and applied to **3** and **4a** in order to examine if this method is also eligible to produce the cationic counterparts. Apparently p-benzoquinone is too strong as an oxidizing agent, because the molecules suffered significant destructive changes. This was revealed by the electrochemical experiments that were conducted to examine the resulting products. The CV of **4a** shows that only a ferrocene moiety was left as the product, and no evidence can be found for the chromocene moieties (Figure 4-18). It seems that during the oxidation reaction the isocyanide bridges as the links between the metal centers broke and the molecule fell apart into at least three parts.

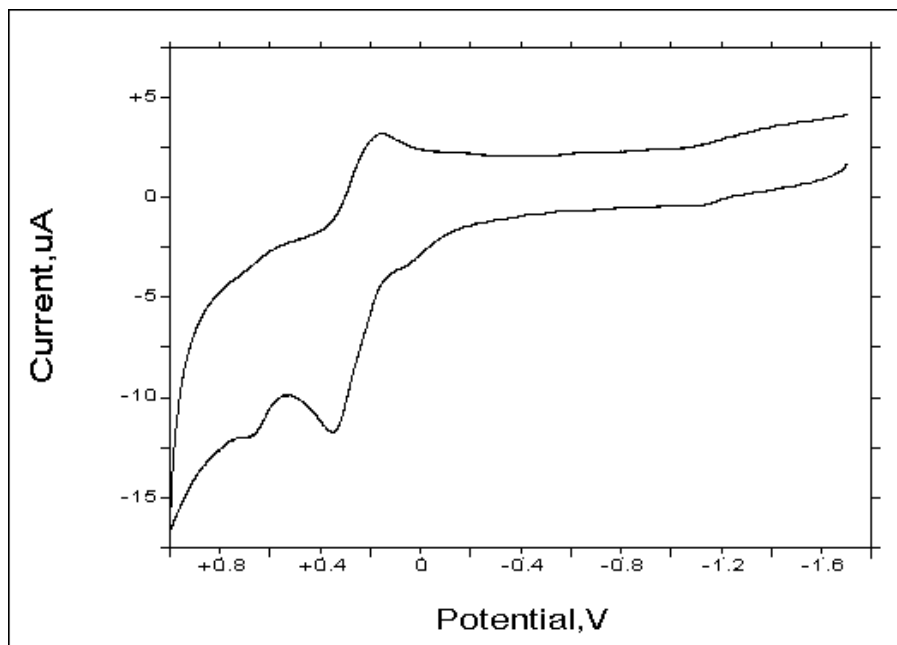


Figure 4-18: CV of **4a** after oxidation with p-benzoquinone with a scan rate of 250 mV/s

Something similar could be observed upon exposing $4a^{2+}(PF_6)^-_2$ to air. The shape of the ferrocenyl redox system looks identical to the one of ferrocenyldiisocyanide.

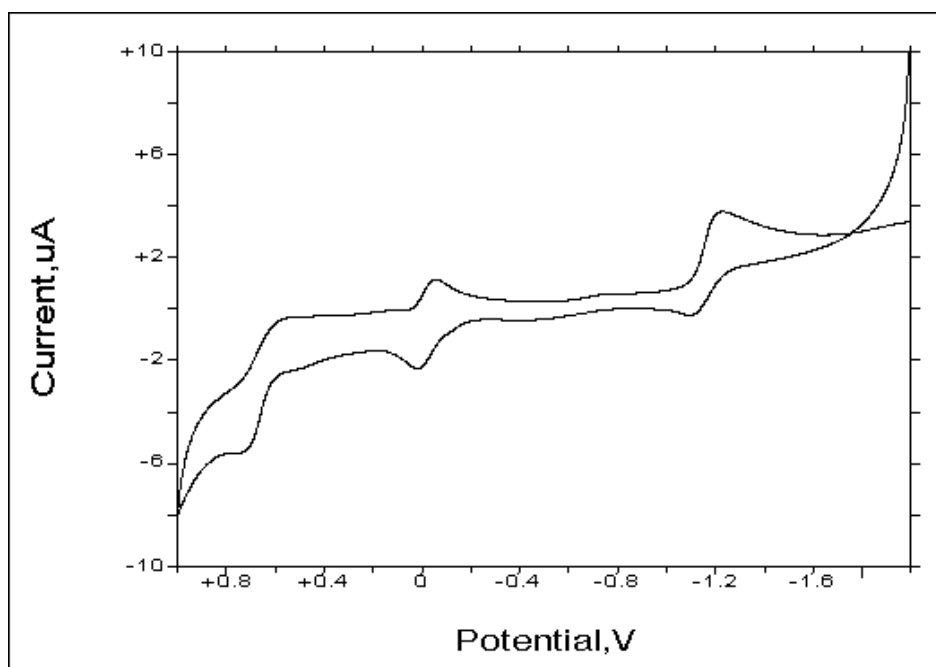


Figure 4-19: CV of $4a^{2+}(PF_6)^-_2$ after exposure to air with a scan rate of 25 mV/s

The reduction of the Cr^{3+} to the Cr^{2+} species appears to be irreversible and at 0 mV a reversible redox system can be observed, which is probably due to ferrocene, generated as a decomposition product. Thus, like the neutral parent complex, $\mathbf{4a}^{2+}(\text{PF}_6)^{-}_2$ suffers decomposition if exposed to air.

The IR absorption band at 2184 cm^{-1} confirms as well that a significant change occurred to $\mathbf{4a}^{2+}(\text{PF}_6)^{-}_2$ upon exposure to air. The original values were observed at 2113 cm^{-1} and 2137 cm^{-1} .

If the obtained ionic species experience electron transfer between the Fe(II) and Cr(III) centers they should show a broad metal to metal charge transfer absorption within the NIR-region. Solutions of $\mathbf{3}^+\text{PF}_6^-$ and $\mathbf{4a}^{2+}(\text{PF}_6)^{-}_2$ in THF as well as in methylene chloride were examined over a broad spectral range between 185 and 2200 nm. No absorption within the NIR region between 800 and 1800 nm could be observed at all. Within the UV-VIS region their spectra look similar to the ones of the neutral counterparts.

Measured values for C, H, and N in $\mathbf{3}^+\text{PF}_6^-$ agree very well with the calculated ones. The value for carbon in $\mathbf{4a}^{2+}(\text{PF}_6)^{-}_2$ appeared to be 3% lower than the theoretical one. This is again attributable to incomplete combustion as mentioned for the neutral species.

4.4.2. Determination of the Effective Magnetic Moments

The effective magnetic moments of both species support the observation that these complexes do not exhibit any mixed valence features. The values were determined by using the Johnson Matthey magnetic susceptibility balance as well as the $^1\text{H-NMR}$ device for the Evans method independently.

For both cationic complexes two experiments of each method were performed and the average of the resulting numbers was taken. A collection of all determined values and the constants that were used for the calculations can be found in the appendix (Chapter 9). $\text{3}^+\text{PF}_6^-$ exhibits an effective magnetic moment of 1.76 BM. This value represents one unpaired electron and the value for $\text{4a}^{2+}(\text{PF}_6)^-_2$ appears to be 2.56 BM, slightly lower than expected for two unpaired electrons. In order to determine the corresponding effective magnetic moment for each metal center separately, the value for both metal centers together has to be divided by the square root of 2, because μ_{eff} is proportional to the square root of χ_M (equation 2-21). Thus, μ_{eff} is proportional to the square root of $(2 \times \chi_M)$ for the two separated metal centers. This results in a value of 1.81 BM per Cr metal center, which is fairly close to the theoretical value of 1.73 BM. If there were any communication between the chromium centers the unpaired electrons on each metal center would pair, resulting in a diamagnetic ionic complex. This apparently does not take place and a variable temperature experiment using the Evans NMR method revealed that the effective magnetic moment does not change within a temperature range between $-90\text{ }^\circ\text{C}$ and $25\text{ }^\circ\text{C}$. As Figure 4-20 shows, no spin state cross-over could be observed during this experiment.

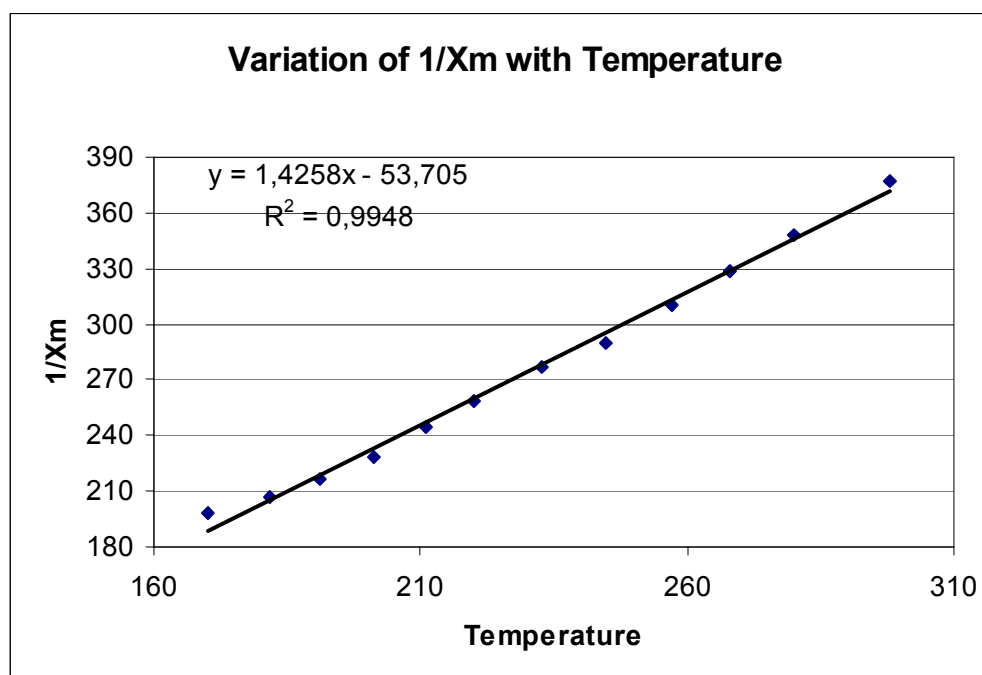


Figure 4-20: values of $1/\chi_m$ as a function of the temperature

Since these complexes seem not to exhibit any electronic communication between the metal centers, both Cr metal centers in complexes **4a** and **4b** are equivalent upon oxidation. Therefore one would expect that a mixture of mono- and di-cation species of **4a** or **4b** could be obtained.

In order to explore this with another experiment, complex **4b** was treated with one equivalent of FcPF₆ on a small scale. The NMR data of the reaction products were not very useful due to the paramagnetic behavior of the oxidized species. However, the IR spectrum of the isolated product shows a broad absorption band at 2115 cm⁻¹ and no band within the region from 1700 to 1900 cm⁻¹. This seems to represent a species in which both chromocene units became oxidized. The slurry that was washed away from this product shows two overlapping IR bands with maxima at 1764 and 1812 cm⁻¹ as well as two other overlapping bands at 2022 and 2049 cm⁻¹. The bands at 2022, 2049 and 1812 cm⁻¹ could possibly belong to the Cr³⁺/Cr²⁺ complex. The maxima at 1764 cm⁻¹ can be assigned to the remaining neutral starting material that did not get used up during the reaction. This is in agreement with the CV, since there is no preference of the oxidant to react only with the starting material. Statistically there should be a 1:2:1 distribution of the starting material, the monocation and the dication. This is the reason why the reaction with one equivalent of FcPF₆ results in a mixture of the monocation and the dication. In the case of a distinct preference to form the monocation, there should be **4b**⁺PF₆⁻ formed as the only product without leaving any **4b** as starting material behind.

5. Discussion

Regarding the experimental results, it seems that none of the polynuclear complexes exhibit any mixed valence behavior. According to the cyclic voltammograms of the cationic complexes, their behavior upon chemical oxidation as well as the absence of NIR-absorption bands, there is no evidence for any electronic communication between the metal centers. This result is somewhat surprising since other organometallic complexes containing more than one metal center linked over conjugated bridging systems were found to exhibit such electronic communication [68]. Also, since the link between the metal centers, the isocyanide group, has been previously found to exhibit the properties of a conducting nanowire between gold layers [69], one would expect electronic interaction to be present to a certain extent in the complexes described herein.

The results revealed some interesting aspects about the electronic properties of the *ansa*-chromocene complexes. One aim was to determine if the electronic effects of isocyanide ligands with different electron donor properties could be detected in the redox potentials of the *ansa*-chromocene complexes. Information from previous electrochemical experiments [37] showed that the carbonyl ligand shifts the Cr^{2+/3+} redox potential to more positive values relative to the *tert*-butyl isocyanide ligand. Therefore, it was expected that varying the substituents on the isocyanide ligands from electron donating to electron withdrawing would tune the redox potential of the complexes. Work by David Foo showed a moderate dependence of the *ansa*-chromocene isocyanide redox potential on the nature of the isocyanide ligand. The homobinuclear complex **5** seems to complement the pattern for a row of *ansa*-chromocene isocyanide complexes synthesized by David Foo [110] (Table 5-1). The 1,4-phenylene diisocyanide ligand appears to fit between *p*-toluenesulfonylmethylisocyanide and *tert*-butyl isocyanide in its electron withdrawing/donating properties.

Table 5-1: *Ansa*-chromocene isocyanide complexes examined by David Foo and complex **5** with their Cr^{2+/3+} redox potentials [110]:

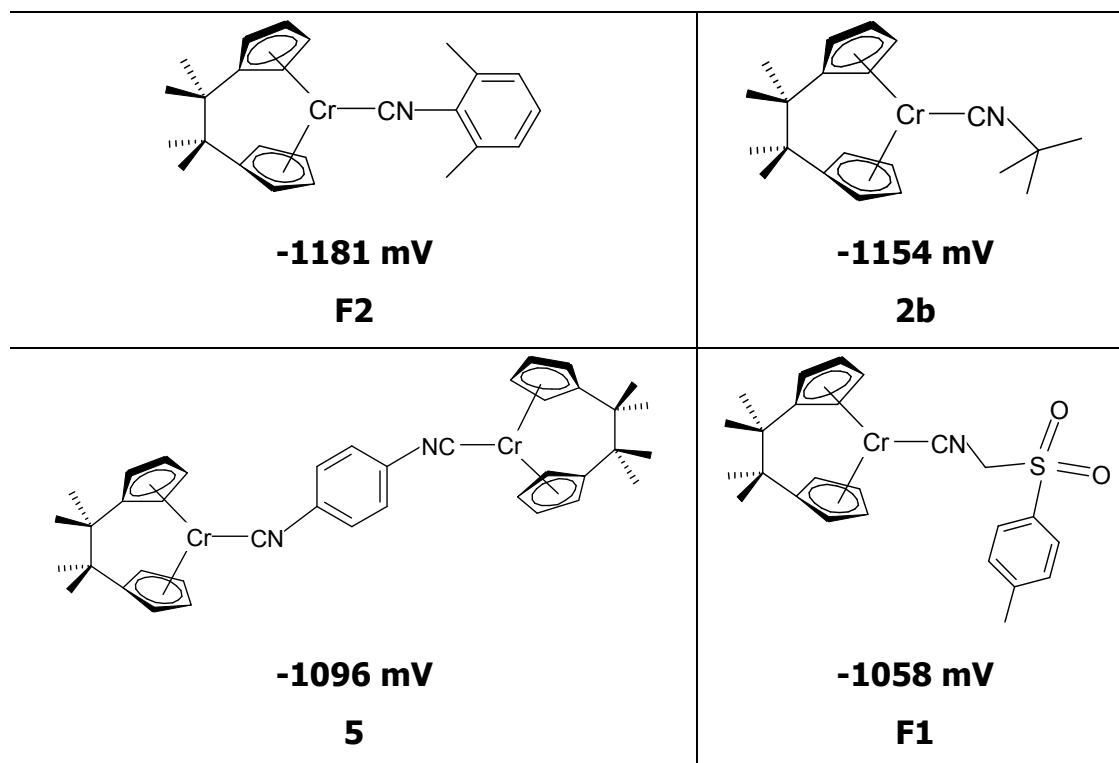


Table 5-2 illustrates that the structural data of these complexes follow a similar trend. The C-N-C bond angles, Cr-C bond distances, and the IR stretching frequencies decrease upon going from xylylisocyanide to *tert*-butyl isocyanide, to 1,4-phenylene diisocyanide, and finally *p*-toluenesulfonylmethylisocyanide.

Table 5-2: Selected data for **F2**, **2b**, **5** and **F1** in the order of decreasing IR stretching frequencies:

Complex	$(E_a + E_c)/2$	$\delta_{(\text{CN})}$	$\nu_{(\text{CN})}$	C-N-C angle	Cr-C distance
F2	-1181 mV	239.7 ppm	2006 cm^{-1}	180.0(1) $^\circ$	1.892(7) Å
2b	-1154 mV	261.2 ppm	1835 cm^{-1}	131.1(3) $^\circ$	1.873(3) Å
5	-1096 mV	278.3 ppm	1766 cm^{-1}	128.6(5) $^\circ$	1.861(5) Å
F1	-1058 mV	290.6 ppm	1752 cm^{-1}	123.1(3) $^\circ$	1.859(3) Å

The $\text{Cr}^{2+/3+}$ redox potentials follow the reverse trend. These data are consistent with the Dewar-Chatt-Duncanson (DCD) model [111,112]. According to the DCD model, π back bonding from the metal to the π^* orbital of the isocyanide ligand should result in the weakening and lengthening of the C-N bond and strengthening and shortening of the M-C bond. It should also result in a rehybridization of the nitrogen atom from sp toward more sp^2 character. The heteronuclear complexes also fit into this row concerning their structural data. In fact, the structural data of **2b** and **3** show very similar values. At the same time, **4b** and **F1** share similar structural features. This is emphasized by the red and blue colored data in Table 5-3. However the green colored values show that the heteronuclear complexes do not follow any trend in respect to their electronic data.

Table 5-3: Similarities between mono- and hetero-nuclear *ansa*-chromocene isocyanides:

Complex	$(E_a + E_c)/2$	$\delta_{(\text{CN})}$	$\nu_{(\text{CN})}$	C-N-C angle	Cr-C distance
2b	-1154 mV	261.2 ppm	1835 cm⁻¹	131.1(3)°	1.873(3) Å
3	-1153 mV	274.0 ppm	1829 cm⁻¹	134.4(4)°	1.879(4) Å
4a	-1152 mV	276.2 ppm	1763 cm⁻¹		
4b	-1149 mV	278.6 ppm	1751 cm⁻¹	125.8(3)°	1.852(4) Å
F1	-1058 mV	290.6 ppm	1752 cm⁻¹	123.1(3)°	1.859(3) Å

Interestingly **3**, **4a** and **4b** share nearly identical chemical shifts for the CN resonance signals in their ¹³C-NMR spectra and the Cr^{2+/3+} redox potentials of these complexes appear to be identical. By contrast, the redox potentials of the monoisocyano- and diisocyano-ferrocene differ dramatically from each other and significant shifts in their redox potentials occur upon their complexation to chromium. Apparently the ferrocene unit as a substituent of an isocyanide ligand behaves differently from the other isocyanide substituents. It appears that in the case of the hetero-binuclear and -trinuclear complexes the ferrocene is acting as an electron reservoir that buffers the redox potential of the chromocene.

Another interesting property of the di- and tri-nuclear *ansa*-chromocene ferrocenyl-isocyanide complexes is their remarkable stability against light and heat. This is similar to what was recently observed for a zerovalent chromium complex exhibiting six ferrocenylisocyanide ligands [113]. The authors reported the remarkable stability of their complex against air, light and heat compared with the *tert*-butyl isocyanide

counterpart. As mentioned on page 66, the *ansa*-chromocene *tert*-butyl isocyanide species decompose if exposed to light or heat, whereas the hetero-binuclear and -trinuclear complexes do not show such a sensitivity.

The collected data suggest that the heteronuclear complexes **3**, **4a** and **4b** are quite sophisticated and complex behaving compounds. At this point, it is hardly possible to entirely explain the nature of these systems. A few aspects however should be discussed that seem to contribute to the interesting behavior of these species.

While different isocyanide ligands act as either electron donors or electron acceptors, it seems that the ferrocene unit can act as both. The iron metal center obviously varies its formal redox potential in order to compensate for electronic changes affecting the aromatic Cp rings. Ferrocenyliisocyanide, for instance, with a redox potential of 186 mV, is more difficult to oxidize than ferrocene (0 mV). This can be attributed to the electron withdrawing effect of the NC group. Two isocyanide groups withdraw even more electron density, resulting in a more positive redox potential of 639 mV for the ferrocenyldiisocyanide species. Upon complexation to the *ansa*-chromocene in **3**, the electron withdrawal from the iron center of the ferrocenyliisocyanide increases (186 mV shifted to 281 mV). However, in **4a** and **4b**, complexation of the ferrocenyldiisocyanide leads to a more negative redox potential for the iron (639 mV shifted to 589 mV).

At the same time, the chromium metal centers maintain their electron densities at constant values. The chromocene moieties vary their π back donation by enlarging or decreasing the C-N-C bond angle of the isocyanide ligand. According to the structural and IR spectroscopic data, **4b** shows more π back bonding than **3**. The ^{13}C chemical shifts however suggest that the electron density at the isocyanide carbon atoms stays constant. Thus, the electron density at the chromocene moieties including the isocyanide carbon atoms seems to be independent from the extent of σ donation and π back bonding.

This might be attributed to partial delocalization of the back donated electron density into the aromatic ring systems of the ferrocene units. It has been proposed that delocalization of charge into π^* orbitals on an aryl ring in aryl isocyanidetransition metal complexes should be possible rather than for alkyl isocyanide transition metal complexes [114,115]. DFT calculations on an optimized model of ferrocenylisocyanide suggest that such delocalization of back donated electron density into the nonbenzoid π^* system of the ferrocenylisocyanide ligand is feasible [113]. This would mean that the ferrocenyl units within the heteronuclear complexes can indeed act as an electron reservoir that is a good σ electron donor as well as an electron sink that is a good π^* acceptor. This feature seems to enable the associated *ansa*-chromocene moieties to act as electronic buffer systems by compensating σ donation with extended π^* back donation and partial delocalization of charge into the aromatic π^* system.

6. Conclusions

The synthesis of *ansa*-chromocene(III) halide complexes turned out to be very difficult. The reaction between the corresponding *ansa*-calcocene complexes and chromium(III) chloride or chromium(III) bromide generates green paramagnetic powders that can hardly be purified. The reaction of *ansa*-chromocene carbonyls with organic bromides results in destruction of the metallocene structure. Ring loss takes place, regenerating the corresponding bridging ligand. The crystal structure of the paramagnetic product was determined, revealing the formation of $\text{CrBr}_2(\text{THF})_2$ in these reactions.

New bimetallic and trimetallic 18 electron *ansa*-chromocene complexes have been synthesized applying a new route to access *ansa*-chromocene isocyanide complexes with yields between 50 and 65% of product. The carbonyl ligands at the metal centers of the *ansa*-chromocene carbonyl complexes were substituted by isoelectronic ferrocenylisocyanide derivatives and 1,4,-phenylene diisocyanide. The electronic and physical properties of these new species were elucidated and revealed that the heteronuclear *ansa*-chromocene isocyanide complexes exhibit a remarkable stability against thermolysis and photolysis. Two of the heteronuclear complexes were successfully oxidized to their cationic counterparts. Electrochemical experiments showed that all heteronuclear complexes possess similar redox potentials for the $\text{Cr}^{2+/3+}$ couples. The analytical characterizations, e.g. electrochemistry, UV-VIS-NIR and IR-spectroscopy do not indicate that these species exhibit any class II or class III mixed valence behavior. At least no common features of conventionally described mixed valence complexes can be observed.

However, the heteronuclear molecules behave like large electron reservoirs. The ferrocene units enable these complexes to modulate the electron density at the Cr metal center. This results in a defined constant redox potential of the $\text{Cr}^{2+/3+}$ couple for all of these species. It has yet to be determined if these constant electronic values result from a complementary synergistic effect of σ donation and π^* back donation with

partial delocalization of charge into the aromatic π^* system. For this purpose Density Functional Theory calculations are currently being performed.

7. Future Work

Some follow up work with the polynuclear complexes could be done concerning their cationic counterparts. Single crystals of these ionic species have not yet been obtained. Therefore the cationic species of complexes **4b** and **5** could be employed to obtain single crystals. In contrast to **3** and **4a**, these species possess the tetramethylethane backbone as the transannular bridge. This should increase the chance to obtain X-ray quality single crystals. The corresponding X-ray structures should reveal if the isocyanide bridges of the cationic complexes assume nearly straight C-N-C bond angles as it was observed for other cationic *ansa*-chromocene isocyanide complexes [110]. In this case, advantage could be taken of the different molecule lengths in respect to their neutral counterparts. Possibly these complexes could be employed as molecular engines by reversibly oxidizing and reducing them, as it happens during CV experiments. Repetitive contracting and stretching due to the changing C-N-C bond angles during the redox process could result in similar mechanical properties as they were observed for azabenzene. The *cis*- and *trans*- azabenzene isomers can be reversibly transformed into the corresponding counter species with photolytic experiments. Seitz and Gaub presented this molecule as the first molecular engine at the beginning of this year [116]. Therefore, customized molecular engines could possibly be created, depending on what kind of substituents are associated with the isocyanide ligand. Individual heteronuclear species could be employed as exchangeable electrical molecular engines, operated by a cycling excitation signal over a constant narrow potential range.

8. References

- [1] Pauson, P. L.; Kealy, T. J. *Nature* **1951**, *168*, 1039.
- [2] Miller, S. A.; Tebboth, J. A. ; Tremaine, J. F. *J. Chem. Soc.* **1952**, 632.
- [3] Wilkinson, G.; Rosenblum, M.; Whiting, M. C.; Woodward, R. B. *J. Am. Chem. Soc.* **1952**, *74*, 2125.
- [4] Wilkinson, G. *J. Am. Chem. Soc.* **1952**, *74*, 6148.
- [5] Eiland, P.; Pepinsky, R. *J. Am. Chem. Soc.* **1952**, *74*, 4971.
- [6] Fisher, E. O.; Pfab, W. Z. *Z. Naturforsch.* **1952**, *76*, 377.
- [7] Woodward, R. B.; Rosenblum, M.; Whiting, M. C. *J. Am. Chem. Soc.* **1952**, *74*, 3458.
- [8] Rosenblum, M.; Woodward, R. B. *J. Am. Chem. Soc.* **1958**, *80*, 5443.
- [9] Spessard, G.O.; Miessler, G. L. *Organometallic Chemistry*; Prentice Hall: New Jersey, 1997; Chapter 4, 5.
- [10] Long, N. J. *Metallocenes An introduction to sandwich complexes*; Blackwell Science: Oxford, 1998; Chapter 3.
- [11] Geiger, W. E. *Adv. Organomet. Chem.* **1984**, *1*, 77.
- [12] Togni, A.; Halterman, R. L. *Metallocenes*; WILEY-VCH: Weinheim, 1998; Chapter 4, 5, 6.
- [13] Brintzinger, H. H.; Lohr, L. L.; Tang Wong, K. L. *J. Am. Chem. Soc.* **1975**, *97*, 5143.
- [14] Wilkinson, G.; Cotton, F. A.; Birmingham, J. M. *J. Inorg. Nucl. Chem.* **1956**, *2*, 95.
- [15] Watt, G. W.; Baye, L. J. *J. Inorg. Nucl. Chem.* **1964**, *26*, 2099.
- [16] Karol, F. J.; Karapinka, G. L.; Wu, C.; Dow, A. W.; Johnson, R. N.; Carric, W. L. *J. Polym. Sci., Polym. Chem. Ed.* **1972**, *10*, 2621.

- [17] Schnellbach, M.; Köhler, F. H.; Blümel, J. *J Organomet. Chem.* **1996**, *520*, 227.
- [18] Hogan, J. P. *J. Polym. Sci., Polym. Chem. Ed.* **1970**, *8*, 2637.
- [19] Theopold, K. H. *Eur. J. Inorg. Chem.* **1998**, 15.
- [20] MacAdams, L. A.; Kim, W. K.; Liable-Sands, L. M.; Guzei, I. A. Rheingold, A. L. Theopold, K. H. *Organometallics* **2002**, *21*, 952.
- [21] Döhring, A.; Göhre, J.; Jolly, P. W.; Kryger, B.; Rust, J.; Verhovnik, G. P. *Organometallics*, **2000**, *19*, 388.
- [22] Emrich, R.; Heinemann, O.; Jolly, P. W. Krüger, C Verhovnik, G. P. *Organometallics* **1997**, *16*, 1511.
- [23] Jensen, V. R.; Angermund, K.; Jolly, P. W. *Organometallics* **2000**, *19*, 403.
- [24] Brintzinger, H. H.; Lohr, L. L.; Tang Wong, K. L. *J. Am. Chem. Soc.* **1975**, *97*, 5146.
- [25] Green, J. C. *Chem. Soc. Rev.* **1998**, *27*, 263.
- [26] Green, J. C.; Jardine, C. N. *J. Chem. Soc., Dalton Trans.* **1999**, 3767.
- [27] Green, J. C.; Jardine, C. N. *J. Chem. Soc., Dalton Trans.* **1998**, 1057.
- [28] Chernega, A.; Cook, J.; Green, M. L.; Labella, L.; Simpson, S. J.; Souter, J.; Stephens, A. H. *J. Chem. Soc., Dalton Trans.* **1997**, 3225.
- [29] Grebrik, R.; Grinter, R.; Perutz, R. N. *Chem. Soc. Rev.* **1988**, *17*, 453.
- [30] Schwemlein, H.; Zsolani, L.; Huttner, G.; Brintzinger, H. H. *J. Organomet. Chem.* **1983**, *256*, 285.
- [31] Schwemlein, H.; Brintzinger, H. H. *J. Organomet. Chem.* **1983**, *254*, 69.
- [32] Rieckhoff, M.; Pieper, U.; Stalke, D.; Edelman, F. T. *Angew. Chem, Int. Ed. Engl.* **1993**, *32*, 1079.
- [33] Foo, D. M.; Shapiro, P. J. *Organometallics* **1995**, *14*, 4957.

- [34] Kane, K. M.; Shapiro, P. J.; Vij, A.; Cubbon R. *Organometallics* **1997**, *16*, 4567.
- [35] Stone, K. J.; Little, R. D. *J. Org. Chem.* **1984**, *49*, 1849.
- [36] Sinnema, P. J.; Shapiro, P. J.; Höhn, B.; Bitterwolf, T. E.; Twamley, B. *Organometallics* **2001**, *20*, 2883.
- [37] Matare, G. J.; Foo, D. M.; Kane, K. M.; Zehnder, R.; Wagener, M.; Shapiro, P. J. *Organometallics* **2000**, *19*, 1534.
- [38] Creutz, C.; Taube, H. *J. Am. Chem. Soc.* **1969**, *91*, 3988.
- [39] Atkins, P. W.; Shriver, D. F. *Anorganische Chemie*; Wiley-VCH: Weinheim, 1997; p 594.
- [40] Crutchley, R. J. *Adv. Inorg. Chem.* **1994**, *41*, 273.
- [41] Mueller-Westerhoff, U. T. *Angew. Chem. Int. Ed. Engl.* **1986**, *25*, 702.
- [42] Demadis, K. D.; Hartshorn, C. M.; Meyer, T. J. *Chem. Rev.* **2001**, *101*, 2655.
- [43] Mosher, P. J.; Yap, G. P.; Crutchley, R. J. *Inorg. Chem.* **2001**, *40*, 1189.
- [44] Brunschwig, B. S.; Sutin, N. *Coord. Chem. Rev.* **1999**, *187*, 233.
- [45] Evans, C. E.; Naklicki, M. L.; Rezvani, A. R.; White, C. A.; Kondratiev, V. V.; Crutchley, R. J. *J. Am. Chem. Soc.* **1998**, *120*, 13096.
- [46] Camire, N.; Mueller-Westerhoff, U. T.; Geiger, W. E. *J. Organomet. Chem.* **2001**, *637-639*, 823.
- [47] Creutz, C. *Prog. Inorg. Chem.* **1983**, *30*, 4.
- [48] Mosher, P. J.; Yap, G. P. A.; Crutchley, R. J. *Inorg. Chem.* **2001**, *40*, 1189.
- [49] Chen, Y. J.; Kao, C. H.; Lin, S. J.; Tai, C. C.; Kwan, K. S. *Inorg. Chem.* **2000**, *39*, 189.
- [50] Foucher, D. A.; Honeyman, C. H.; Nelson, J. M.; Tang, B. Z.; Manners, I. *Angew. Chem. Int. Ed. Engl.* **1993**, *32*, 1709.
- [51] Cotton, F. A.; Donahue, J. P.; Lin, C.; Murillo, C. A. *Inorg. Chem.* **2001**, *40*, 1234.

- [52] Neve, F.; Crispini, A.; Serroni, S.; Loiseau, F.; Campagna, S. *Inorg. Chem.* **2001**, *40*, 1093.
- [53] Barlow, S.; O' Hare, D. *Chem. Rev.* **1997**, *97*, 637.
- [54] Mata, J.; Falomir, E.; Llusar, R.; Peris, E. *J. Organomet. Chem.* **2000**, *616*, 80.
- [55] Mata, J.; Uriel, S.; Peris, E.; Llusar, R.; Houbrechts, S.; Persoons, A. *J. Organomet. Chem.* **1998**, *562*, 197.
- [56] Lin, J. T.; Wu, J. J.; Li, Ch. Sh.; Wen, Y. S.; Lin, K. J. *Organometallics* **1996**, *15*, 5028.
- [57] Heck, J.; Dabeck, S. Meyer-Fridrichsen, T.; Wong, H. *Coord. Chem. Rev.* **1999**, *190-192*, 1217.
- [58] Zhu, Y.; Clot, O.; Wolf, M. O.; Yap, G. P. *J. Am. Chem. Soc.* **1998**, *120*, 1812.
- [59] Colbert, M. C.; Lewis, J.; Long, N. J.; Raithby, P. R.; White, A. J.; Williams, D. J. *J. Chem. Soc., Dalton Trans.* **1997**, 99.
- [60] Jones, N. D.; Wolf, M. O. *Organometallics* **1997**, *16*, 1352.
- [61] Liu, S. H.; Chen, Y.; Wan, K. L.; Wen, T. B. Zhou, Z.; Lo, M. F.; Williams, I. D.; Jia, G. *Organometallics*, **2002**, *21*, 4984.
- [62] Scheiring, T.; Fiedler, J.; Kaim, W. *Organometallics* **2001**, *20*, 1437.
- [63] Johnson, R. C.; Hupp, J. T. *J. Am. Chem. Soc.* **2001**, *123*, 2053.
- [64] Glöckle, M.; Kaim, W. *Z. Anorg. Allg. Chem.* **2001**, *627*, 1441.
- [65] Ota, K. I.; Sasaki, H.; Matsui, T.; Hamaguchi, T. Y.; Ito, T.; Kido, H.; Kubiak, C. P. *Inorg. Chem.* **1999**, *38*, 4070.
- [66] Bayly, S.; McCleverty, J.; Ward, M. D.; Gatteschi, D., Totti, F. *Inorg. Chem.* **2000**, *39*, 1288.
- [67] Ung, V. A.; Couchman, S. M.; Jeffery, J. C.; McCleverty, J.; Ward, M. D.; Totti, F.; Gatteschi, D. *Inorg. Chem.* **1999**, *38*, 365.
- [68] McCleverty, J.; Ward, M. D. *Acc. Chem. Res.* **1998**, *31*, 842.

- [69] Henderson, J. I.; Feng, S.; Bein, T.; Kubiak, C. P. *Langmuir* **2000**, *16*, 6183.
- [70] Chen, J.; Calvet, L. C.; Reed, M. A.; Carr, D. W.; Grubisha, D. S.; Bennett, D. W. *Chem. Phys. Lett.* **1999**, *313*, 741.
- [71] Glöckle, M.; Kaim, W.; Klein, A.; Roduner, E.; Hübner, G.; Zalis, S.; Van Slageren, J.; Renz, F.; Güttlich, P. *Inorg. Chem.* **2001**, *40*, 2256.
- [72] Kaim, W.; Bruns, W.; Poppe, J.; Kasack, V. *J. Mol. Struct.* **1993**, *292*, 221.
- [73] Taube, H. *Angew. Chem. Int. Ed. Engl.* **1984**, *23*, 329.
- [74] Ward, M. D. *Chem. Soc. Rev.* **1995**, *34*, 121.
- [75] Bencini, A.; Ciofini, I.; Daul, C. A.; Ferretti, A. *J. Am. Chem. Soc.* **1999**, *121*, 11418.
- [76] Tarraga, A.; Molina, P.; Curiel, D.; Velasco, M. D. *Organometallics* **2001**, *20*, 2145.
- [77] Vollhardt, P. K.; Schore, N. E. *Organische Chemie*; Wiley-VCH: Weinheim, 1998; p 362.
- [78] Atkins, P. W. *Physical Chemistry*, 6th ed.; Oxford University: Oxford, 1998; pp 527-539.
- [79] Günther, H. *NMR Spectroscopy An Introduction*, 2nd ed.; John Wiley & Sons: Chichester, West Sussex, 1995; chapter 1, 2.
- [80] Fox, M. A.; Whitesell, J. K. *Organic chemistry*, 2nd ed.; Jones and Bartlett: Sudbury, Massachusetts, 1997; p 191.
- [81] Skoog, D. A.; Holler, F. J.; Nieman, T. A. *Principles of Instrumental Analysis*, 5th ed.; Thomson Learning: Crawfordsville, MD, 1998; p 119, 654.
- [82] Günzler, H.; Gremlich, H. U. *IR Spectroscopy*; Wiley-VCH: Weinheim, 2002; p 53.
- [83] Sohn, Y. S.; Hendrickson, D. N.; Gray, H. B., *J. Amer. Chem. Soc.*, **1971**, *93*, 3603.
- [84] Wedler, G. *Lehrbuch der Physikalischen Chemie*, 3rd ed.; Wiley-VCH: Weinheim, 1987; p 532.

- [85] Kissinger, P. T.; Heineman, W. R. *J. Chem. Educ.*, **1983**, *60*, 702.
- [86] Bovey, F. A. *Nuclear Magnetic Resonance Spectroscopy*, 2nd ed.; Academic: San Diego, California, 1988; p 131.
- [87] Hollemann, A. F; Wiberg, E. *Lehrbuch der Anorganischen Chemie*; Walter de Gruyter Verlag: Berlin, 1985; p 986.
- [88] Magnetic Susceptibility Balance Instruction manual; Johnson Matthey: Wayne, PA, 1990; pp 13-18
- [89] Scherwood Scientific Ltd web address:
<http://www.gemini.co.uk/biopages/co/sherwood/msb/shmagway.html>
- [90] Sur, S. K. *J. Magn. Reson.* **1989**, *82*, 169.
- [91] Bildstein, B.; Malaun, M.; Kopacka, H.; Wurst, K.; Mitterboeck, M.; Ongania, K. H.; Opromolla, G.; Zanello, P. *Organometallics* **1999**, *18*, 4325.
- [92] Knox, G. R.; Pauson, P. L.; Willison, D. *Organometallics* **1990**, *9*, 301.
- [93] Sonoda, A.; Moritani, I. *J. Organometal. Chem.* **1971**, *26*, 133.
- [94] Leusen, D.; Hessen, B. *Organometallics* **2001**, *20*, 224.
- [95] Doty, F. D.; Entzminger, G; Yang, Y. A. *Conc. in Magn. Reson.* **1998**, *10*, 133.
- [96] CRC Handbook of Chemistry and Physics, 73rd ed.; Boca Raton, Fla.: The Chemical Rubber Co., 1992-1993; pp 9.62-9.125
- [97] Holloway, J. D.; Bowden, W. L.; Geiger, W. E. *J. Am. Chem. Soc.* **1977**, *99*, 7089
- [98] Van Raaij, E. U.; Mönkeberg, S.; Kiesele, H.; Brintzinger, H. H. *J. Organomet. Chem.* **1988**, *356*, 307.
- [99] Cotton, F. A.; Wilkinson, G.; Murillo, C. A.; Bochmann, M. *Advanced Inorg. Chem.*, 6th ed.; John Wiley & Sons: New York, NY, 1999; p 246.
- [100] Edelman, F. T.; Rieckhoff, M.; Haiduc, I.; Silaghi-Dumitrescu, I. *J. Organomet. Chem.* **1993**, *447*, 203.

- [101] Twamley, B.; Zehnder, R.; Shapiro, P. J. *Acta. Cryst.* **2001**, *E57*, 80.
- [102] Elschenbroich, C.; Salzer, A. *Organometallics A concise introduction*, 2nd ed.; Wiley-VCH: Weinheim, 1991; pp 220-222.
- [103] Powell, P. *Principles of organometallic chemistry*, 2nd ed.; Chapman and Hall: London, 1988; pp 167-173.
- [104] Bochmann, M. *Organometallics 1: Complexes with Metal Carbon σ Bonds*, Oxford University: Oxford, 1994; pp 15-18.
- [105] Basolo, F. *Inorg. Chim. Acta.* **1981**, *50*, 65.
- [106] Bartolomäs, T.; Lentz, D.; Neubert, I; Röttger, M. *Z. Anorg. Allg. Chem.* **2002**, *628*, 863.
- [107] Connelly, N. G.; Geiger, W. E. *Chem. Rev.* **1996**, *96*, 877.
- [108] Carney, M. J.; Lesniak, J. S.; Likar, M. D. Pladziewicz, J. R. *J. Am. Chem. Soc.* **1984**, *106*, 2565.
- [109] Santi, S.; Ceccon, A.; Crociani, L.; Gambaro, A.; Ganis, P.; Tiso, M.; Venzo, A.; Bacchi, A. *Organometallics* **2002**, *21*, 565.
- [110] Foo, D. M. Ph.D. Dissertation, University of Idaho, 2002.
- [111] Dewar, M. J. S.; *Bull. Soc. Chim., Fr.*, **1951**, *18*, C71.
- [112] Chatt, J.; Duncanson, L.A. *J. Chem. Soc.*, **1953**, 2939.
- [113] Barybin, M. V.; Holovics, T. C.; Deplazes, S. F.; Lushington, G. H.; Powell, D. R.; Toriyama, M. *J. Am. Chem. Soc.* **2002**, *46*, 13668.
- [114] Singleton, E.; Oosthuizen, H. E. *Adv. Organomet.Chem.* **1983**, *22*, 209.
- [115] Treichel, P. M. *Adv. Organomet. Chem.* **1973**, *11*, 21.
- [116] Hugel, T.; Holland, N. B.; Cattani, A.; Moroder, L.; Seitz, M.; Gaub, H. E. *Science* **2002**, *296*, 1103.

9. Appendix

9.1. Magnetic Susceptibility

9.1.1. Determination of the Effective Magnetic Moment using the Evans NMR Method

Table 9-1: Used Abbreviations:

f:	Frequency of NMR-device
d_{solvent} :	Density of solvent
χ_{solvent} :	Diamagnetic susceptibility of solvent
χ_{diam} :	Diamagnetic contribution of ligands of the complex
T:	Temperature
m_{sample} :	Mass of sample
m_{solvent} :	Mass of solvent
V_{solvent} :	Volume of solvent
n:	Mass of sample in one ml solvent
Δf :	Difference of peaks in spectrum
χ_g :	Magnetic susceptibility
χ_M :	Molar magnetic susceptibility
$\chi_{M\text{corr.}}$:	Corrected molar magnetic susceptibility
μ_{eff} :	Effective magnetic moment
M:	Molar weight

Equations:

$$\chi_g = \frac{3 \times \Delta f}{4 \times \pi \times f \times n} + \chi_{\text{solvent}} ; \quad \chi_M = \chi_g \times M$$

$$\chi_{M\text{corr.}} = \chi_M + \chi_{\text{diam.}} ; \quad \mu_{\text{eff}} = 2.84 \times \sqrt{\chi_{M\text{corr.}} \times T}$$

Table 9-2: Experimental data for complexes $[3]^+ PF_6^-$ and $[4]^{2+}(PF_6^-)_2$:

$[3]^+ PF_6^-$	Experiment 1	f:	300 MHz
m_{sample} :	8.0 mg	solvent:	DMSO
m_{solvent} :	732 mg	d_{solvent} :	1.10 g/ml
V_{solvent} :	0.666 ml	χ_{solvent} :	$-0.660 \times 10^{-6} \text{ cgs/g}$
n:	0.012 g/ml	T:	293.13 K
Δf :	50.623 Hz	M:	716.12 g/mol
χ_M :	$1.932 \times 10^{-3} \text{ cgs/mol}$	$\chi_{\text{diam.}}$:	$-0.349 \times 10^{-3} \text{ cgs/mol}$
$\chi_{M\text{corr}}$:	$1.583 \times 10^{-3} \text{ cgs/mol}$	μ_{eff} :	1.93 BM
$[3]^+ PF_6^-$	Experiment 2	f:	300 MHz
m_{sample} :	8 mg	solvent:	DMSO
m_{solvent} :	601 mg	d_{solvent} :	1.10 g/ml
V_{solvent} :	0.546 ml	χ_{solvent} :	$-0.660 \times 10^{-6} \text{ cgs/g}$
n:	0.015 g/ml	T:	293.13 K
Δf :	52.401 Hz	M:	M= 716.12 g/mol
χ_M :	$1.567 \times 10^{-3} \text{ cgs/mol}$	$\chi_{\text{diam.}}$:	$-0.349 \times 10^{-3} \text{ cgs/mol}$
$\chi_{M\text{corr}}$:	$1.218 \times 10^{-3} \text{ cgs/mol}$	μ_{eff} :	1.69 BM
$[4]^{2+}(PF_6^-)_2$	Experiment 1	f:	300 MHz
m_{sample} :	9 mg	solvent:	DMSO
m_{solvent} :	616 mg	d_{solvent} :	1.10 g/ml
V_{solvent} :	0.560 ml	χ_{solvent} :	$-0.660 \times 10^{-6} \text{ cgs/g}$
n:	0.016 g/ml	T:	293.13 K
Δf :	70.339 Hz	M:	1246.82 g/mol
χ_M :	$3.520 \times 10^{-3} \text{ cgs/mol}$	$\chi_{\text{diam.}}$:	$-0.573 \times 10^{-3} \text{ cgs/mol}$
$\chi_{M\text{corr}}$:	$2.947 \times 10^{-3} \text{ cgs/mol}$	μ_{eff} :	2.63 BM

[4]²⁺(PF₆⁻)₂	Experiment 2	f:	300 MHz
m _{sample} :	8 mg	solvent:	DMSO
m _{solvent} :	631 mg	d _{solvent} :	1.10 g/ml
V _{solvent} :	0.574 ml	χ _{solvent} :	-0.66 x 10 ⁻⁶ cgs/g
n:	0.014 g/ml	T:	293.13 K
Δf:	64.814 Hz	M:	1246.82 g/mol
χ _M :	3.788 x 10 ⁻³ cgs/mol	χ _{diam} :	-0.573 x 10 ⁻³ cgs/mol
χ _{Mcorr.} :	3.215 x 10 ⁻³ cgs/mol	μ _{eff} :	2.76 BM

9.1.2. Determination of the Effective Magnetic Moment using the Evans Matthey Johnson Magnetic Susceptibility Balance

Table 9-3: Used Abbreviations:

R ₀ :	Value for the empty sample tube
R _{full} :	Value for the filled sample tube
R:	Net value for R
l:	Length in cm the tube is filled with sample
T:	Temperature
m _{sample} :	Mass of sample
c:	Specific coefficient of the magnetic balance
χ _g :	Magnetic susceptibility
χ _M :	Molar magnetic susceptibility
χ _{diam} :	Diamagnetic contribution of ligands of the complex
χ _{Mcorr.} :	Corrected molar magnetic susceptibility
μ _{eff} :	Effective magnetic moment
MW	Molar weight

Equations:

$$R = R_{full} - R_0; \quad \chi_g = \frac{c \times l \times R}{m \times 10^9}; \quad \chi_M = \chi_g \times M$$

$$\chi_{Mcorr.} = \chi_M + \chi_{diam.}; \quad \mu_{eff} = 2.84 \times \sqrt{\chi_{Mcorr.} \times T}$$

Table 9-4: Experimental data for complexes **[3]⁺ PF₆⁻** and **[4]²⁺(PF₆⁻)₂**:

[3]⁺ PF₆⁻	Experiment 1	R _{full} :	67
R ₀ :	-33	c:	1.071
R:	100	T:	294.4 K
l:	2.15 cm	M:	716.12 g/mol
m _{sample} :	0.111 g	χ _g :	2.075 × 10 ⁻⁶ cg/g
χ _M :	1.486 × 10 ⁻³ cg/mol	χ _{diam.} :	-0.349 × 10 ⁻³ cg/mol
χ _{Mcorr.} :	1.137 × 10 ⁻³ cg/mol	μ _{eff} :	1.64 BM
[3]⁺ PF₆⁻	Experiment 2	R _{full} :	70
R ₀ :	-33	c:	1.071
R:	103	T:	293.9 K
l:	1.45 cm	M:	716.12 g/mol
m _{sample} :	0.069 g	χ _g :	2.318 × 10 ⁻⁶ cg/g
χ _M :	1.660 × 10 ⁻³ cg/mol	χ _{diam.} :	-0.349 × 10 ⁻³ cg/mol
χ _{Mcorr.} :	1.311 × 10 ⁻³ cg/mol	μ _{eff} :	1.76 BM
[4]²⁺(PF₆⁻)₂	Experiment 1	R _{full} :	50
R ₀ :	-30	c:	1.071
R:	80	T:	296.0 K
l:	2.8 cm	M:	1246.82 g/mol
m _{sample} :	0.094 g	χ _g :	2.552 × 10 ⁻⁶ cg/g
χ _M :	3.182 × 10 ⁻³ cg/mol	χ _{diam.} :	-0.573 × 10 ⁻³ cg/mol
χ _{Mcorr.} :	2.609 × 10 ⁻³ cg/mol	μ _{eff} :	2.50 BM

[4]²⁺(PF₆⁻)₂	Experiment 2	R _{full} :	50
R ₀ :	-30	c:	1.071
R:	80	T:	296.0 K
l:	2.7 cm	M:	1246.82 g/mol
m _{sample} :	0.100 g	χ _g :	2.313 x 10 ⁻⁶ cgs/g
χ _M :	2.884 x 10 ⁻³ cgs/mol	χ _{diam.} :	-0.573 x 10 ⁻³ cgs/mol
χ _{Mcorr.} :	2.311 x 10 ⁻³ cgs/mol	μ _{eff} :	2.35 BM

Average value for **[3]⁺ PF₆⁻**: 1.76 BM

Average value for **[4]²⁺(PF₆⁻)₂**: 2.56 BM (1.81 BM/Cr atom)

Table 9-5: Data of variable temperature experiment for **[4]²⁺(PF₆⁻)₂** in THF-d₈:

T [°C]	T [K]	Δf [Hz]	χ _g [x 10 ⁻⁶ cgs/g]	χ _M [x 10 ⁻³ cgs/mol]	χ _{Mcorr.} [x 10 ⁻³ cgs/mol]	1/χ _{Mcorr.} [mol/cgs]	μ _{eff} [BM]
-105.0	170.13	329	6.544	5.635	5.062	197.6	2.64
-93.5	181.63	317	6.284	5.411	4.838	206.7	2.66
-84.0	191.13	305	6.023	5.186	4.613	216.8	2.67
-74.0	201.13	293	5.762	4.962	4.389	227.8	2.67
-64.0	211.13	277	5.415	4.663	4.090	244.5	2.64
-53.0	220.13	265	5.154	4.438	3.865	258.7	2.62
-40.5	232.63	251	4.861	4.186	3.613	276.8	2.60
-28.5	244.63	242	4.655	4.008	3.435	289.6	2.60
-16.0	257.13	231	4.416	3.803	3.230	309.6	2.59
-5.0	268.13	221	4.199	3.616	3.043	328.6	2.57
+7.0	280.13	212	4.004	3.448	2.875	347.8	2.55
+25.0	298.13	200	3.743	3.223	2.650	377.3	2.52

9.2. X-Ray Single Crystal Structure Data

Table 9-6: Crystal data and structure refinement for **3**:

Formula weight	571.44
Temperature	203(2) K
Wavelength	0.71073 Å
Crystal system	Monoclinic
Space group	P2 ₁ /c
Unit cell dimensions	a = 7.641(3) Å α = 90°.
	b = 10.176(7) Å β = 95.51(5)°.
	c = 34.17(2) Å γ = 90°.
Volume	2644(3) Å ³
Z	4
Density (calculated)	1.435 Mg/m ³
Absorption coefficient	0.985 mm ⁻¹
F(000)	1184
Crystal size	0.29 x 0.21 x 0.05 mm ³
Crystal color and habit	orange needle
Diffractometer	Siemens SMART 1K
Theta range for data collection	2.09 to 27.49°.
Index ranges	-9 ≤ h ≤ 9, -8 ≤ k ≤ 13, -35 ≤ l ≤ 44
Reflections collected	23445
Independent reflections	6072 [R(int) = 0.0655]
Completeness to theta = 27.49°	100.0 %
Absorption correction	†Empirical
Max. and min. transmission	0.9524 and 0.7633
Solution method	XS, Bruker SHELXTL v. 5.10
Refinement method	Full-matrix least-squares on F ²
Data / restraints / parameters	6072 / 0 / 349
Goodness-of-fit on F ²	1.073
Final R indices [I > 2σ(I)]	R1 = 0.0609, wR2 = 0.1390
R indices (all data)	R1 = 0.1050, wR2 = 0.1535
Largest diff. peak and hole	0.789 and -0.494 e.Å ⁻³

†**SADABS**: an empirical absorption correction program, Sheldrick, G.M., Bruker AXS Inc., Madison, WI, 1999.

Refinement Note: The hydrogen atoms on the bridgehead carbons(C6 and C7) were located on the difference map and refined.

Table 9-7: Atomic coordinates ($\times 10^4$) and equivalent isotropic displacement parameters ($\text{\AA}^2 \times 10^3$) for **3** U(eq) is defined as one third of the trace of the orthogonalized U_{ij} tensor:

	x	y	z	U(eq)
Cr(1)	6480(1)	-141(1)	2987(1)	27(1)
Fe(1)	8285(1)	-97(1)	1437(1)	32(1)
N(1)	5773(4)	-156(3)	2085(1)	33(1)
C(1)	4002(5)	-41(4)	3243(1)	34(1)
C(2)	3821(5)	646(4)	2889(1)	35(1)
C(3)	5038(5)	1716(4)	2907(1)	32(1)
C(4)	5992(5)	1677(4)	3282(1)	33(1)
C(5)	5338(5)	595(4)	3494(1)	32(1)
C(6)	6014(5)	85(4)	3896(1)	35(1)
C(7)	7966(5)	-267(4)	3882(1)	33(1)
C(8)	8182(5)	-839(4)	3476(1)	32(1)
C(9)	9231(5)	-236(4)	3206(1)	35(1)
C(10)	9011(5)	-955(4)	2860(1)	41(1)
C(11)	7830(5)	-2002(4)	2905(1)	41(1)
C(12)	7295(5)	-1937(4)	3285(1)	35(1)
C(13)	8711(5)	-1153(4)	4216(1)	32(1)
C(14)	10092(6)	-728(5)	4470(1)	44(1)
C(15)	10849(6)	-1542(5)	4768(1)	54(1)
C(16)	10239(6)	-2790(5)	4812(1)	46(1)
C(17)	8821(6)	-3229(4)	4562(1)	46(1)
C(18)	8071(6)	-2411(4)	4270(1)	40(1)
C(19)	5617(5)	1037(4)	4221(1)	32(1)
C(20)	6315(5)	2297(4)	4245(1)	39(1)
C(21)	5812(6)	3180(4)	4519(1)	44(1)

C(22)	4619(6)	2798(5)	4781(1)	49(1)
C(23)	3952(6)	1541(5)	4765(1)	51(1)
C(24)	4463(6)	665(4)	4486(1)	41(1)
C(25)	6133(5)	-108(4)	2436(1)	30(1)
C(26)	6349(5)	527(4)	1761(1)	29(1)
C(27)	5684(5)	319(4)	1367(1)	35(1)
C(28)	6617(6)	1164(5)	1128(1)	46(1)
C(29)	7844(6)	1874(4)	1375(1)	45(1)
C(30)	7722(6)	1492(4)	1769(1)	40(1)
C(31)	9244(6)	-1775(4)	1690(2)	53(1)
C(32)	8564(6)	-2028(5)	1304(2)	56(1)
C(33)	9464(7)	-1237(5)	1052(2)	57(1)
C(34)	10727(6)	-498(5)	1283(2)	55(1)
C(35)	10613(6)	-836(5)	1679(2)	52(1)

Table 9-8: Bond lengths [\AA] and angles [$^\circ$] for **3** :

Cr(1)-C(25)	1.879(4)	Fe(1)-C(28)	2.032(4)
Cr(1)-C(8)	2.136(4)	Fe(1)-C(32)	2.033(5)
Cr(1)-C(5)	2.147(4)	Fe(1)-C(29)	2.042(4)
Cr(1)-C(12)	2.154(4)	Fe(1)-C(30)	2.043(4)
Cr(1)-C(4)	2.155(4)	N(1)-C(25)	1.205(5)
Cr(1)-C(1)	2.162(4)	N(1)-C(26)	1.411(5)
Cr(1)-C(9)	2.165(4)	C(1)-C(2)	1.393(5)
Cr(1)-C(2)	2.180(4)	C(1)-C(5)	1.424(5)
Cr(1)-C(10)	2.186(4)	C(1)-H(1)	0.9400
Cr(1)-C(11)	2.188(4)	C(2)-C(3)	1.430(5)
Cr(1)-C(3)	2.192(4)	C(2)-H(2)	0.9400
Fe(1)-C(31)	2.018(5)	C(3)-C(4)	1.414(5)
Fe(1)-C(27)	2.024(4)	C(3)-H(3)	0.9400
Fe(1)-C(33)	2.028(4)	C(4)-C(5)	1.434(5)
Fe(1)-C(34)	2.029(4)	C(4)-H(4)	0.9400
Fe(1)-C(35)	2.032(4)	C(5)-C(6)	1.513(5)
Fe(1)-C(26)	2.033(4)	C(6)-C(19)	1.525(5)

C(6)-C(7)	1.539(5)	C(26)-C(27)	1.411(5)
C(6)-H(6)	1.13(4)	C(26)-C(30)	1.436(6)
C(7)-C(13)	1.521(5)	C(27)-C(28)	1.422(6)
C(7)-C(8)	1.529(5)	C(27)-H(27)	0.9400
C(7)-H(7)	1.05(4)	C(28)-C(29)	1.399(6)
C(8)-C(9)	1.417(6)	C(28)-H(28)	0.9400
C(8)-C(12)	1.430(5)	C(29)-C(30)	1.412(6)
C(9)-C(10)	1.387(5)	C(29)-H(29)	0.9400
C(9)-H(9)	0.9400	C(30)-H(30)	0.9400
C(10)-C(11)	1.415(6)	C(31)-C(32)	1.393(7)
C(10)-H(10)	0.9400	C(31)-C(35)	1.420(7)
C(11)-C(12)	1.400(6)	C(31)-H(31)	0.9400
C(11)-H(11)	0.9400	C(32)-C(33)	1.404(7)
C(12)-H(12)	0.9400	C(32)-H(32)	0.9400
C(13)-C(14)	1.372(6)	C(33)-C(34)	1.403(7)
C(13)-C(18)	1.389(6)	C(33)-H(33)	0.9400
C(14)-C(15)	1.393(6)	C(34)-C(35)	1.409(7)
C(14)-H(14)	0.9400	C(34)-H(34)	0.9400
C(15)-C(16)	1.366(7)	C(35)-H(35)	0.9400
C(15)-H(15)	0.9400		
C(16)-C(17)	1.387(6)	C(25)-Cr(1)-C(8)	143.72(16)
C(16)-H(16)	0.9400	C(25)-Cr(1)-C(5)	140.69(16)
C(17)-C(18)	1.382(6)	C(8)-Cr(1)-C(5)	75.57(15)
C(17)-H(17)	0.9400	C(25)-Cr(1)-C(12)	119.73(16)
C(18)-H(18)	0.9400	C(8)-Cr(1)-C(12)	38.96(15)
C(19)-C(24)	1.378(5)	C(5)-Cr(1)-C(12)	92.10(15)
C(19)-C(20)	1.388(6)	C(25)-Cr(1)-C(4)	116.04(15)
C(20)-C(21)	1.378(6)	C(8)-Cr(1)-C(4)	92.31(15)
C(20)-H(20)	0.9400	C(5)-Cr(1)-C(4)	38.93(14)
C(21)-C(22)	1.393(6)	C(12)-Cr(1)-C(4)	124.23(15)
C(21)-H(21)	0.9400	C(25)-Cr(1)-C(1)	111.11(16)
C(22)-C(23)	1.377(7)	C(8)-Cr(1)-C(1)	101.05(15)
C(22)-H(22)	0.9400	C(5)-Cr(1)-C(1)	38.60(15)
C(23)-C(24)	1.387(6)	C(12)-Cr(1)-C(1)	94.23(16)
C(23)-H(23)	0.9400	C(4)-Cr(1)-C(1)	64.77(16)
C(24)-H(24)	0.9400	C(25)-Cr(1)-C(9)	112.68(16)

C(8)-Cr(1)-C(9)	38.46(15)	C(2)-Cr(1)-C(3)	38.17(14)
C(5)-Cr(1)-C(9)	101.17(15)	C(10)-Cr(1)-C(3)	138.17(16)
C(12)-Cr(1)-C(9)	64.66(15)	C(11)-Cr(1)-C(3)	165.45(15)
C(4)-Cr(1)-C(9)	94.74(15)	C(31)-Fe(1)-C(27)	122.69(19)
C(1)-Cr(1)-C(9)	136.20(16)	C(31)-Fe(1)-C(33)	68.1(2)
C(25)-Cr(1)-C(2)	78.40(16)	C(27)-Fe(1)-C(33)	122.31(19)
C(8)-Cr(1)-C(2)	137.03(15)	C(31)-Fe(1)-C(34)	68.7(2)
C(5)-Cr(1)-C(2)	63.34(15)	C(27)-Fe(1)-C(34)	158.1(2)
C(12)-Cr(1)-C(2)	127.42(16)	C(33)-Fe(1)-C(34)	40.5(2)
C(4)-Cr(1)-C(2)	63.67(15)	C(31)-Fe(1)-C(35)	41.04(19)
C(1)-Cr(1)-C(2)	37.42(14)	C(27)-Fe(1)-C(35)	159.58(19)
C(9)-Cr(1)-C(2)	158.38(16)	C(33)-Fe(1)-C(35)	68.1(2)
C(25)-Cr(1)-C(10)	81.31(16)	C(34)-Fe(1)-C(35)	40.60(19)
C(8)-Cr(1)-C(10)	62.96(16)	C(31)-Fe(1)-C(26)	106.56(17)
C(5)-Cr(1)-C(10)	136.78(16)	C(27)-Fe(1)-C(26)	40.69(15)
C(12)-Cr(1)-C(10)	63.37(16)	C(33)-Fe(1)-C(26)	157.4(2)
C(4)-Cr(1)-C(10)	127.87(16)	C(34)-Fe(1)-C(26)	160.1(2)
C(1)-Cr(1)-C(10)	157.55(16)	C(35)-Fe(1)-C(26)	123.26(19)
C(9)-Cr(1)-C(10)	37.18(15)	C(31)-Fe(1)-C(28)	160.1(2)
C(2)-Cr(1)-C(10)	159.69(15)	C(27)-Fe(1)-C(28)	41.05(17)
C(25)-Cr(1)-C(11)	84.81(16)	C(33)-Fe(1)-C(28)	108.7(2)
C(8)-Cr(1)-C(11)	63.45(15)	C(34)-Fe(1)-C(28)	122.57(19)
C(5)-Cr(1)-C(11)	129.71(16)	C(35)-Fe(1)-C(28)	157.8(2)
C(12)-Cr(1)-C(11)	37.61(15)	C(26)-Fe(1)-C(28)	68.43(16)
C(4)-Cr(1)-C(11)	155.18(15)	C(31)-Fe(1)-C(32)	40.2(2)
C(1)-Cr(1)-C(11)	122.33(16)	C(27)-Fe(1)-C(32)	107.36(19)
C(9)-Cr(1)-C(11)	63.33(15)	C(33)-Fe(1)-C(32)	40.5(2)
C(2)-Cr(1)-C(11)	137.95(16)	C(34)-Fe(1)-C(32)	68.2(2)
C(10)-Cr(1)-C(11)	37.75(16)	C(35)-Fe(1)-C(32)	68.1(2)
C(25)-Cr(1)-C(3)	80.64(15)	C(26)-Fe(1)-C(32)	121.44(18)
C(8)-Cr(1)-C(3)	130.25(14)	C(28)-Fe(1)-C(2)	124.6(2)
C(5)-Cr(1)-C(3)	64.04(14)	C(31)-Fe(1)-C(29)	157.7(2)
C(12)-Cr(1)-C(3)	155.50(15)	C(27)-Fe(1)-C(29)	68.39(18)
C(4)-Cr(1)-C(3)	37.94(14)	C(33)-Fe(1)-C(29)	124.9(2)
C(1)-Cr(1)-C(3)	63.98(15)	C(34)-Fe(1)-C(29)	108.46(19)
C(9)-Cr(1)-C(3)	122.79(15)	C(35)-Fe(1)-C(29)	122.4(2)

C(26)-Fe(1)-C(29)	68.22(16)	Cr(1)-C(4)-H(4)	122.9
C(28)-Fe(1)-C(29)	40.18(18)	C(1)-C(5)-C(4)	108.0(3)
C(32)-Fe(1)-C(29)	161.0(2)	C(1)-C(5)-C(6)	123.6(4)
C(31)-Fe(1)-C(8)	121.4(2)	C(4)-C(5)-C(6)	128.1(4)
C(27)-Fe(1)-C(30)	69.13(17)	C(1)-C(5)-Cr(1)	71.3(2)
C(33)-Fe(1)-C(30)	160.4(2)	C(4)-C(5)-Cr(1)	70.9(2)
C(34)-Fe(1)-C(30)	123.5(2)	C(6)-C(5)-Cr(1)	118.8(3)
C(35)-Fe(1)-C(30)	106.87(19)	C(5)-C(6)-C(19)	111.6(3)
C(26)-Fe(1)-C(30)	41.25(16)	C(5)-C(6)-C(7)	107.4(3)
C(28)-Fe(1)-C(30)	68.45(19)	C(19)-C(6)-C(7)	115.6(3)
C(32)-Fe(1)-C(30)	157.1(2)	C(5)-C(6)-H(6)	106(2)
C(29)-Fe(1)-C(30)	40.46(17)	C(19)-C(6)-H(6)	108.6(19)
C(25)-N(1)-C(8)	134.4(4)	C(7)-C(6)-H(6)	107(2)
C(2)-C(1)-C(5)	107.5(4)	C(13)-C(7)-C(8)	113.0(3)
C(2)-C(1)-Cr(1)	72.0(2)	C(13)-C(7)-C(6)	114.1(3)
C(5)-C(1)-Cr(1)	70.1(2)	C(8)-C(7)-C(6)	107.9(3)
C(2)-C(1)-H(1)	126.3	C(13)-C(7)-H(7)	107(2)
C(5)-C(1)-H(1)	126.3	C(8)-C(7)-H(7)	108(2)
Cr(1)-C(1)-H(1)	123.3	C(6)-C(7)-H(7)	107(2)
C(1)-C(2)-C(3)	109.6(4)	C(9)-C(8)-C(12)	108.4(3)
C(1)-C(2)-Cr(1)	70.6(2)	C(9)-C(8)-C(7)	122.9(4)
C(3)-C(2)-Cr(1)	71.4(2)	C(12)-C(8)-C(7)	128.5(4)
C(1)-C(2)-H(2)	125.2	C(9)-C(8)-Cr(1)	71.9(2)
C(3)-C(2)-H(2)	125.2	C(12)-C(8)-Cr(1)	71.2(2)
Cr(1)-C(2)-H(2)	124.4	C(7)-C(8)-Cr(1)	118.2(3)
C(4)-C(3)-C(2)	107.1(3)	C(10)-C(9)-C(8)	107.2(4)
C(4)-C(3)-Cr(1)	69.6(2)	C(10)-C(9)-Cr(1)	72.2(2)
C(2)-C(3)-Cr(1)	70.5(2)	C(8)-C(9)-Cr(1)	69.6(2)
C(4)-C(3)-H(3)	126.5	C(10)-C(9)-H(9)	126.4
C(2)-C(3)-H(3)	126.5	C(8)-C(9)-H(9)	126.4
Cr(1)-C(3)-H(3)	125.0	Cr(1)-C(9)-H(9)	123.4
C(3)-C(4)-C(5)	107.8(3)	C(9)-C(10)-C(11)	109.3(4)
C(3)-C(4)-Cr(1)	72.4(2)	C(9)-C(10)-Cr(1)	70.6(2)
C(5)-C(4)-Cr(1)	70.2(2)	C(11)-C(10)-Cr(1)	71.2(2)
C(3)-C(4)-H(4)	126.1	C(9)-C(10)-H(10)	125.4
C(5)-C(4)-H(4)	126.1	C(11)-C(10)-H(10)	125.4

Cr(1)-C(10)-H(10)	124.5	C(19)-C(20)-H(20)	119.6
C(12)-C(11)-C(10)	108.2(4)	C(20)-C(21)-C(22)	119.8(4)
C(12)-C(11)-Cr(1)	69.9(2)	C(20)-C(21)-H(21)	120.1
C(10)-C(11)-Cr(1)	71.1(2)	C(22)-C(21)-H(21)	120.1
C(12)-C(11)-H(11)	125.9	C(23)-C(22)-C(21)	119.7(4)
C(10)-C(11)-H(11)	125.9	C(23)-C(22)-H(22)	120.1
Cr(1)-C(11)-H(11)	124.7	C(21)-C(22)-H(22)	120.1
C(11)-C(12)-C(8)	106.9(4)	C(22)-C(23)-C(24)	119.9(4)
C(11)-C(12)-Cr(1)	72.5(2)	C(22)-C(23)-H(23)	120.1
C(8)-C(12)-Cr(1)	69.8(2)	C(24)-C(23)-H(23)	120.1
C(11)-C(12)-H(12)	126.6	C(19)-C(24)-C(23)	121.0(4)
C(8)-C(12)-H(12)	126.6	C(19)-C(24)-H(24)	119.5
Cr(1)-C(12)-H(12)	122.8	C(23)-C(24)-H(24)	119.5
C(14)-C(13)-C(18)	117.8(4)	N(1)-C(25)-Cr(1)	173.9(3)
C(14)-C(13)-C(7)	119.9(4)	N(1)-C(26)-C(27)	124.3(4)
C(18)-C(13)-C(7)	122.3(4)	N(1)-C(26)-C(30)	127.3(4)
C(13)-C(14)-C(15)	121.0(4)	C(27)-C(26)-C(30)	108.3(3)
C(13)-C(14)-H(14)	119.5	N(1)-C(26)-Fe(1)	124.8(3)
C(15)-C(14)-H(14)	119.5	C(27)-C(26)-Fe(1)	69.3(2)
C(16)-C(15)-C(14)	120.7(4)	C(30)-C(26)-Fe(1)	69.8(2)
C(16)-C(15)-H(15)	119.7	C(26)-C(27)-C(28)	107.6(4)
C(14)-C(15)-H(15)	119.7	C(26)-C(27)-Fe(1)	70.0(2)
C(15)-C(16)-C(17)	119.2(4)	C(28)-C(27)-Fe(1)	69.8(2)
C(15)-C(16)-H(16)	120.4	C(26)-C(27)-H(27)	126.2
C(17)-C(16)-H(16)	120.4	C(28)-C(27)-H(27)	126.2
C(18)-C(17)-C(16)	119.7(4)	Fe(1)-C(27)-H(27)	125.6
C(18)-C(17)-H(17)	120.1	C(29)-C(28)-C(27)	108.2(4)
C(16)-C(17)-H(17)	120.1	C(29)-C(28)-Fe(1)	70.3(2)
C(17)-C(18)-C(13)	121.6(4)	C(27)-C(28)-Fe(1)	69.2(2)
C(17)-C(18)-H(18)	119.2	C(29)-C(28)-H(28)	125.9
C(13)-C(18)-H(18)	119.2	C(27)-C(28)-H(28)	125.9
C(24)-C(19)-C(20)	118.8(4)	Fe(1)-C(28)-H(28)	126.2
C(24)-C(19)-C(6)	119.3(4)	C(28)-C(29)-C(30)	109.2(4)
C(20)-C(19)-C(6)	121.9(3)	C(28)-C(29)-Fe(1)	69.5(3)
C(21)-C(20)-C(19)	120.8(4)	C(30)-C(29)-Fe(1)	69.8(2)
C(21)-C(20)-H(20)	119.6	C(28)-C(29)-H(29)	125.4

C(30)-C(29)-H(29)	125.4	Fe(1)-C(32)-H(32)	126.8
Fe(1)-C(29)-H(29)	126.8	C(34)-C(33)-C(32)	108.4(5)
C(29)-C(30)-C(26)	106.7(4)	C(34)-C(33)-Fe(1)	69.8(3)
C(29)-C(30)-Fe(1)	69.7(2)	C(32)-C(33)-Fe(1)	69.9(3)
C(26)-C(30)-Fe(1)	69.0(2)	C(34)-C(33)-H(33)	125.8
C(29)-C(30)-H(30)	126.7	C(32)-C(33)-H(33)	125.8
C(26)-C(30)-H(30)	126.7	Fe(1)-C(33)-H(33)	126.0
Fe(1)-C(30)-H(30)	126.2	C(33)-C(34)-C(35)	107.8(5)
C(32)-C(31)-C(35)	108.0(4)	C(33)-C(34)-Fe(1)	69.7(3)
C(32)-C(31)-Fe(1)	70.4(3)	C(35)-C(34)-Fe(1)	69.8(3)
C(35)-C(31)-Fe(1)	70.0(3)	C(33)-C(34)-H(34)	126.1
C(32)-C(31)-H(31)	126.0	C(35)-C(34)-H(34)	126.1
C(35)-C(31)-H(31)	126.0	Fe(1)-C(34)-H(34)	125.9
Fe(1)-C(31)-H(31)	125.2	C(34)-C(35)-C(31)	107.6(4)
C(31)-C(32)-C(33)	108.2(4)	C(34)-C(35)-Fe(1)	69.6(3)
C(31)-C(32)-Fe(1)	69.3(3)	C(31)-C(35)-Fe(1)	69.0(3)
C(33)-C(32)-Fe(1)	69.6(3)	C(34)-C(35)-H(35)	126.2
C(31)-C(32)-H(32)	125.9	C(31)-C(35)-H(35)	126.2
C(33)-C(32)-H(32)	125.9	Fe(1)-C(35)-H(35)	126.8

Table 9-9: Anisotropic displacement parameters for **3** ($\text{\AA}^2 \times 10^3$). The anisotropic displacement factor exponent takes the form: $-2\pi^2 [h^2 a^{*2} U_{11} + 2hk a^* b^* U_{12}]$:

	U ₁₁	U ₂₂	U ₃₃	U ₂₃	U ₁₃	U ₁₂
Cr(1)	23(1)	22(1)	35(1)	0(1)	0(1)	2(1)
Fe(1)	24(1)	25(1)	47(1)	-1(1)	5(1)	2(1)
N(1)	32(2)	28(2)	39(2)	1(1)	2(1)	3(1)
C(1)	20(2)	36(2)	47(2)	4(2)	5(2)	5(2)
C(2)	21(2)	39(2)	43(2)	3(2)	-4(2)	5(2)
C(3)	28(2)	29(2)	37(2)	2(2)	3(2)	7(2)
C(4)	29(2)	29(2)	40(2)	-3(2)	2(2)	5(2)
C(5)	24(2)	33(2)	39(2)	0(2)	6(2)	10(2)
C(6)	31(2)	33(2)	42(2)	2(2)	3(2)	2(2)

C(7)	28(2)	32(2)	39(2)	-2(2)	1(2)	2(2)
C(8)	25(2)	33(2)	37(2)	-2(2)	-6(2)	9(2)
C(9)	22(2)	33(2)	49(2)	-3(2)	-3(2)	3(2)
C(10)	34(2)	44(3)	45(2)	-3(2)	9(2)	16(2)
C(11)	37(2)	39(2)	42(2)	-12(2)	-12(2)	14(2)
C(12)	31(2)	29(2)	43(2)	6(2)	-1(2)	5(2)
C(13)	27(2)	40(2)	31(2)	-2(2)	3(2)	9(2)
C(14)	37(2)	45(3)	46(2)	10(2)	-5(2)	-6(2)
C(15)	36(3)	68(3)	55(3)	16(2)	-13(2)	-1(2)
C(16)	37(3)	57(3)	44(2)	17(2)	-1(2)	9(2)
C(17)	46(3)	38(3)	55(3)	6(2)	12(2)	-1(2)
C(18)	36(2)	45(3)	37(2)	-5(2)	-3(2)	-1(2)
C(19)	25(2)	40(2)	32(2)	4(2)	2(2)	6(2)
C(20)	33(2)	45(3)	39(2)	6(2)	4(2)	-3(2)
C(21)	45(3)	39(3)	46(3)	-3(2)	-4(2)	-1(2)
C(22)	47(3)	57(3)	42(3)	-12(2)	5(2)	11(2)
C(23)	42(3)	61(3)	52(3)	-6(2)	17(2)	-3(2)
C(24)	40(2)	41(2)	43(2)	-2(2)	9(2)	-8(2)
C(25)	28(2)	22(2)	41(2)	0(2)	2(2)	-1(2)
C(26)	25(2)	24(2)	38(2)	0(2)	3(2)	6(2)
C(27)	24(2)	43(2)	40(2)	-3(2)	5(2)	9(2)
C(28)	39(3)	57(3)	44(2)	11(2)	12(2)	19(2)
C(29)	35(2)	28(2)	73(3)	8(2)	16(2)	9(2)
C(30)	34(2)	30(2)	57(3)	-6(2)	5(2)	1(2)
C(31)	52(3)	35(3)	74(3)	11(2)	20(3)	17(2)
C(32)	37(3)	35(3)	98(4)	-19(3)	13(3)	5(2)
C(33)	49(3)	61(3)	59(3)	-13(3)	8(2)	25(3)
C(34)	30(2)	48(3)	89(4)	7(3)	21(2)	8(2)
C(35)	31(3)	45(3)	78(4)	-1(2)	-8(2)	16(2)

Table 9-10: Hydrogen coordinates ($\times 10^4$) and isotropic displacement parameters for **3** ($\text{\AA}^2 \times 10^3$):

	x	y	z	U(eq)
H(1)	3360	-788	3305	41
H(2)	3020	4382671	42	
H(3)	5178	2330	2706	38
H(4)	6895	2256	3376	39
H(6)	5290(50)	-870(40)	3938(11)	42
H(7)	8680(50)	610(40)	3908(11)	39
H(9)	9944	511	3253	42
H(10)	9561	-774	2631	49
H(11)	7468	-2633	2714	49
H(12)	6503	-2505	3395	41
H(14)	10534	126	4444	52
H(15)	11789	-1228	4941	65
H(16)	10773	-3344	5008	55
H(17)	8372	-4079	4592	55
H(18)	7105	-2714	4103	48
H(20)	7141	2551	4073	47
H(21)	6273	4037	4529	53
H(22)	4271	3397	4968	58
H(23)	3152	1276	4942	61
H(24)	4015	-196	4479	49
H(27)	4786	-271	1277	42
H(28)	6439	1234	853	55
H(29)	8627	2504	1291	54
H(30)	8406	1809	1992	48
H(31)	8864	-2159	1917	63
H(32)	7659	-2625	1226	68
H(33)	9256	-1208	777	68
H(34)	11509	113	1189	66
H(35)	11315	-500	1897	63

Table 9-11: Torsion angles for **3** [°]:

C(25)-Cr(1)-C(1)-C(2)	-30.8(3)	C(4)-Cr(1)-C(2)-C(3)	37.4(2)
C(8)-Cr(1)-C(1)-C(2)	166.3(2)	C(1)-Cr(1)-C(2)-C(3)	119.6(3)
C(5)-Cr(1)-C(1)-C(2)	117.0(4)	C(9)-Cr(1)-C(2)-C(3)	33.8(5)
C(12)-Cr(1)-C(1)-C(2)	-155.0(3)	C(10)-Cr(1)-C(2)-C(3)	-92.1(5)
C(4)-Cr(1)-C(1)-C(2)	79.0(3)	C(11)-Cr(1)-C(2)-C(3)	-158.1(2)
C(9)-Cr(1)-C(1)-C(2)	147.9(3)	C(1)-C(2)-C(3)-C(4)	0.2(4)
C(10)-Cr(1)-C(1)-C(2)	-151.5(4)	Cr(1)-C(2)-C(3)-C(4)	-60.3(3)
C(11)-Cr(1)-C(1)-C(2)	-128.2(3)	C(1)-C(2)-C(3)-Cr(1)	60.5(3)
C(3)-Cr(1)-C(1)-C(2)	36.7(2)	C(25)-Cr(1)-C(3)-C(4)	-159.2(2)
C(25)-Cr(1)-C(1)-C(5)	-147.8(2)	C(8)-Cr(1)-C(3)-C(4)	-0.7(3)
C(8)-Cr(1)-C(1)-C(5)	49.3(3)	C(5)-Cr(1)-C(3)-C(4)	38.5(2)
C(12)-Cr(1)-C(1)-C(5)	88.1(2)	C(12)-Cr(1)-C(3)-C(4)	52.5(5)
C(4)-Cr(1)-C(1)-C(5)	-38.0(2)	C(1)-Cr(1)-C(3)-C(4)	81.7(2)
C(9)-Cr(1)-C(1)-C(5)	31.0(3)	C(9)-Cr(1)-C(3)-C(4)	-48.2(3)
C(2)-Cr(1)-C(1)-C(5)	-117.0(4)	C(2)-Cr(1)-C(3)-C(4)	117.7(3)
C(10)-Cr(1)-C(1)-C(5)	91.6(5)	C(10)-Cr(1)-C(3)-C(4)	-93.7(3)
C(11)-Cr(1)-C(1)-C(5)	114.8(2)	C(11)-Cr(1)-C(3)-C(4)	-159.2(6)
C(3)-Cr(1)-C(1)-C(5)	-80.3(2)	C(25)-Cr(1)-C(3)-C(2)	83.1(2)
C(5)-C(1)-C(2)-C(3)	0.5(4)	C(8)-Cr(1)-C(3)-C(2)	-118.3(3)
Cr(1)-C(1)-C(2)-C(3)	-61.0(3)	C(5)-Cr(1)-C(3)-C(2)	-79.2(2)
C(5)-C(1)-C(2)-Cr(1)	61.5(3)	C(12)-Cr(1)-C(3)-C(2)	-65.1(4)
C(25)-Cr(1)-C(2)-C(1)	150.8(3)	C(4)-Cr(1)-C(3)-C(2)	-117.7(3)
C(8)-Cr(1)-C(2)-C(1)	-19.9(4)	C(1)-Cr(1)-C(3)-C(2)	-36.0(2)
C(5)-Cr(1)-C(2)-C(1)	-38.5(2)	C(9)-Cr(1)-C(3)-C(2)	-165.9(2)
C(12)-Cr(1)-C(2)-C(1)	32.1(3)	C(10)-Cr(1)-C(3)-C(2)	148.7(2)
C(4)-Cr(1)-C(2)-C(1)	-82.2(3)	C(11)-Cr(1)-C(3)-C(2)	83.2(7)
C(9)-Cr(1)-C(2)-C(1)	-85.8(5)	C(2)-C(3)-C(4)-C(5)	-0.8(4)
C(10)-Cr(1)-C(2)-C(1)	148.3(4)	Cr(1)-C(3)-C(4)-C(5)	-61.7(3)
C(11)-Cr(1)-C(2)-C(1)	82.2(3)	C(2)-C(3)-C(4)-Cr(1)	60.8(3)
C(3)-Cr(1)-C(2)-C(1)	-119.6(3)	C(25)-Cr(1)-C(4)-C(3)	22.9(3)
C(25)-Cr(1)-C(2)-C(3)	-89.6(2)	C(8)-Cr(1)-C(4)-C(3)	179.5(2)
C(8)-Cr(1)-C(2)-C(3)	99.7(3)	C(5)-Cr(1)-C(4)-C(3)	-117.0(3)
C(5)-Cr(1)-C(2)-C(3)	81.1(2)	C(12)-Cr(1)-C(4)-C(3)	-156.5(2)
C(12)-Cr(1)-C(2)-C(3)	151.7(2)	C(1)-Cr(1)-C(4)-C(3)	-79.4(2)

C(9)-Cr(1)-C(4)-C(3)	141.0(2)	C(9)-Cr(1)-C(5)-C(4)	83.7(2)
C(2)-Cr(1)-C(4)-C(3)	-37.6(2)	C(2)-Cr(1)-C(5)-C(4)	-80.3(2)
C(10)-Cr(1)-C(4)-C(3)	122.5(3)	C(10)-Cr(1)-C(5)-C(4)	96.3(3)
C(11)-Cr(1)-C(4)-C(3)	167.7(3)	C(11)-Cr(1)-C(5)-C(4)	148.2(2)
C(25)-Cr(1)-C(4)-C(5)	140.0(2)	C(3)-Cr(1)-C(5)-C(4)	-37.5(2)
C(8)-Cr(1)-C(4)-C(5)	-63.5(2)	C(25)-Cr(1)-C(5)-C(6)	170.5(3)
C(12)-Cr(1)-C(4)-C(5)	-39.5(3)	C(8)-Cr(1)-C(5)-C(6)	-11.0(3)
C(1)-Cr(1)-C(4)-C(5)	37.7(2)	C(12)-Cr(1)-C(5)-C(6)	24.6(3)
C(9)-Cr(1)-C(4)-C(5)	-101.9(2)	C(4)-Cr(1)-C(5)-C(6)	-123.7(4)
C(2)-Cr(1)-C(4)-C(5)	79.4(2)	C(1)-Cr(1)-C(5)-C(6)	118.7(4)
C(10)-Cr(1)-C(4)-C(5)	-120.4(2)	C(9)-Cr(1)-C(5)-C(6)	-40.0(3)
C(11)-Cr(1)-C(4)-C(5)	-75.3(4)	C(2)-Cr(1)-C(5)-C(6)	156.0(4)
C(3)-Cr(1)-C(4)-C(5)	117.0(3)	C(10)-Cr(1)-C(5)-C(6)	-27.4(4)
C(2)-C(1)-C(5)-C(4)	-1.0(4)	C(11)-Cr(1)-C(5)-C(6)	24.5(4)
Cr(1)-C(1)-C(5)-C(4)	61.7(3)	C(3)-Cr(1)-C(5)-C(6)	-161.2(4)
C(2)-C(1)-C(5)-C(6)	-175.4(3)	C(1)-C(5)-C(6)-C(19)	-116.2(4)
Cr(1)-C(1)-C(5)-C(6)	-112.7(3)	C(4)-C(5)-C(6)-C(19)	70.5(5)
C(2)-C(1)-C(5)-Cr(1)	-62.7(3)	Cr(1)-C(5)-C(6)-C(19)	158.0(3)
C(3)-C(4)-C(5)-C(1)	1.1(4)	C(1)-C(5)-C(6)-C(7)	116.2(4)
Cr(1)-C(4)-C(5)-C(1)	-62.0(3)	C(4)-C(5)-C(6)-C(7)	-57.1(5)
C(3)-C(4)-C(5)-C(6)	175.2(3)	Cr(1)-C(5)-C(6)-C(7)	30.4(4)
Cr(1)-C(4)-C(5)-C(6)	112.1(4)	C(5)-C(6)-C(7)-C(13)	-163.0(3)
C(3)-C(4)-C(5)-Cr(1)	63.1(3)	C(19)-C(6)-C(7)-C(13)	71.7(5)
C(25)-Cr(1)-C(5)-C(1)	51.8(3)	C(5)-C(6)-C(7)-C(8)	-36.7(4)
C(8)-Cr(1)-C(5)-C(1)	-129.8(3)	C(19)-C(6)-C(7)-C(8)	-161.9(3)
C(12)-Cr(1)-C(5)-C(1)	-94.1(2)	C(13)-C(7)-C(8)-C(9)	-115.9(4)
C(4)-Cr(1)-C(5)-C(1)	117.6(3)	C(6)-C(7)-C(8)-C(9)	117.1(4)
C(9)-Cr(1)-C(5)-C(1)	-158.7(2)	C(13)-C(7)-C(8)-C(12)	70.7(5)
C(2)-Cr(1)-C(5)-C(1)	37.3(2)	C(6)-C(7)-C(8)-C(12)	-56.3(5)
C(10)-Cr(1)-C(5)-C(1)	-146.1(3)	C(13)-C(7)-C(8)-Cr(1)	158.4(3)
C(11)-Cr(1)-C(5)-C(1)	-94.2(3)	C(6)-C(7)-C(8)-Cr(1)	31.3(4)
C(3)-Cr(1)-C(5)-C(1)	80.1(2)	C(25)-Cr(1)-C(8)-C(9)	48.2(4)
C(25)-Cr(1)-C(5)-C(4)	-65.8(3)	C(5)-Cr(1)-C(8)-C(9)	-130.2(3)
C(8)-Cr(1)-C(5)-C(4)	112.6(2)	C(12)-Cr(1)-C(8)-C(9)	117.5(3)
C(12)-Cr(1)-C(5)-C(4)	148.2(2)	C(4)-Cr(1)-C(8)-C(9)	-94.7(2)
C(1)-Cr(1)-C(5)-C(4)	-117.6(3)	C(1)-Cr(1)-C(8)-C(9)	-159.5(2)

C(2)-Cr(1)-C(8)-C(9)	-147.3(2)	C(3)-Cr(1)-C(9)-C(10)	-128.1(3)
C(10)-Cr(1)-C(8)-C(9)	37.3(2)	C(25)-Cr(1)-C(9)-C(8)	-151.5(2)
C(11)-Cr(1)-C(8)-C(9)	79.8(3)	C(5)-Cr(1)-C(9)-C(8)	48.9(3)
C(3)-Cr(1)-C(8)-C(9)	-94.3(3)	C(12)-Cr(1)-C(9)-C(8)	-38.1(2)
C(25)-Cr(1)-C(8)-C(12)	-69.4(3)	C(4)-Cr(1)-C(9)-C(8)	87.7(2)
C(5)-Cr(1)-C(8)-C(12)	112.2(3)	C(1)-Cr(1)-C(9)-C(8)	29.8(3)
C(4)-Cr(1)-C(8)-C(12)	147.7(2)	C(2)-Cr(1)-C(9)-C(8)	91.0(5)
C(1)-Cr(1)-C(8)-C(12)	83.0(2)	C(10)-Cr(1)-C(9)-C(8)	-116.8(4)
C(9)-Cr(1)-C(8)-C(12)	-117.5(3)	C(11)-Cr(1)-C(9)-C(8)	-80.1(3)
C(2)-Cr(1)-C(8)-C(12)	95.2(3)	C(3)-Cr(1)-C(9)-C(8)	115.1(2)
C(10)-Cr(1)-C(8)-C(12)	-80.3(3)	C(8)-C(9)-C(10)-C(11)	0.3(4)
C(11)-Cr(1)-C(8)-C(12)	-37.8(2)	Cr(1)-C(9)-C(10)-C(11)	-60.9(3)
C(3)-Cr(1)-C(8)-C(12)	148.1(2)	C(8)-C(9)-C(10)-Cr(1)	61.2(3)
C(25)-Cr(1)-C(8)-C(7)	166.3(3)	C(25)-Cr(1)-C(10)-C(9)	147.9(3)
C(5)-Cr(1)-C(8)-C(7)	-12.0(3)	C(8)-Cr(1)-C(10)-C(9)	-38.6(2)
C(12)-Cr(1)-C(8)-C(7)	-124.3(4)	C(5)-Cr(1)-C(10)-C(9)	-20.7(4)
C(4)-Cr(1)-C(8)-C(7)	23.5(3)	C(12)-Cr(1)-C(10)-C(9)	-82.5(3)
C(1)-Cr(1)-C(8)-C(7)	-41.3(3)	C(4)-Cr(1)-C(10)-C(9)	31.6(3)
C(9)-Cr(1)-C(8)-C(7)	118.2(4)	C(1)-Cr(1)-C(10)-C(9)	-86.4(5)
C(2)-Cr(1)-C(8)-C(7)	-29.1(4)	C(2)-Cr(1)-C(10)-C(9)	150.4(4)
C(10)-Cr(1)-C(8)-C(7)	155.5(4)	C(11)-Cr(1)-C(10)-C(9)	-119.3(4)
C(11)-Cr(1)-C(8)-C(7)	-162.0(4)	C(3)-Cr(1)-C(10)-C(9)	82.6(3)
C(3)-Cr(1)-C(8)-C(7)	23.9(4)	C(25)-Cr(1)-C(10)-C(11)	-92.8(3)
C(12)-C(8)-C(9)-C(10)	-0.7(4)	C(8)-Cr(1)-C(10)-C(11)	80.8(3)
C(7)-C(8)-C(9)-C(10)	-175.2(3)	C(5)-Cr(1)-C(10)-C(11)	98.6(3)
Cr(1)-C(8)-C(9)-C(10)	-62.9(3)	C(12)-Cr(1)-C(10)-C(11)	36.9(2)
C(12)-C(8)-C(9)-Cr(1)	62.2(3)	C(4)-Cr(1)-C(10)-C(11)	150.9(2)
C(7)-C(8)-C(9)-Cr(1)	-112.3(3)	C(1)-Cr(1)-C(10)-C(11)	33.0(5)
C(25)-Cr(1)-C(9)-C(10)	-34.7(3)	C(9)-Cr(1)-C(10)-C(11)	119.3(4)
C(8)-Cr(1)-C(9)-C(10)	116.8(4)	C(2)-Cr(1)-C(10)-C(11)	-90.2(5)
C(5)-Cr(1)-C(9)-C(10)	165.7(3)	C(3)-Cr(1)-C(10)-C(11)	-158.1(2)
C(12)-Cr(1)-C(9)-C(10)	78.7(3)	C(9)-C(10)-C(11)-C(12)	0.2(5)
C(4)-Cr(1)-C(9)-C(10)	-155.5(3)	Cr(1)-C(10)-C(11)-C(12)	-60.3(3)
C(1)-Cr(1)-C(9)-C(10)	146.6(3)	C(9)-C(10)-C(11)-Cr(1)	60.6(3)
C(2)-Cr(1)-C(9)-C(10)	-152.3(4)	C(25)-Cr(1)-C(11)-C(12)	-159.0(3)
C(11)-Cr(1)-C(9)-C(10)	36.7(3)	C(8)-Cr(1)-C(11)-C(12)	39.1(2)

C(5)-Cr(1)-C(11)-C(12)	0.1(3)	C(1)-Cr(1)-C(12)-C(8)	-102.4(2)
C(4)-Cr(1)-C(11)-C(12)	52.3(5)	C(9)-Cr(1)-C(12)-C(8)	37.6(2)
C(1)-Cr(1)-C(11)-C(12)	-47.3(3)	C(2)-Cr(1)-C(12)-C(8)	-121.3(2)
C(9)-Cr(1)-C(11)-C(12)	82.4(3)	C(10)-Cr(1)-C(12)-C(8)	79.1(3)
C(2)-Cr(1)-C(11)-C(12)	-92.7(3)	C(11)-Cr(1)-C(12)-C(8)	116.1(3)
C(10)-Cr(1)-C(11)-C(12)	118.5(3)	C(3)-Cr(1)-C(12)-C(8)	-76.3(4)
C(3)-Cr(1)-C(11)-C(12)	-159.1(6)	C(8)-C(7)-C(13)-C(14)	116.6(4)
C(25)-Cr(1)-C(11)-C(10)	82.5(3)	C(6)-C(7)-C(13)-C(14)	-119.7(4)
C(8)-Cr(1)-C(11)-C(10)	-79.4(3)	C(8)-C(7)-C(13)-C(18)	-61.7(5)
C(5)-Cr(1)-C(11)-C(10)	-118.3(3)	C(6)-C(7)-C(13)-C(18)	62.0(5)
C(12)-Cr(1)-C(11)-C(10)	-118.5(3)	C(18)-C(13)-C(14)-C(15)	1.2(6)
C(4)-Cr(1)-C(11)-C(10)	-66.1(5)	C(7)-C(13)-C(14)-C(15)	-177.2(4)
C(1)-Cr(1)-C(11)-C(10)	-165.8(2)	C(13)-C(14)-C(15)-C(16)	0.5(7)
C(9)-Cr(1)-C(11)-C(10)	-36.1(2)	C(14)-C(15)-C(16)-C(17)	-1.7(7)
C(2)-Cr(1)-C(11)-C(10)	148.8(3)	C(15)-C(16)-C(17)-C(18)	1.2(7)
C(3)-Cr(1)-C(11)-C(10)	82.4(7)	C(16)-C(17)-C(18)-C(13)	0.5(6)
C(10)-C(11)-C(12)-C(8)	-0.7(4)	C(14)-C(13)-C(18)-C(17)	-1.7(6)
Cr(1)-C(11)-C(12)-C(8)	-61.7(3)	C(7)-C(13)-C(18)-C(17)	176.6(4)
C(10)-C(11)-C(12)-Cr(1)	61.1(3)	C(5)-C(6)-C(19)-C(24)	113.9(4)
C(9)-C(8)-C(12)-C(11)	0.8(4)	C(7)-C(6)-C(19)-C(24)	-123.0(4)
C(7)-C(8)-C(12)-C(11)	175.0(4)	C(5)-C(6)-C(19)-C(20)	-62.8(5)
Cr(1)-C(8)-C(12)-C(11)	63.5(3)	C(7)-C(6)-C(19)-C(20)	60.3(5)
C(9)-C(8)-C(12)-Cr(1)	-62.7(3)	C(24)-C(19)-C(20)-C(21)	-2.6(6)
C(7)-C(8)-C(12)-Cr(1)	111.5(4)	C(6)-C(19)-C(20)-C(21)	174.0(4)
C(25)-Cr(1)-C(12)-C(11)	24.2(3)	C(19)-C(20)-C(21)-C(22)	1.5(6)
C(8)-Cr(1)-C(12)-C(11)	-116.1(3)	C(20)-C(21)-C(22)-C(23)	0.0(7)
C(5)-Cr(1)-C(12)-C(11)	-179.9(3)	C(21)-C(22)-C(23)-C(24)	-0.4(7)
C(4)-Cr(1)-C(12)-C(11)	-156.3(2)	C(20)-C(19)-C(24)-C(23)	2.3(6)
C(1)-Cr(1)-C(12)-C(11)	141.5(3)	C(6)-C(19)-C(24)-C(23)	-174.5(4)
C(9)-Cr(1)-C(12)-C(11)	-78.5(3)	C(22)-C(23)-C(24)-C(19)	-0.8(7)
C(2)-Cr(1)-C(12)-C(11)	122.6(3)	C(26)-N(1)-C(25)-Cr(1)	166(3)
C(10)-Cr(1)-C(12)-C(11)	-37.0(2)	C(8)-Cr(1)-C(25)-N(1)	114(3)
C(3)-Cr(1)-C(12)-C(11)	167.5(3)	C(5)-Cr(1)-C(25)-N(1)	-68(3)
C(25)-Cr(1)-C(12)-C(8)	140.4(2)	C(12)-Cr(1)-C(25)-N(1)	71(3)
C(5)-Cr(1)-C(12)-C(8)	-63.8(2)	C(4)-Cr(1)-C(25)-N(1)	-108(3)
C(4)-Cr(1)-C(12)-C(8)	-40.2(3)	C(1)-Cr(1)-C(25)-N(1)	-37(3)

C(9)-Cr(1)-C(25)-N(1)	144(3)	N(1)-C(26)-C(27)-Fe(1)	-118.7(4)
C(2)-Cr(1)-C(25)-N(1)	-55(3)	C(30)-C(26)-C(27)-Fe(1)	59.0(3)
C(10)-Cr(1)-C(25)-N(1)	124(3)	C(31)-Fe(1)-C(27)-C(26)	76.9(3)
C(11)-Cr(1)-C(25)-N(1)	86(3)	C(33)-Fe(1)-C(27)-C(26)	160.1(3)
C(3)-Cr(1)-C(25)-N(1)	-94(3)	C(34)-Fe(1)-C(27)-C(26)	-167.1(5)
C(25)-N(1)-C(26)-C(27)	-178.1(4)	C(35)-Fe(1)-C(27)-C(26)	44.6(6)
C(25)-N(1)-C(26)-C(30)	4.5(7)	C(28)-Fe(1)-C(27)-C(26)	-118.5(4)
C(25)-N(1)-C(26)-Fe(1)	94.5(5)	C(32)-Fe(1)-C(27)-C(26)	118.3(3)
C(31)-Fe(1)-C(26)-N(1)	-3.1(4)	C(29)-Fe(1)-C(27)-C(26)	-81.3(3)
C(27)-Fe(1)-C(26)-N(1)	118.1(4)	C(30)-Fe(1)-C(27)-C(26)	-37.7(2)
C(33)-Fe(1)-C(26)-N(1)	69.6(6)	C(31)-Fe(1)-C(27)-C(28)	-164.6(3)
C(34)-Fe(1)-C(26)-N(1)	-76.0(6)	C(33)-Fe(1)-C(27)-C(28)	-81.4(3)
C(35)-Fe(1)-C(26)-N(1)	-44.9(4)	C(34)-Fe(1)-C(27)-C(28)	-48.6(6)
C(28)-Fe(1)-C(26)-N(1)	156.5(4)	C(35)-Fe(1)-C(27)-C(28)	163.1(5)
C(32)-Fe(1)-C(26)-N(1)	38.2(4)	C(26)-Fe(1)-C(27)-C(28)	118.5(4)
C(29)-Fe(1)-C(26)-N(1)	-160.1(4)	C(32)-Fe(1)-C(27)-C(28)	-123.2(3)
C(30)-Fe(1)-C(26)-N(1)	-122.0(4)	C(29)-Fe(1)-C(27)-C(28)	37.2(3)
C(31)-Fe(1)-C(26)-C(27)	-121.2(3)	C(30)-Fe(1)-C(27)-C(28)	80.7(3)
C(33)-Fe(1)-C(26)-C(27)	-48.5(6)	C(26)-C(27)-C(28)-C(29)	0.3(5)
C(34)-Fe(1)-C(26)-C(27)	165.9(5)	Fe(1)-C(27)-C(28)-C(29)	-59.7(3)
C(35)-Fe(1)-C(26)-C(27)	-163.0(3)	C(26)-C(27)-C(28)-Fe(1)	60.0(3)
C(28)-Fe(1)-C(26)-C(27)	38.4(3)	C(31)-Fe(1)-C(28)-C(29)	160.3(5)
C(32)-Fe(1)-C(26)-C(27)	-80.0(3)	C(27)-Fe(1)-C(28)-C(29)	119.4(4)
C(29)-Fe(1)-C(26)-C(27)	81.7(3)	C(33)-Fe(1)-C(28)-C(29)	-122.5(3)
C(30)-Fe(1)-C(26)-C(27)	119.8(3)	C(34)-Fe(1)-C(28)-C(29)	-80.0(3)
C(31)-Fe(1)-C(26)-C(30)	119.0(3)	C(35)-Fe(1)-C(28)-C(29)	-45.0(6)
C(27)-Fe(1)-C(26)-C(30)	-119.8(3)	C(26)-Fe(1)-C(28)-C(29)	81.4(3)
C(33)-Fe(1)-C(26)-C(30)	-168.3(5)	C(32)-Fe(1)-C(28)-C(29)	-164.5(3)
C(34)-Fe(1)-C(26)-C(30)	46.1(6)	C(30)-Fe(1)-C(28)-C(29)	36.8(2)
C(35)-Fe(1)-C(26)-C(30)	77.2(3)	C(31)-Fe(1)-C(28)-C(27)	40.9(6)
C(28)-Fe(1)-C(26)-C(30)	-81.5(3)	C(33)-Fe(1)-C(28)-C(27)	118.1(3)
C(32)-Fe(1)-C(26)-C(30)	160.2(3)	C(34)-Fe(1)-C(28)-C(27)	160.6(3)
C(29)-Fe(1)-C(26)-C(30)	-38.1(3)	C(35)-Fe(1)-C(28)-C(27)	-164.4(5)
N(1)-C(26)-C(27)-C(28)	-178.6(3)	C(26)-Fe(1)-C(28)-C(27)	-38.0(2)
C(30)-C(26)-C(27)-C(28)	-0.9(4)	C(32)-Fe(1)-C(28)-C(27)	76.1(3)
Fe(1)-C(26)-C(27)-C(28)	-59.9(3)	C(29)-Fe(1)-C(28)-C(27)	-119.4(4)

C(30)-Fe(1)-C(28)-C(27)	-82.5(3)	C(31)-Fe(1)-C(30)-C(26)	-79.1(3)
C(27)-C(28)-C(29)-C(30)	0.3(5)	C(27)-Fe(1)-C(30)-C(26)	37.3(2)
Fe(1)-C(28)-C(29)-C(30)	-58.7(3)	C(33)-Fe(1)-C(30)-C(26)	166.6(5)
C(27)-C(28)-C(29)-Fe(1)	59.0(3)	C(34)-Fe(1)-C(30)-C(26)	-162.9(3)
C(31)-Fe(1)-C(29)-C(28)	-162.4(4)	C(35)-Fe(1)-C(30)-C(26)	-121.6(3)
C(27)-Fe(1)-C(29)-C(28)	-38.0(2)	C(28)-Fe(1)-C(30)-C(26)	81.4(3)
C(33)-Fe(1)-C(29)-C(28)	77.1(3)	C(32)-Fe(1)-C(30)-C(26)	-48.0(6)
C(34)-Fe(1)-C(29)-C(28)	119.0(3)	C(29)-Fe(1)-C(30)-C(26)	118.0(4)
C(35)-Fe(1)-C(29)-C(28)	161.6(3)	C(27)-Fe(1)-C(31)-C(32)	77.9(3)
C(26)-Fe(1)-C(29)-C(28)	-81.9(3)	C(33)-Fe(1)-C(31)-C(32)	-37.4(3)
C(32)-Fe(1)-C(29)-C(28)	42.5(7)	C(34)-Fe(1)-C(31)-C(32)	-81.0(3)
C(30)-Fe(1)-C(29)-C(28)	-120.7(4)	C(35)-Fe(1)-C(31)-C(32)	-118.6(4)
C(31)-Fe(1)-C(29)-C(30)	-41.7(6)	C(26)-Fe(1)-C(31)-C(32)	119.4(3)
C(27)-Fe(1)-C(29)-C(30)	82.8(3)	C(28)-Fe(1)-C(31)-C(32)	47.2(6)
C(33)-Fe(1)-C(29)-C(30)	-162.1(3)	C(29)-Fe(1)-C(31)-C(32)	-167.8(4)
C(34)-Fe(1)-C(29)-C(30)	-120.3(3)	C(30)-Fe(1)-C(31)-C(32)	161.9(3)
C(35)-Fe(1)-C(29)-C(30)	-77.7(3)	C(27)-Fe(1)-C(31)-C(35)	-163.5(3)
C(26)-Fe(1)-C(29)-C(30)	38.8(2)	C(33)-Fe(1)-C(31)-C(35)	81.3(3)
C(28)-Fe(1)-C(29)-C(30)	120.7(4)	C(34)-Fe(1)-C(31)-C(35)	37.6(3)
C(32)-Fe(1)-C(29)-C(30)	163.2(5)	C(26)-Fe(1)-C(31)-C(35)	-122.0(3)
C(28)-C(29)-C(30)-C(26)	-0.8(5)	C(28)-Fe(1)-C(31)-C(35)	165.8(5)
Fe(1)-C(29)-C(30)-C(26)	-59.3(3)	C(32)-Fe(1)-C(31)-C(35)	118.6(4)
C(28)-C(29)-C(30)-Fe(1)	58.5(3)	C(29)-Fe(1)-C(31)-C(35)	-49.2(6)
N(1)-C(26)-C(30)-C(29)	178.7(4)	C(30)-Fe(1)-C(31)-C(35)	-79.5(3)
C(27)-C(26)-C(30)-C(29)	1.0(4)	C(35)-C(31)-C(32)-C(33)	-1.3(5)
Fe(1)-C(26)-C(30)-C(29)	59.8(3)	Fe(1)-C(31)-C(32)-C(33)	58.9(3)
N(1)-C(26)-C(30)-Fe(1)	118.9(4)	C(35)-C(31)-C(32)-Fe(1)	-60.2(3)
C(27)-C(26)-C(30)-Fe(1)	-58.8(3)	C(27)-Fe(1)-C(32)-C(31)	-120.4(3)
C(31)-Fe(1)-C(30)-C(29)	162.8(3)	C(33)-Fe(1)-C(32)-C(31)	119.8(4)
C(27)-Fe(1)-C(30)-C(29)	-80.8(3)	C(34)-Fe(1)-C(32)-C(31)	82.3(3)
C(33)-Fe(1)-C(30)-C(29)	48.6(7)	C(35)-Fe(1)-C(32)-C(31)	38.4(3)
C(34)-Fe(1)-C(30)-C(29)	79.0(3)	C(26)-Fe(1)-C(32)-C(31)	-78.2(3)
C(35)-Fe(1)-C(30)-C(29)	120.4(3)	C(28)-Fe(1)-C(32)-C(31)	-162.3(3)
C(26)-Fe(1)-C(30)-C(29)	-118.0(4)	C(29)-Fe(1)-C(32)-C(31)	165.7(5)
C(28)-Fe(1)-C(30)-C(29)	-36.6(3)	C(30)-Fe(1)-C(32)-C(31)	-43.1(6)
C(32)-Fe(1)-C(30)-C(29)	-166.1(5)	C(31)-Fe(1)-C(32)-C(33)	-119.8(4)

C(27)-Fe(1)-C(32)-C(33)	119.8(3)	C(30)-Fe(1)-C(34)-C(33)	-164.8(3)
C(34)-Fe(1)-C(32)-C(33)	-37.5(3)	C(31)-Fe(1)-C(34)-C(35)	-38.0(3)
C(35)-Fe(1)-C(32)-C(33)	-81.4(3)	C(27)-Fe(1)-C(34)-C(35)	-163.6(4)
C(26)-Fe(1)-C(32)-C(33)	162.0(3)	C(33)-Fe(1)-C(34)-C(35)	-118.9(4)
C(28)-Fe(1)-C(32)-C(33)	77.9(3)	C(26)-Fe(1)-C(34)-C(35)	41.6(7)
C(29)-Fe(1)-C(32)-C(33)	45.9(7)	C(28)-Fe(1)-C(34)-C(35)	160.6(3)
C(30)-Fe(1)-C(32)-C(33)	-162.9(4)	C(32)-Fe(1)-C(34)-C(35)	-81.4(3)
C(31)-C(32)-C(33)-C(34)	0.7(5)	C(29)-Fe(1)-C(34)-C(35)	118.5(3)
Fe(1)-C(32)-C(33)-C(34)	59.4(3)	C(30)-Fe(1)-C(34)-C(35)	76.3(3)
C(31)-C(32)-C(33)-Fe(1)	-58.7(3)	C(33)-C(34)-C(35)-C(31)	-0.9(5)
C(31)-Fe(1)-C(33)-C(34)	-82.3(3)	Fe(1)-C(34)-C(35)-C(31)	58.7(3)
C(27)-Fe(1)-C(33)-C(34)	161.9(3)	C(33)-C(34)-C(35)-Fe(1)	-59.6(3)
C(35)-Fe(1)-C(33)-C(34)	-37.9(3)	C(32)-C(31)-C(35)-C(34)	1.4(5)
C(26)-Fe(1)-C(33)-C(34)	-162.8(4)	Fe(1)-C(31)-C(35)-C(34)	-59.1(3)
C(28)-Fe(1)-C(33)-C(34)	118.7(3)	C(32)-C(31)-C(35)-Fe(1)	60.4(3)
C(32)-Fe(1)-C(33)-C(34)	-119.5(4)	C(31)-Fe(1)-C(35)-C(34)	119.2(4)
C(29)-Fe(1)-C(33)-C(34)	77.1(4)	C(27)-Fe(1)-C(35)-C(34)	162.5(5)
C(30)-Fe(1)-C(33)-C(34)	40.7(7)	C(33)-Fe(1)-C(35)-C(34)	37.8(3)
C(31)-Fe(1)-C(33)-C(32)	37.1(3)	C(26)-Fe(1)-C(35)-C(34)	-164.3(3)
C(27)-Fe(1)-C(33)-C(32)	-78.6(3)	C(28)-Fe(1)-C(35)-C(34)	-47.9(6)
C(34)-Fe(1)-C(33)-C(32)	119.5(4)	C(32)-Fe(1)-C(35)-C(34)	81.6(3)
C(35)-Fe(1)-C(33)-C(32)	81.5(3)	C(29)-Fe(1)-C(35)-C(34)	-80.6(3)
C(26)-Fe(1)-C(33)-C(32)	-43.3(6)	C(30)-Fe(1)-C(35)-C(34)	-122.1(3)
C(28)-Fe(1)-C(33)-C(32)	-121.9(3)	C(27)-Fe(1)-C(35)-C(31)	43.3(7)
C(29)-Fe(1)-C(33)-C(32)	-163.5(3)	C(33)-Fe(1)-C(35)-C(31)	-81.4(3)
C(30)-Fe(1)-C(33)-C(32)	160.1(5)	C(34)-Fe(1)-C(35)-C(31)	-119.2(4)
C(32)-C(33)-C(34)-C(35)	0.2(5)	C(26)-Fe(1)-C(35)-C(31)	76.5(3)
Fe(1)-C(33)-C(34)-C(35)	59.7(3)	C(28)-Fe(1)-C(35)-C(31)	-167.2(4)
C(32)-C(33)-C(34)-Fe(1)	-59.5(3)	C(32)-Fe(1)-C(35)-C(31)	-37.7(3)
C(31)-Fe(1)-C(34)-C(33)	80.9(3)	C(29)-Fe(1)-C(35)-C(31)	160.1(3)
C(27)-Fe(1)-C(34)-C(33)	-44.8(6)	C(30)-Fe(1)-C(35)-C(31)	118.7(3)
C(35)-Fe(1)-C(34)-C(33)	118.9(4)		
C(26)-Fe(1)-C(34)-C(33)	160.5(5)		
C(28)-Fe(1)-C(34)-C(33)	-80.6(4)		
C(32)-Fe(1)-C(34)-C(33)	37.5(3)		
C(29)-Fe(1)-C(34)-C(33)	-122.6(3)		

Table 9-12: Crystal data and structure refinement for **4b**:

Empirical formula	C ₅₀ H ₅₄ Cr ₂ Fe N ₂
Formula weight	842.80
Temperature	81(2) K
Wavelength	0.71073 Å
Crystal system	Triclinic
Space group	P-1
Unit cell dimensions	a = 12.8945(5) Å α = 69.17(1)°.
	b = 13.3213(5) Å β = 68.65(1)°.
	c = 13.4444(5) Å γ = 71.84(1)°.
Volume	1965.77(13) Å ³
Z	2
Density (calculated)	1.424 Mg/m ³
Absorption coefficient	0.946 mm ⁻¹
F(000)	884
Crystal size	0.19 x 0.10 x 0.04 mm ³
Crystal color and habit	Red Parallelepiped
Diffractionmeter	Bruker/Siemens SMART APEX
Theta range for data collection	1.67 to 28.29°.
Index ranges	-17 ≤ h ≤ 17, -17 ≤ k ≤ 17, -17 ≤ l ≤ 17
Reflections collected	24182
Independent reflections	9731 [R(int) = 0.0868]
Completeness to theta = 28.29°	99.6 %
Absorption correction	Empirical
Max. and min. transmission	0.9631 and 0.8407
Solution method	XS, Bruker SHELXTL v. 6.10
Refinement method	Full-matrix least-squares on F ²
Data / restraints / parameters	9731 / 0 / 504
Goodness-of-fit on F ²	0.967
Final R indices [I > 2σ(I)]	R1 = 0.0625, wR2 = 0.1115
R indices (all data)	R1 = 0.1093, wR2 = 0.1275
Largest diff. peak and hole	0.565 and -0.523 e.Å ⁻³

Table 9-13: Atomic coordinates ($\times 10^4$) and equivalent isotropic displacement parameters for **4b** ($\text{\AA}^2 \times 10^3$). $U(\text{eq})$ is defined as one third of the trace of the orthogonalized U_{ij} tensor:

	x	y	z	U(eq)
C(1)	11881(3)	2685(3)	578(3)	16(1)
C(2)	10785(3)	3322(3)	878(3)	16(1)
C(3)	10533(3)	3384(3)	1986(3)	15(1)
C(4)	11477(3)	2777(3)	2367(3)	15(1)
C(5)	12336(3)	2332(3)	1502(3)	14(1)
C(6)	13489(3)	1574(3)	1575(3)	15(1)
C(7)	13246(3)	472(3)	2495(3)	16(1)
C(8)	12112(3)	306(3)	2542(3)	16(1)
C(9)	11862(3)	134(3)	1672(3)	17(1)
C(10)	10707(3)	69(3)	2023(3)	22(1)
C(11)	10233(3)	207(3)	3112(3)	20(1)
C(12)	11081(3)	361(3)	3434(3)	18(1)
C(13)	14196(3)	-535(3)	2266(3)	22(1)
C(14)	13191(3)	498(3)	3656(3)	23(1)
C(15)	14171(3)	1378(3)	435(3)	20(1)
C(16)	14179(3)	2158(3)	1833(3)	24(1)
C(17)	9349(3)	2070(3)	1955(3)	13(1)
C(18)	7376(3)	2547(3)	2783(3)	12(1)
C(19)	7334(3)	2420(3)	3891(3)	14(1)
C(20)	6158(3)	2642(3)	4499(3)	15(1)
C(21)	5500(3)	2906(3)	3760(3)	16(1)
C(22)	6246(3)	2856(3)	2694(3)	14(1)
C(23)	6187(3)	5267(3)	3878(3)	14(1)
C(24)	5558(3)	5546(3)	3107(3)	17(1)
C(25)	6350(3)	5470(3)	2060(3)	16(1)
C(26)	7470(3)	5164(3)	2173(3)	13(1)
C(27)	7377(3)	5034(3)	3304(3)	13(1)
C(28)	6994(3)	5371(3)	6999(3)	15(1)
C(29)	7551(3)	5906(3)	5909(3)	15(1)

C(30)	8733(3)	5683(3)	5790(3)	14(1)
C(31)	8918(3)	5007(3)	6801(3)	14(1)
C(32)	7844(3)	4809(3)	7576(3)	11(1)
C(33)	7631(3)	4085(3)	8768(3)	14(1)
C(34)	8278(3)	2868(3)	8734(3)	13(1)
C(35)	8324(3)	2748(3)	7630(3)	14(1)
C(36)	9328(3)	2610(3)	6722(3)	16(1)
C(37)	8991(3)	2565(3)	5857(3)	17(1)
C(38)	7788(3)	2666(3)	6218(3)	18(1)
C(39)	7378(3)	2771(3)	7304(3)	17(1)
C(40)	7685(3)	2001(3)	9696(3)	21(1)
C(41)	9499(3)	2618(3)	8814(3)	21(1)
C(42)	6335(3)	4167(3)	9302(3)	20(1)
C(43)	8026(3)	4522(3)	9452(3)	19(1)
C(44)	8231(3)	4529(3)	4735(3)	12(1)
C(45)	7242(3)	8142(3)	2392(3)	23(1)
C(46)	6580(3)	8022(3)	3485(3)	22(1)
C(47)	6362(4)	8831(3)	3992(3)	26(1)
C(48)	6816(4)	9754(3)	3412(4)	29(1)
C(49)	7466(4)	9881(3)	2324(4)	31(1)
C(50)	7673(4)	9068(3)	1818(3)	27(1)
Cr(1)	10849(1)	1674(1)	1989(1)	12(1)
Cr(2)	8188(1)	4141(1)	6221(1)	11(1)
Fe(1)	6550(1)	3987(1)	3214(1)	12(1)
N(1)	8363(3)	2350(2)	1904(2)	14(1)
N(2)	8294(2)	4752(2)	3752(2)	12(1)

Table 9-14: Bond lengths [\AA] and angles [$^\circ$]:

C(1)-C(2)	1.401(5)	C(12)-Cr(1)	2.147(4)
C(1)-C(5)	1.433(5)	C(12)-H(12)	1.0000
C(1)-Cr(1)	2.155(4)	C(13)-H(13A)	0.9800
C(1)-H(1)	1.0000	C(13)-H(13B)	0.9800
C(2)-C(3)	1.430(5)	C(13)-H(13C)	0.9800
C(2)-Cr(1)	2.168(3)	C(14)-H(14A)	0.9800
C(2)-H(2)	1.0000	C(14)-H(14B)	0.9800
C(3)-C(4)	1.395(5)	C(14)-H(14C)	0.9800
C(3)-Cr(1)	2.184(3)	C(15)-H(15A)	0.9800
C(3)-H(3)	1.0000	C(15)-H(15B)	0.9800
C(4)-C(5)	1.440(5)	C(15)-H(15C)	0.9800
C(4)-Cr(1)	2.155(3)	C(16)-H(16A)	0.9800
C(4)-H(4)	1.0000	C(16)-H(16B)	0.9800
C(5)-C(6)	1.529(5)	C(16)-H(16C)	0.9800
C(5)-Cr(1)	2.145(3)	C(17)-N(1)	1.230(4)
C(6)-C(15)	1.534(5)	C(17)-Cr(1)	1.852(4)
C(6)-C(16)	1.538(5)	C(18)-N(1)	1.415(4)
C(6)-C(7)	1.580(5)	C(18)-C(19)	1.421(5)
C(7)-C(8)	1.522(5)	C(18)-C(22)	1.424(5)
C(7)-C(13)	1.546(5)	C(18)-Fe(1)	2.053(3)
C(7)-C(14)	1.549(5)	C(19)-C(20)	1.429(5)
C(8)-C(9)	1.427(5)	C(19)-Fe(1)	2.052(3)
C(8)-C(12)	1.433(5)	C(19)-H(19)	1.0000
C(8)-Cr(1)	2.144(4)	C(20)-C(21)	1.417(5)
C(9)-C(10)	1.410(5)	C(20)-Fe(1)	2.043(3)
C(9)-Cr(1)	2.155(3)	C(20)-H(20)	1.0000
C(9)-H(9)	1.0000	C(21)-C(22)	1.417(5)
C(10)-C(11)	1.422(5)	C(21)-Fe(1)	2.045(4)
C(10)-Cr(1)	2.185(4)	C(21)-H(21)	1.0000
C(10)-H(10)	1.0000	C(22)-Fe(1)	2.055(3)
C(11)-C(12)	1.404(5)	C(22)-H(22)	1.0000
C(11)-Cr(1)	2.175(4)	C(23)-C(24)	1.422(5)
C(11)-H(11)	1.0000	C(23)-C(27)	1.434(5)

C(23)-Fe(1)	2.051(3)	C(35)-Cr(2)	2.145(3)
C(23)-H(23)	1.0000	C(36)-C(37)	1.406(5)
C(24)-C(25)	1.423(5)	C(36)-Cr(2)	2.156(4)
C(24)-Fe(1)	2.059(3)	C(36)-H(36)	1.0000
C(24)-H(24)	1.0000	C(37)-C(38)	1.424(5)
C(25)-C(26)	1.423(5)	C(37)-Cr(2)	2.174(3)
C(25)-Fe(1)	2.042(3)	C(37)-H(37)	1.0000
C(25)-H(25)	1.0000	C(38)-C(39)	1.403(5)
C(26)-C(27)	1.431(5)	C(38)-Cr(2)	2.184(3)
C(26)-Fe(1)	2.054(4)	C(38)-H(38)	1.0000
C(26)-H(26)	1.0000	C(39)-Cr(2)	2.175(4)
C(27)-N(2)	1.409(4)	C(39)-H(39)	1.0000
C(27)-Fe(1)	2.060(4)	C(40)-H(40A)	0.9800
C(28)-C(29)	1.407(5)	C(40)-H(40B)	0.9800
C(28)-C(32)	1.435(5)	C(40)-H(40C)	0.9800
C(28)-Cr(2)	2.150(3)	C(41)-H(41A)	0.9800
C(28)-H(28)	1.0000	C(41)-H(41B)	0.9800
C(29)-C(30)	1.418(5)	C(41)-H(41C)	0.9800
C(29)-Cr(2)	2.174(3)	C(42)-H(42A)	0.9800
C(29)-H(29)	1.0000	C(42)-H(42B)	0.9800
C(30)-C(31)	1.396(5)	C(42)-H(42C)	0.9800
C(30)-Cr(2)	2.193(3)	C(43)-H(43A)	0.9800
C(30)-H(30)	1.0000	C(43)-H(43B)	0.9800
C(31)-C(32)	1.433(5)	C(43)-H(43C)	0.9800
C(31)-Cr(2)	2.163(3)	C(44)-N(2)	1.224(4)
C(31)-H(31)	1.0000	C(44)-Cr(2)	1.862(4)
C(32)-C(33)	1.523(5)	C(45)-C(50)	1.365(5)
C(32)-Cr(2)	2.149(3)	C(45)-C(46)	1.385(5)
C(33)-C(43)	1.533(5)	C(45)-H(45)	0.9500
C(33)-C(42)	1.545(5)	C(46)-C(47)	1.378(5)
C(33)-C(34)	1.584(5)	C(46)-H(46)	0.9500
C(34)-C(35)	1.528(5)	C(47)-C(48)	1.378(5)
C(34)-C(40)	1.535(5)	C(47)-H(47)	0.9500
C(34)-C(41)	1.540(5)	C(48)-C(49)	1.375(6)
C(35)-C(39)	1.426(5)	C(48)-H(48)	0.9500
C(35)-C(36)	1.436(5)	C(49)-C(50)	1.385(6)

C(49)-H(49)	0.9500	C(5)-C(6)-C(7)	107.3(3)
C(50)-H(50)	0.9500	C(15)-C(6)-C(7)	112.0(3)
		C(16)-C(6)-C(7)	113.1(3)
C(2)-C(1)-C(5)	107.7(3)	C(8)-C(7)-C(13)	109.9(3)
C(2)-C(1)-Cr(1)	71.6(2)	C(8)-C(7)-C(14)	109.0(3)
C(5)-C(1)-Cr(1)	70.2(2)	C(13)-C(7)-C(14)	104.9(3)
C(2)-C(1)-H(1)	126.1	C(8)-C(7)-C(6)	108.3(3)
C(5)-C(1)-H(1)	126.1	C(13)-C(7)-C(6)	112.5(3)
Cr(1)-C(1)-H(1)	126.1	C(14)-C(7)-C(6)	112.1(3)
C(1)-C(2)-C(3)	109.1(3)	C(9)-C(8)-C(12)	107.3(3)
C(1)-C(2)-Cr(1)	70.6(2)	C(9)-C(8)-C(7)	126.0(3)
C(3)-C(2)-Cr(1)	71.4(2)	C(12)-C(8)-C(7)	126.7(3)
C(1)-C(2)-H(2)	125.4	C(9)-C(8)-Cr(1)	71.0(2)
C(3)-C(2)-H(2)	125.4	C(12)-C(8)-Cr(1)	70.6(2)
Cr(1)-C(2)-H(2)	125.4	C(7)-C(8)-Cr(1)	120.8(2)
C(4)-C(3)-C(2)	107.5(3)	C(10)-C(9)-C(8)	108.5(3)
C(4)-C(3)-Cr(1)	70.1(2)	C(10)-C(9)-Cr(1)	72.2(2)
C(2)-C(3)-Cr(1)	70.20(19)	C(8)-C(9)-Cr(1)	70.22(19)
C(4)-C(3)-H(3)	126.2	C(10)-C(9)-H(9)	125.7
C(2)-C(3)-H(3)	126.2	C(8)-C(9)-H(9)	125.7
Cr(1)-C(3)-H(3)	126.2	Cr(1)-C(9)-H(9)	125.7
C(3)-C(4)-C(5)	108.8(3)	C(9)-C(10)-C(11)	107.5(3)
C(3)-C(4)-Cr(1)	72.4(2)	C(9)-C(10)-Cr(1)	69.9(2)
C(5)-C(4)-Cr(1)	70.07(19)	C(11)-C(10)-Cr(1)	70.6(2)
C(3)-C(4)-H(4)	125.6	C(9)-C(10)-H(10)	126.2
C(5)-C(4)-H(4)	125.6	C(11)-C(10)-H(10)	126.2
Cr(1)-C(4)-H(4)	125.6	Cr(1)-C(10)-H(10)	126.2
C(1)-C(5)-C(4)	107.0(3)	C(12)-C(11)-C(10)	109.0(3)
C(1)-C(5)-C(6)	126.3(3)	C(12)-C(11)-Cr(1)	70.0(2)
C(4)-C(5)-C(6)	126.7(3)	C(10)-C(11)-Cr(1)	71.4(2)
C(1)-C(5)-Cr(1)	70.9(2)	C(12)-C(11)-H(11)	125.5
C(4)-C(5)-Cr(1)	70.8(2)	C(10)-C(11)-H(11)	125.5
C(6)-C(5)-Cr(1)	120.9(2)	Cr(1)-C(11)-H(11)	125.5
C(5)-C(6)-C(15)	109.1(3)	C(11)-C(12)-C(8)	107.7(3)
C(5)-C(6)-C(16)	109.2(3)	C(11)-C(12)-Cr(1)	72.1(2)
C(15)-C(6)-C(16)	106.1(3)	C(8)-C(12)-Cr(1)	70.4(2)

C(11)-C(12)-H(12)	126.1	C(20)-C(19)-Fe(1)	69.3(2)
C(8)-C(12)-H(12)	126.1	C(18)-C(19)-H(19)	126.5
Cr(1)-C(12)-H(12)	126.1	C(20)-C(19)-H(19)	126.5
C(7)-C(13)-H(13A)	109.5	Fe(1)-C(19)-H(19)	126.5
C(7)-C(13)-H(13B)	109.5	C(21)-C(20)-C(19)	108.1(3)
H(13A)-C(13)-H(13B)	109.5	C(21)-C(20)-Fe(1)	69.8(2)
C(7)-C(13)-H(13C)	109.5	C(19)-C(20)-Fe(1)	69.89(19)
H(13A)-C(13)-H(13C)	109.5	C(21)-C(20)-H(20)	126.0
H(13B)-C(13)-H(13C)	109.5	C(19)-C(20)-H(20)	126.0
C(7)-C(14)-H(14A)	109.5	Fe(1)-C(20)-H(20)	126.0
C(7)-C(14)-H(14B)	109.5	C(20)-C(21)-C(22)	108.8(3)
H(14A)-C(14)-H(14B)	109.5	C(20)-C(21)-Fe(1)	69.7(2)
C(7)-C(14)-H(14C)	109.5	C(22)-C(21)-Fe(1)	70.2(2)
H(14A)-C(14)-H(14C)	109.5	C(20)-C(21)-H(21)	125.6
H(14B)-C(14)-H(14C)	109.5	C(22)-C(21)-H(21)	125.6
C(6)-C(15)-H(15A)	109.5	Fe(1)-C(21)-H(21)	125.6
C(6)-C(15)-H(15B)	109.5	C(21)-C(22)-C(18)	107.1(3)
H(15A)-C(15)-H(15B)	109.5	C(21)-C(22)-Fe(1)	69.4(2)
C(6)-C(15)-H(15C)	109.5	C(18)-C(22)-Fe(1)	69.66(19)
H(15A)-C(15)-H(15C)	109.5	C(21)-C(22)-H(22)	126.5
H(15B)-C(15)-H(15C)	109.5	C(18)-C(22)-H(22)	126.5
C(6)-C(16)-H(16A)	109.5	Fe(1)-C(22)-H(22)	126.5
C(6)-C(16)-H(16B)	109.5	C(24)-C(23)-C(27)	108.4(3)
H(16A)-C(16)-H(16B)	109.5	C(24)-C(23)-Fe(1)	70.0(2)
C(6)-C(16)-H(16C)	109.5	C(27)-C(23)-Fe(1)	69.90(19)
H(16A)-C(16)-H(16C)	109.5	C(24)-C(23)-H(23)	125.8
H(16B)-C(16)-H(16C)	109.5	C(27)-C(23)-H(23)	125.8
N(1)-C(17)-Cr(1)	178.3(3)	Fe(1)-C(23)-H(23)	125.8
N(1)-C(18)-C(19)	126.8(3)	C(25)-C(24)-C(23)	107.8(3)
N(1)-C(18)-C(22)	124.1(3)	C(25)-C(24)-Fe(1)	69.1(2)
C(19)-C(18)-C(22)	109.1(3)	C(23)-C(24)-Fe(1)	69.5(2)
N(1)-C(18)-Fe(1)	129.0(2)	C(25)-C(24)-H(24)	126.1
C(19)-C(18)-Fe(1)	69.69(19)	C(23)-C(24)-H(24)	126.1
C(22)-C(18)-Fe(1)	69.78(19)	Fe(1)-C(24)-H(24)	126.1
C(18)-C(19)-C(20)	107.0(3)	C(24)-C(25)-C(26)	108.5(3)
C(18)-C(19)-Fe(1)	69.8(2)	C(24)-C(25)-Fe(1)	70.3(2)

C(26)-C(25)-Fe(1)	70.1(2)	C(32)-C(31)-Cr(2)	70.08(19)
C(24)-C(25)-H(25)	125.7	C(30)-C(31)-H(31)	125.7
C(26)-C(25)-H(25)	125.7	C(32)-C(31)-H(31)	125.7
Fe(1)-C(25)-H(25)	125.7	Cr(2)-C(31)-H(31)	125.7
C(25)-C(26)-C(27)	107.9(3)	C(31)-C(32)-C(28)	107.1(3)
C(25)-C(26)-Fe(1)	69.2(2)	C(31)-C(32)-C(33)	127.3(3)
C(27)-C(26)-Fe(1)	69.9(2)	C(28)-C(32)-C(33)	125.5(3)
C(25)-C(26)-H(26)	126.0	C(31)-C(32)-Cr(2)	71.10(19)
C(27)-C(26)-H(26)	126.0	C(28)-C(32)-Cr(2)	70.52(19)
Fe(1)-C(26)-H(26)	126.0	C(33)-C(32)-Cr(2)	120.9(2)
N(2)-C(27)-C(26)	125.7(3)	C(32)-C(33)-C(43)	109.9(3)
N(2)-C(27)-C(23)	126.9(3)	C(32)-C(33)-C(42)	109.0(3)
C(26)-C(27)-C(23)	107.4(3)	C(43)-C(33)-C(42)	106.1(3)
N(2)-C(27)-Fe(1)	127.6(2)	C(32)-C(33)-C(34)	107.6(3)
C(26)-C(27)-Fe(1)	69.4(2)	C(43)-C(33)-C(34)	112.7(3)
C(23)-C(27)-Fe(1)	69.3(2)	C(42)-C(33)-C(34)	111.6(3)
C(29)-C(28)-C(32)	107.3(3)	C(35)-C(34)-C(40)	109.6(3)
C(29)-C(28)-Cr(2)	71.94(19)	C(35)-C(34)-C(41)	109.3(3)
C(32)-C(28)-Cr(2)	70.48(19)	C(40)-C(34)-C(41)	106.0(3)
C(29)-C(28)-H(28)	126.3	C(35)-C(34)-C(33)	107.1(3)
C(32)-C(28)-H(28)	126.3	C(40)-C(34)-C(33)	112.7(3)
Cr(2)-C(28)-H(28)	126.3	C(41)-C(34)-C(33)	112.1(3)
C(28)-C(29)-C(30)	109.0(3)	C(39)-C(35)-C(36)	107.5(3)
C(28)-C(29)-Cr(2)	70.09(19)	C(39)-C(35)-C(34)	126.4(3)
C(30)-C(29)-Cr(2)	71.76(19)	C(36)-C(35)-C(34)	126.1(3)
C(28)-C(29)-H(29)	125.5	C(39)-C(35)-Cr(2)	71.9(2)
C(30)-C(29)-H(29)	125.5	C(36)-C(35)-Cr(2)	70.9(2)
Cr(2)-C(29)-H(29)	125.5	C(34)-C(35)-Cr(2)	121.9(2)
C(31)-C(30)-C(29)	108.0(3)	C(37)-C(36)-C(35)	107.7(3)
C(31)-C(30)-Cr(2)	70.2(2)	C(37)-C(36)-Cr(2)	71.7(2)
C(29)-C(30)-Cr(2)	70.3(2)	C(35)-C(36)-Cr(2)	70.1(2)
C(31)-C(30)-H(30)	126.0	C(37)-C(36)-H(36)	126.1
C(29)-C(30)-H(30)	126.0	C(35)-C(36)-H(36)	126.1
Cr(2)-C(30)-H(30)	126.0	Cr(2)-C(36)-H(36)	126.1
C(30)-C(31)-C(32)	108.5(3)	C(36)-C(37)-C(38)	108.2(3)
C(30)-C(31)-Cr(2)	72.5(2)	C(36)-C(37)-Cr(2)	70.36(19)

C(38)-C(37)-Cr(2)	71.3(2)	H(43A)-C(43)-H(43B)	109.5
C(36)-C(37)-H(37)	125.9	C(33)-C(43)-H(43C)	109.5
C(38)-C(37)-H(37)	125.9	H(43A)-C(43)-H(43C)	109.5
Cr(2)-C(37)-H(37)	125.9	H(43B)-C(43)-H(43C)	109.5
C(39)-C(38)-C(37)	108.5(3)	N(2)-C(44)-Cr(2)	177.6(3)
C(39)-C(38)-Cr(2)	70.9(2)	C(50)-C(45)-C(46)	119.7(4)
C(37)-C(38)-Cr(2)	70.54(19)	C(50)-C(45)-H(45)	120.2
C(39)-C(38)-H(38)	125.8	C(46)-C(45)-H(45)	120.2
C(37)-C(38)-H(38)	125.8	C(47)-C(46)-C(45)	120.2(4)
Cr(2)-C(38)-H(38)	125.8	C(47)-C(46)-H(46)	119.9
C(38)-C(39)-C(35)	108.0(3)	C(45)-C(46)-H(46)	119.9
C(38)-C(39)-Cr(2)	71.6(2)	C(46)-C(47)-C(48)	119.7(4)
C(35)-C(39)-Cr(2)	69.6(2)	C(46)-C(47)-H(47)	120.2
C(38)-C(39)-H(39)	126.0	C(48)-C(47)-H(47)	120.2
C(35)-C(39)-H(39)	126.0	C(49)-C(48)-C(47)	120.3(4)
Cr(2)-C(39)-H(39)	126.0	C(49)-C(48)-H(48)	119.8
C(34)-C(40)-H(40A)	109.5	C(47)-C(48)-H(48)	119.8
C(34)-C(40)-H(40B)	109.5	C(48)-C(49)-C(50)	119.6(4)
H(40A)-C(40)-H(40B)	109.5	C(48)-C(49)-H(49)	120.2
C(34)-C(40)-H(40C)	109.5	C(50)-C(49)-H(49)	120.2
H(40A)-C(40)-H(40C)	109.5	C(45)-C(50)-C(49)	120.6(4)
H(40B)-C(40)-H(40C)	109.5	C(45)-C(50)-H(50)	119.7
C(34)-C(41)-H(41A)	109.5	C(49)-C(50)-H(50)	119.7
C(34)-C(41)-H(41B)	109.5	C(17)-Cr(1)-C(8)	142.73(15)
H(41A)-C(41)-H(41B)	109.5	C(17)-Cr(1)-C(5)	142.15(14)
C(34)-C(41)-H(41C)	109.5	C(8)-Cr(1)-C(5)	75.11(14)
H(41A)-C(41)-H(41C)	109.5	C(17)-Cr(1)-C(12)	111.63(15)
H(41B)-C(41)-H(41C)	109.5	C(8)-Cr(1)-C(12)	39.01(13)
C(33)-C(42)-H(42A)	109.5	C(5)-Cr(1)-C(12)	101.23(14)
C(33)-C(42)-H(42B)	109.5	C(17)-Cr(1)-C(9)	118.57(14)
H(42A)-C(42)-H(42B)	109.5	C(8)-Cr(1)-C(9)	38.76(13)
C(33)-C(42)-H(42C)	109.5	C(5)-Cr(1)-C(9)	91.83(14)
H(42A)-C(42)-H(42C)	109.5	C(12)-Cr(1)-C(9)	64.73(14)
H(42B)-C(42)-H(42C)	109.5	C(17)-Cr(1)-C(4)	117.86(14)
C(33)-C(43)-H(43A)	109.5	C(8)-Cr(1)-C(4)	91.41(14)
C(33)-C(43)-H(43B)	109.5	C(5)-Cr(1)-C(4)	39.11(13)

C(12)-Cr(1)-C(4)	93.92(14)	C(9)-Cr(1)-C(10)	37.92(13)
C(9)-Cr(1)-C(4)	123.57(14)	C(4)-Cr(1)-C(10)	155.10(14)
C(17)-Cr(1)-C(1)	111.08(15)	C(1)-Cr(1)-C(10)	122.94(14)
C(8)-Cr(1)-C(1)	101.85(14)	C(2)-Cr(1)-C(10)	138.52(14)
C(5)-Cr(1)-C(1)	38.92(13)	C(11)-Cr(1)-C(10)	38.07(14)
C(12)-Cr(1)-C(1)	137.27(15)	C(3)-Cr(1)-C(10)	165.49(14)
C(9)-Cr(1)-C(1)	95.53(14)	C(44)-Cr(2)-C(35)	142.29(14)
C(4)-Cr(1)-C(1)	64.76(14)	C(44)-Cr(2)-C(32)	143.04(14)
C(17)-Cr(1)-C(2)	78.72(14)	C(35)-Cr(2)-C(32)	74.50(13)
C(8)-Cr(1)-C(2)	137.83(14)	C(44)-Cr(2)-C(28)	110.13(14)
C(5)-Cr(1)-C(2)	64.07(14)	C(35)-Cr(2)-C(28)	101.66(13)
C(12)-Cr(1)-C(2)	157.26(14)	C(32)-Cr(2)-C(28)	39.00(13)
C(9)-Cr(1)-C(2)	129.49(14)	C(44)-Cr(2)-C(36)	113.45(14)
C(4)-Cr(1)-C(2)	63.61(13)	C(35)-Cr(2)-C(36)	39.01(13)
C(1)-Cr(1)-C(2)	37.82(13)	C(32)-Cr(2)-C(36)	99.87(14)
C(17)-Cr(1)-C(11)	79.30(15)	C(28)-Cr(2)-C(36)	136.42(14)
C(8)-Cr(1)-C(11)	64.08(14)	C(44)-Cr(2)-C(31)	121.19(14)
C(5)-Cr(1)-C(11)	137.53(14)	C(35)-Cr(2)-C(31)	90.26(14)
C(12)-Cr(1)-C(11)	37.92(14)	C(32)-Cr(2)-C(31)	38.82(13)
C(9)-Cr(1)-C(11)	63.68(14)	C(28)-Cr(2)-C(31)	64.70(14)
C(4)-Cr(1)-C(11)	127.74(15)	C(36)-Cr(2)-C(31)	91.94(14)
C(1)-Cr(1)-C(11)	159.05(14)	C(44)-Cr(2)-C(29)	79.23(14)
C(2)-Cr(1)-C(11)	158.00(15)	C(35)-Cr(2)-C(29)	137.38(13)
C(17)-Cr(1)-C(3)	82.58(14)	C(32)-Cr(2)-C(29)	63.95(13)
C(8)-Cr(1)-C(3)	128.86(14)	C(28)-Cr(2)-C(29)	37.98(13)
C(5)-Cr(1)-C(3)	64.30(13)	C(36)-Cr(2)-C(29)	154.94(14)
C(12)-Cr(1)-C(3)	120.68(14)	C(31)-Cr(2)-C(29)	63.32(14)
C(9)-Cr(1)-C(3)	155.91(14)	C(44)-Cr(2)-C(37)	79.73(14)
C(4)-Cr(1)-C(3)	37.49(13)	C(35)-Cr(2)-C(37)	64.22(13)
C(1)-Cr(1)-C(3)	64.21(13)	C(32)-Cr(2)-C(37)	136.51(14)
C(2)-Cr(1)-C(3)	38.37(13)	C(28)-Cr(2)-C(37)	160.53(14)
C(11)-Cr(1)-C(3)	136.54(14)	C(36)-Cr(2)-C(37)	37.90(13)
C(17)-Cr(1)-C(10)	82.97(15)	C(31)-Cr(2)-C(37)	125.52(14)
C(8)-Cr(1)-C(10)	64.27(14)	C(29)-Cr(2)-C(37)	158.38(14)
C(5)-Cr(1)-C(10)	129.74(14)	C(44)-Cr(2)-C(39)	115.68(14)
C(12)-Cr(1)-C(10)	64.15(15)	C(35)-Cr(2)-C(39)	38.54(13)

C(32)-Cr(2)-C(39)	92.39(13)	C(20)-Fe(1)-C(18)	68.00(14)
C(28)-Cr(2)-C(39)	96.89(14)	C(21)-Fe(1)-C(18)	67.76(14)
C(36)-Cr(2)-C(39)	64.41(14)	C(19)-Fe(1)-C(18)	40.50(13)
C(31)-Cr(2)-C(39)	123.13(14)	C(23)-Fe(1)-C(18)	159.91(14)
C(29)-Cr(2)-C(39)	131.42(14)	C(25)-Fe(1)-C(22)	107.86(14)
C(37)-Cr(2)-C(39)	63.66(14)	C(20)-Fe(1)-C(22)	68.40(14)
C(44)-Cr(2)-C(38)	81.24(14)	C(21)-Fe(1)-C(22)	40.43(14)
C(35)-Cr(2)-C(38)	63.85(13)	C(19)-Fe(1)-C(22)	68.68(14)
C(32)-Cr(2)-C(38)	129.93(13)	C(23)-Fe(1)-C(22)	157.97(14)
C(28)-Cr(2)-C(38)	124.75(15)	C(18)-Fe(1)-C(22)	40.56(13)
C(36)-Cr(2)-C(38)	63.78(14)	C(25)-Fe(1)-C(26)	40.64(14)
C(31)-Cr(2)-C(38)	153.16(14)	C(20)-Fe(1)-C(26)	157.49(14)
C(29)-Cr(2)-C(38)	141.23(14)	C(21)-Fe(1)-C(26)	160.32(14)
C(37)-Cr(2)-C(38)	38.15(14)	C(19)-Fe(1)-C(26)	121.48(14)
C(39)-Cr(2)-C(38)	37.54(13)	C(23)-Fe(1)-C(26)	68.45(14)
C(44)-Cr(2)-C(30)	85.55(14)	C(18)-Fe(1)-C(26)	107.74(14)
C(35)-Cr(2)-C(30)	127.59(14)	C(22)-Fe(1)-C(26)	123.71(14)
C(32)-Cr(2)-C(30)	63.85(13)	C(25)-Fe(1)-C(24)	40.59(14)
C(28)-Cr(2)-C(30)	63.96(13)	C(20)-Fe(1)-C(24)	123.90(15)
C(36)-Cr(2)-C(30)	118.84(14)	C(21)-Fe(1)-C(24)	108.32(15)
C(31)-Cr(2)-C(30)	37.37(13)	C(19)-Fe(1)-C(24)	160.02(14)
C(29)-Cr(2)-C(30)	37.90(13)	C(23)-Fe(1)-C(24)	40.48(14)
C(37)-Cr(2)-C(30)	134.96(14)	C(18)-Fe(1)-C(24)	158.27(14)
C(39)-Cr(2)-C(30)	156.17(13)	C(22)-Fe(1)-C(24)	122.51(14)
C(38)-Cr(2)-C(30)	166.18(14)	C(26)-Fe(1)-C(24)	68.33(14)
C(25)-Fe(1)-C(20)	160.40(15)	C(25)-Fe(1)-C(27)	68.47(14)
C(25)-Fe(1)-C(21)	124.25(15)	C(20)-Fe(1)-C(27)	121.76(14)
C(20)-Fe(1)-C(21)	40.55(14)	C(21)-Fe(1)-C(27)	157.89(14)
C(25)-Fe(1)-C(19)	157.54(15)	C(19)-Fe(1)-C(27)	106.73(14)
C(20)-Fe(1)-C(19)	40.85(14)	C(23)-Fe(1)-C(27)	40.83(13)
C(21)-Fe(1)-C(19)	68.43(14)	C(18)-Fe(1)-C(27)	123.46(14)
C(25)-Fe(1)-C(23)	68.29(14)	C(22)-Fe(1)-C(27)	159.91(14)
C(20)-Fe(1)-C(23)	107.53(14)	C(26)-Fe(1)-C(27)	40.71(13)
C(21)-Fe(1)-C(23)	122.47(14)	C(24)-Fe(1)-C(27)	68.43(14)
C(19)-Fe(1)-C(23)	123.33(14)	C(17)-N(1)-C(18)	125.8(3)
C(25)-Fe(1)-C(18)	122.53(14)	C(44)-N(2)-C(27)	126.4(3)

Table 9-15: Anisotropic displacement parameters ($\text{\AA}^2 \times 10^3$) for **4b**. The anisotropic displacement factor exponent takes the form: $-2\pi^2 [h^2 a^{*2} U_{11} + \dots + 2 h k a^* b^* U_{12}]$:

	U ₁₁	U ₂₂	U ₃₃	U ₂₃	U ₁₃	U ₁₂
C(1)	19(2)	14(2)	13(2)	-3(2)	-2(2)	-6(2)
C(2)	20(2)	13(2)	17(2)	-1(2)	-9(2)	-7(2)
C(3)	15(2)	12(2)	17(2)	-2(2)	-4(2)	-5(2)
C(4)	19(2)	10(2)	17(2)	-5(2)	-7(2)	-3(2)
C(5)	13(2)	12(2)	19(2)	-5(2)	-2(2)	-7(2)
C(6)	16(2)	14(2)	19(2)	-9(2)	-5(2)	-3(2)
C(7)	16(2)	16(2)	18(2)	-4(2)	-7(2)	-1(2)
C(8)	19(2)	10(2)	18(2)	-2(2)	-6(2)	-1(2)
C(9)	18(2)	10(2)	22(2)	-6(2)	-8(2)	1(2)
C(10)	23(2)	14(2)	32(2)	-9(2)	-12(2)	-1(2)
C(11)	20(2)	9(2)	25(2)	0(2)	-3(2)	-5(2)
C(12)	19(2)	16(2)	14(2)	-1(2)	-4(2)	-2(2)
C(13)	21(2)	19(2)	22(2)	-6(2)	-5(2)	-2(2)
C(14)	27(2)	23(2)	20(2)	-6(2)	-10(2)	-2(2)
C(15)	21(2)	17(2)	19(2)	-5(2)	-3(2)	-3(2)
C(16)	20(2)	24(2)	32(2)	-8(2)	-7(2)	-8(2)
C(17)	23(2)	10(2)	8(2)	-2(1)	-3(2)	-6(2)
C(18)	14(2)	12(2)	14(2)	-5(2)	-5(2)	-5(1)
C(19)	18(2)	11(2)	15(2)	-2(2)	-7(2)	-5(2)
C(20)	16(2)	17(2)	11(2)	-1(2)	-1(2)	-10(2)
C(21)	12(2)	19(2)	17(2)	-5(2)	-3(2)	-6(2)
C(22)	15(2)	10(2)	17(2)	-1(2)	-10(2)	-2(1)
C(23)	18(2)	14(2)	12(2)	-4(2)	-3(2)	-7(2)
C(24)	16(2)	14(2)	24(2)	-8(2)	-8(2)	-1(2)
C(25)	28(2)	9(2)	14(2)	-3(2)	-9(2)	-4(2)
C(26)	15(2)	12(2)	9(2)	0(1)	-4(2)	-2(2)
C(27)	15(2)	12(2)	12(2)	-3(2)	-5(2)	-2(2)
C(28)	12(2)	13(2)	16(2)	-6(2)	-1(2)	1(2)
C(29)	20(2)	11(2)	14(2)	-5(2)	-5(2)	1(2)
C(30)	17(2)	13(2)	13(2)	-8(2)	1(2)	-5(2)
C(31)	15(2)	11(2)	20(2)	-10(2)	-4(2)	-1(2)

C(32)	14(2)	11(2)	11(2)	-6(1)	0(2)	-7(1)
C(33)	21(2)	11(2)	11(2)	-3(2)	-3(2)	-5(2)
C(34)	17(2)	14(2)	12(2)	-6(2)	-6(2)	-3(2)
C(35)	21(2)	7(2)	13(2)	-1(1)	-5(2)	-4(2)
C(36)	20(2)	12(2)	17(2)	-4(2)	-7(2)	-3(2)
C(37)	28(2)	10(2)	14(2)	-6(2)	-5(2)	-3(2)
C(38)	30(2)	14(2)	15(2)	-1(2)	-11(2)	-11(2)
C(39)	23(2)	14(2)	16(2)	-1(2)	-7(2)	-7(2)
C(40)	33(2)	17(2)	15(2)	-5(2)	-7(2)	-8(2)
C(41)	25(2)	19(2)	20(2)	-5(2)	-12(2)	-1(2)
C(42)	25(2)	20(2)	11(2)	-1(2)	-1(2)	-8(2)
C(43)	29(2)	17(2)	11(2)	-6(2)	-1(2)	-7(2)
C(44)	8(2)	12(2)	19(2)	-7(2)	-3(2)	-4(1)
C(45)	23(2)	22(2)	26(2)	-10(2)	-11(2)	2(2)
C(46)	26(2)	16(2)	25(2)	1(2)	-12(2)	-8(2)
C(47)	36(3)	22(2)	16(2)	1(2)	-9(2)	-9(2)
C(48)	48(3)	20(2)	25(2)	-1(2)	-18(2)	-10(2)
C(49)	34(3)	26(2)	32(3)	8(2)	-14(2)	-16(2)
C(50)	24(2)	31(2)	17(2)	-2(2)	-2(2)	-4(2)
Cr(1)	13(1)	10(1)	14(1)	-4(1)	-3(1)	-3(1)
Cr(2)	14(1)	11(1)	9(1)	-3(1)	-3(1)	-4(1)
Fe(1)	13(1)	12(1)	11(1)	-3(1)	-4(1)	-3(1)
N(1)	17(2)	16(2)	12(2)	-5(1)	-5(1)	-5(1)
N(2)	14(2)	12(2)	13(2)	-4(1)	-4(1)	-5(1)

Table 9-16: Hydrogen coordinates ($\times 10^4$) and isotropic displacement parameters for **4b** ($\text{\AA}^2 \times 10^3$):

	x	y	z	U(eq)
H(1)	12289	2537	-162	19
H(2)	10269	3693	390	19
H(3)	9819	3803	2402	18
H(4)	11557	2692	3107	18
H(9)	12422	39	950	20
H(10)	10301	-70	1592	26
H(11)	9430	184	3579	24
H(12)	10993	443	4173	22
H(13A)	14024	-1192	2871	32
H(13B)	14927	-414	2217	32
H(13C)	14240	-637	1564	32
H(14A)	12618	1136	3848	35
H(14B)	13937	550	3646	35
H(14C)	12983	-176	4210	35
H(15A)	13792	963	251	30
H(15B)	14941	960	454	30
H(15C)	14215	2086	-129	30
H(16A)	14353	2803	1211	37
H(16B)	14890	1652	1944	37
H(16C)	13733	2390	2509	37
H(19)	8000	2208	4192	17
H(20)	5853	2616	5304	17
H(21)	4650	3103	3958	19
H(22)	6020	3004	2010	16
H(23)	5856	5238	4683	16
H(24)	4709	5747	3274	20
H(25)	6153	5613	1362	19
H(26)	8195	5053	1570	16
H(28)	6154	5420	7326	18
H(29)	7172	6383	5321	19

H(30)	9328	5972	5106	17
H(31)	9668	4739	6969	17
H(36)	10128	2521	6720	19
H(37)	9510	2452	5126	20
H(38)	7317	2642	5781	21
H(39)	6569	2828	7776	21
H(40A)	6943	2050	9619	31
H(40B)	7577	2134	10403	31
H(40C)	8158	1268	9681	31
H(41A)	9471	2601	9558	31
H(41B)	9896	3190	8259	31
H(41C)	9906	1903	8676	31
H(42A)	5951	4941	9225	30
H(42B)	6186	3766	10091	30
H(42C)	6046	3848	8927	30
H(43A)	8831	4559	9103	28
H(43B)	7929	4029	10206	28
H(43C)	7570	5258	9484	28
H(45)	7395	7583	2043	28
H(46)	6275	7381	3886	27
H(47)	5900	8752	4739	31
H(48)	6679	10306	3764	35
H(49)	7772	10521	1922	37
H(50)	8118	9155	1065	32

Table 9-17: Crystal data and structure refinement for **5**:

Formula weight	656.77
Temperature	81(2) K
Wavelength	0.71073 Å
Crystal system	Monoclinic
Space group	P2(1)/n
Unit cell dimensions	a = 10.551(9) Å $\alpha = 90^\circ$.
	b = 9.168(8) Å $\beta = 107.79(4)^\circ$.
	c = 17.063(18) Å $\gamma = 90^\circ$.
Volume	1572(3) Å ³
Z	2
Density (calculated)	1.388 Mg/m ³
Absorption coefficient	0.724 mm ⁻¹
F(000)	692
Crystal size	0.23 x 0.08 x 0.03 mm ³
Crystal color and habit	orange plate
Diffractometer	Bruker/Siemens SMART APEX
Theta range for data collection	2.03 to 25.47°.
Index ranges	-12 ≤ h ≤ 10, -11 ≤ k ≤ 10, -20 ≤ l ≤ 20
Reflections collected	10327
Independent reflections	2873 [R(int) = 0.1740]
Completeness to theta = 25.47°	98.6 %
Absorption correction	†Empirical
Max. and min. transmission	0.9786 and 0.8512
Solution method	XS, Bruker SHELXTL v. 6.10
Refinement method	Full-matrix least-squares on F ²
Data / restraints / parameters	2873 / 12 / 199
Goodness-of-fit on F ²	0.894
Final R indices [I > 2σ(I)]	R1 = 0.0640, wR2 = 0.1251
R indices (all data)	R1 = 0.1412, wR2 = 0.1520
Largest diff. peak and hole	0.927 and -0.773 e.Å ⁻³

†**SADABS**: an empirical absorption correction program, Saint+ 6.22, Bruker AXS Inc., Madison, WI, 2001.

Table 9-18: Atomic coordinates ($\times 10^4$) and equivalent isotropic displacement parameters for **5** ($\text{\AA}^2 \times 10^3$). $U(\text{eq})$ is defined as one third of the trace of the orthogonalized U_{ij} tensor:

	x	y	z	$U(\text{eq})$
C(1)	5849(4)	10067(6)	6642(3)	19(1)
C(2)	6522(5)	11068(6)	7239(3)	24(1)
C(3)	5564(5)	12001(6)	7426(3)	22(1)
C(4)	4289(5)	11549(6)	6931(3)	21(1)
C(5)	4452(5)	10372(6)	6430(3)	19(1)
C(6)	3330(5)	9510(6)	5814(3)	21(1)
C(7)	2515(5)	8676(6)	6323(3)	20(1)
C(8)	3477(5)	8356(6)	7189(3)	17(1)
C(9)	3398(5)	8995(6)	7935(3)	19(1)
C(10)	4500(5)	8497(6)	8586(3)	23(1)
C(11)	5290(5)	7567(7)	8247(3)	24(1)
C(12)	4660(5)	7481(6)	7383(3)	20(1)
C(13)	1884(5)	7258(6)	5908(3)	25(1)
C(14)	1361(4)	9631(7)	6416(3)	23(1)
C(15)	3940(5)	8441(6)	5338(3)	23(1)
C(16)	2477(5)	10572(6)	5169(3)	24(1)
C(17)	6458(5)	10247(6)	8689(3)	18(1)
C(18)	8646(5)	10299(6)	9662(3)	18(1)
C(19)	9319(5)	9567(6)	9200(3)	19(1)
C(20)	10674(5)	9264(6)	9534(3)	18(1)
Cr(1)	5187(1)	9739(1)	7704(1)	19(1)
N(1)	7261(4)	10628(5)	9346(3)	20(1)

Table 9-19: Bond lengths [\AA] and angles for **5** [$^\circ$]

C(1)-C(2)	1.393(7)	C(12)-Cr(1)	2.170(6)
C(1)-C(5)	1.434(6)	C(12)-H(12A)	1.0000
C(1)-Cr(1)	2.152(5)	C(13)-H(13A)	0.9800
C(1)-H(1A)	1.0000	C(13)-H(13B)	0.9800
C(2)-C(3)	1.432(8)	C(13)-H(13C)	0.9800
C(2)-Cr(1)	2.186(6)	C(14)-H(14A)	0.9800
C(2)-H(2A)	1.0000	C(14)-H(14B)	0.9800
C(3)-C(4)	1.415(7)	C(14)-H(14C)	0.9800
C(3)-Cr(1)	2.191(6)	C(15)-H(15A)	0.9800
C(3)-H(3A)	1.0000	C(15)-H(15B)	0.9800
C(4)-C(5)	1.418(8)	C(15)-H(15C)	0.9800
C(4)-Cr(1)	2.151(6)	C(16)-H(16A)	0.9800
C(4)-H(4A)	1.0000	C(16)-H(16B)	0.9800
C(5)-C(6)	1.540(7)	C(16)-H(16C)	0.9800
C(5)-Cr(1)	2.151(5)	C(17)-N(1)	1.232(6)
C(6)-C(15)	1.534(7)	C(17)-Cr(1)	1.861(5)
C(6)-C(16)	1.537(7)	C(18)-C(19)	1.386(7)
C(6)-C(7)	1.592(7)	C(18)-C(20)#1	1.399(7)
C(7)-C(13)	1.532(7)	C(18)-N(1)	1.427(6)
C(7)-C(8)	1.543(6)	C(19)-C(20)	1.395(6)
C(7)-C(14)	1.547(7)	C(19)-H(19A)	0.9500
C(8)-C(9)	1.427(7)	C(20)-C(18)#1	1.399(7)
C(8)-C(12)	1.435(7)	C(20)-H(20A)	0.9500
C(8)-Cr(1)	2.160(5)		
C(9)-C(10)	1.416(7)	C(2)-C(1)-C(5)	108.1(5)
C(9)-Cr(1)	2.154(5)	C(2)-C(1)-Cr(1)	72.6(3)
C(9)-H(9A)	1.0000	C(5)-C(1)-Cr(1)	70.5(3)
C(10)-C(11)	1.431(8)	C(2)-C(1)-H(1A)	125.9
C(10)-Cr(1)	2.180(6)	C(5)-C(1)-H(1A)	125.9
C(10)-H(10A)	1.0000	Cr(1)-C(1)-H(1A)	125.9
C(11)-C(12)	1.421(7)	C(1)-C(2)-C(3)	108.7(5)
C(11)-Cr(1)	2.185(6)	C(1)-C(2)-Cr(1)	69.9(3)
C(11)-H(11A)	1.0000	C(3)-C(2)-Cr(1)	71.1(3)

C(1)-C(2)-H(2A)	125.7	C(12)-C(8)-Cr(1)	71.0(3)
C(3)-C(2)-H(2A)	125.7	C(7)-C(8)-Cr(1)	120.1(4)
Cr(1)-C(2)-H(2A)	125.7	C(10)-C(9)-C(8)	108.0(5)
C(4)-C(3)-C(2)	107.4(5)	C(10)-C(9)-Cr(1)	71.9(3)
C(4)-C(3)-Cr(1)	69.5(3)	C(8)-C(9)-Cr(1)	70.9(3)
C(2)-C(3)-Cr(1)	70.7(3)	C(10)-C(9)-H(9A)	125.9
C(4)-C(3)-H(3A)	126.3	C(8)-C(9)-H(9A)	125.9
C(2)-C(3)-H(3A)	126.3	Cr(1)-C(9)-H(9A)	125.9
Cr(1)-C(3)-H(3A)	126.3	C(9)-C(10)-C(11)	108.4(5)
C(3)-C(4)-C(5)	108.3(5)	C(9)-C(10)-Cr(1)	69.9(3)
C(3)-C(4)-Cr(1)	72.5(3)	C(11)-C(10)-Cr(1)	71.1(3)
C(5)-C(4)-Cr(1)	70.8(3)	C(9)-C(10)-H(10A)	125.8
C(3)-C(4)-H(4A)	125.8	C(11)-C(10)-H(10A)	125.8
C(5)-C(4)-H(4A)	125.8	Cr(1)-C(10)-H(10A)	125.8
Cr(1)-C(4)-H(4A)	125.8	C(12)-C(11)-C(10)	107.8(5)
C(4)-C(5)-C(1)	107.5(4)	C(12)-C(11)-Cr(1)	70.4(3)
C(4)-C(5)-C(6)	126.3(5)	C(10)-C(11)-Cr(1)	70.7(3)
C(1)-C(5)-C(6)	126.0(5)	C(12)-C(11)-H(11A)	126.1
C(4)-C(5)-Cr(1)	70.7(3)	C(10)-C(11)-H(11A)	126.1
C(1)-C(5)-Cr(1)	70.6(3)	Cr(1)-C(11)-H(11A)	126.1
C(6)-C(5)-Cr(1)	121.0(4)	C(11)-C(12)-C(8)	107.9(5)
C(15)-C(6)-C(16)	105.9(4)	C(11)-C(12)-Cr(1)	71.5(3)
C(15)-C(6)-C(5)	109.3(4)	C(8)-C(12)-Cr(1)	70.3(3)
C(16)-C(6)-C(5)	108.9(5)	C(11)-C(12)-H(12A)	126.0
C(15)-C(6)-C(7)	111.5(5)	C(8)-C(12)-H(12A)	126.0
C(16)-C(6)-C(7)	113.5(4)	Cr(1)-C(12)-H(12A)	126.0
C(5)-C(6)-C(7)	107.8(4)	C(7)-C(13)-H(13A)	109.5
C(13)-C(7)-C(8)	110.3(4)	C(7)-C(13)-H(13B)	109.5
C(13)-C(7)-C(14)	106.5(4)	H(13A)-C(13)-H(13B)	109.5
C(8)-C(7)-C(14)	108.5(4)	C(7)-C(13)-H(13C)	109.5
C(13)-C(7)-C(6)	112.7(4)	H(13A)-C(13)-H(13C)	109.5
C(8)-C(7)-C(6)	107.8(4)	H(13B)-C(13)-H(13C)	109.5
C(14)-C(7)-C(6)	111.0(5)	C(7)-C(14)-H(14A)	109.5
C(9)-C(8)-C(12)	107.8(4)	C(7)-C(14)-H(14B)	109.5
C(9)-C(8)-C(7)	125.1(5)	H(14A)-C(14)-H(14B)	109.5
C(12)-C(8)-C(7)	126.8(5)	C(7)-C(14)-H(14C)	109.5
C(9)-C(8)-Cr(1)	70.5(3)	H(14A)-C(14)-H(14C)	109.5

H(14B)-C(14)-H(14C)	109.5	C(9)-Cr(1)-C(8)	38.64(19)
C(6)-C(15)-H(15A)	109.5	C(17)-Cr(1)-C(12)	121.6(2)
C(6)-C(15)-H(15B)	109.5	C(4)-Cr(1)-C(12)	123.4(2)
H(15A)-C(15)-H(15B)	109.5	C(5)-Cr(1)-C(12)	91.0(2)
C(6)-C(15)-H(15C)	109.5	C(1)-Cr(1)-C(12)	92.6(2)
H(15A)-C(15)-H(15C)	109.5	C(9)-Cr(1)-C(12)	64.7(2)
H(15B)-C(15)-H(15C)	109.5	C(8)-Cr(1)-C(12)	38.71(18)
C(6)-C(16)-H(16A)	109.5	C(17)-Cr(1)-C(10)	78.9(2)
C(6)-C(16)-H(16B)	109.5	C(4)-Cr(1)-C(10)	130.5(2)
H(16A)-C(16)-H(16B)	109.5	C(5)-Cr(1)-C(10)	138.15(19)
C(6)-C(16)-H(16C)	109.5	C(1)-Cr(1)-C(10)	156.3(2)
H(16A)-C(16)-H(16C)	109.5	C(9)-Cr(1)-C(10)	38.13(18)
H(16B)-C(16)-H(16C)	109.5	C(8)-Cr(1)-C(10)	64.0(2)
N(1)-C(17)-Cr(1)	177.2(5)	C(12)-Cr(1)-C(10)	64.0(2)
C(19)-C(18)-C(20)#1	119.9(4)	C(17)-Cr(1)-C(2)	79.7(2)
C(19)-C(18)-N(1)	122.1(4)	C(4)-Cr(1)-C(2)	63.9(2)
C(20)#1-C(18)-N(1)	118.0(5)	C(5)-Cr(1)-C(2)	63.7(2)
C(18)-C(19)-C(20)	120.2(4)	C(9)-Cr(1)-C(2)	160.2(2)
C(18)-C(19)-H(19A)	119.9	C(8)-Cr(1)-C(2)	136.9(2)
C(20)-C(19)-H(19A)	119.9	C(12)-Cr(1)-C(2)	125.8(2)
C(19)-C(20)-C(18)#1	119.9(5)	C(10)-Cr(1)-C(2)	158.16(19)
C(19)-C(20)-H(20A)	120.1	C(17)-Cr(1)-C(11)	85.2(2)
C(18)#1-C(20)-H(20A)	120.1	C(4)-Cr(1)-C(11)	156.7(2)
C(17)-Cr(1)-C(4)	114.9(2)	C(5)-Cr(1)-C(11)	129.1(2)
C(17)-Cr(1)-C(5)	141.5(2)	C(1)-Cr(1)-C(11)	119.8(2)
C(4)-Cr(1)-C(5)	38.5(2)	C(9)-Cr(1)-C(11)	64.3(2)
C(17)-Cr(1)-C(1)	113.3(2)	C(8)-Cr(1)-C(11)	64.2(2)
C(4)-Cr(1)-C(1)	64.7(2)	C(12)-Cr(1)-C(11)	38.10(19)
C(5)-Cr(1)-C(1)	38.94(17)	C(10)-Cr(1)-C(11)	38.3(2)
C(17)-Cr(1)-C(9)	110.1(2)	C(2)-Cr(1)-C(11)	135.1(2)
C(4)-Cr(1)-C(9)	96.3(2)	C(17)-Cr(1)-C(3)	80.2(2)
C(5)-Cr(1)-C(9)	101.83(19)	C(4)-Cr(1)-C(3)	38.03(18)
C(1)-Cr(1)-C(9)	136.60(18)	C(5)-Cr(1)-C(3)	63.9(2)
C(17)-Cr(1)-C(8)	142.8(2)	C(1)-Cr(1)-C(3)	63.8(2)
C(4)-Cr(1)-C(8)	92.7(2)	C(9)-Cr(1)-C(3)	124.5(2)
C(5)-Cr(1)-C(8)	75.5(2)	C(8)-Cr(1)-C(3)	130.70(19)
C(1)-Cr(1)-C(8)	100.7(2)	C(12)-Cr(1)-C(3)	153.9(2)

Table 9-20: Anisotropic displacement parameters for **5** ($\text{\AA}^2 \times 10^3$). The anisotropic displacement factor exponent takes the form: $-2\pi^2 [h^2 a^{*2} U_{11} + 2hk a^* b^* U_{12}]$:

	U ₁₁	U ₂₂	U ₃₃	U ₂₃	U ₁₃	U ₁₂
C(1)	9(2)	37(4)	12(2)	6(3)	6(2)	3(2)
C(2)	11(3)	43(4)	17(3)	12(3)	5(2)	0(2)
C(3)	26(3)	30(4)	12(3)	3(3)	9(2)	-5(3)
C(4)	18(3)	34(4)	12(3)	3(3)	6(2)	-4(2)
C(5)	16(3)	33(3)	11(2)	6(3)	8(2)	3(2)
C(6)	16(3)	31(4)	14(3)	-3(3)	2(2)	0(2)
C(7)	12(3)	31(4)	18(3)	2(3)	6(2)	2(2)
C(8)	16(1)	18(2)	17(2)	0(1)	6(1)	-2(1)
C(9)	15(3)	26(4)	21(3)	2(3)	10(2)	-5(2)
C(10)	24(3)	32(4)	13(3)	0(3)	8(2)	-11(3)
C(11)	13(3)	36(4)	20(3)	8(3)	2(2)	-3(2)
C(12)	14(3)	21(3)	23(3)	-2(3)	1(2)	-1(2)
C(13)	20(3)	37(4)	18(3)	1(3)	6(2)	-4(3)
C(14)	10(2)	39(4)	22(3)	-2(3)	8(2)	-1(2)
C(15)	18(3)	31(4)	20(3)	2(3)	6(2)	1(2)
C(16)	14(3)	36(4)	17(3)	0(3)	-1(2)	1(2)
C(17)	17(1)	19(2)	18(1)	1(1)	7(1)	0(1)
C(18)	12(2)	22(3)	19(3)	2(3)	5(2)	-3(2)
C(19)	17(3)	22(3)	13(3)	-1(3)	-2(2)	-5(2)
C(20)	12(3)	23(3)	19(3)	-1(3)	5(2)	-1(2)
Cr(1)	9(1)	33(1)	16(1)	2(1)	2(1)	-3(1)
N(1)	11(2)	29(3)	21(2)	1(2)	5(2)	-1(2)

Table 9-21: Hydrogen coordinates ($\times 10^4$) and isotropic displacement parameters for **5** ($\text{\AA}^2 \times 10^{-3}$):

	x	y	z	U(eq)
H(1A)	6271	9314	6378	23
H(2A)	7509	11135	7488	28
H(3A)	5762	12835	7823	26
H(4A)	3425	12023	6908	25
H(9A)	2660	9628	7994	23
H(10A)	4685	8737	9182	27
H(11A)	6119	7044	8564	28
H(12A)	4963	6878	6986	24
H(13A)	1374	6804	6236	38
H(13B)	2586	6588	5867	38
H(13C)	1290	7474	5355	38
H(14A)	870	9093	6727	35
H(14B)	759	9875	5870	35
H(14C)	1723	10530	6711	35
H(15A)	4450	8986	5042	34
H(15B)	3229	7893	4944	34
H(15C)	4532	7763	5725	34
H(16A)	3033	11041	4875	35
H(16B)	2100	11317	5445	35
H(16C)	1755	10034	4777	35
H(19A)	8857	9271	8653	22
H(20A)	11134	8762	9216	2

The research for this Dissertation was performed from August 1999 to August 2002 in the laboratory of Prof. Pamela Shapiro at the Department of Chemistry, University of Idaho under the supervision of Prof. Pamela Shapiro (University of Idaho) and Prof. Dr. Bernd Wenclawiak (Universität – GH Siegen).

Acknowledgments

I like to thank Prof. Pamela Shapiro for her great supervision during this challenging and interesting project. The use of laboratory space, materials and the financial support for this work is greatly acknowledged.

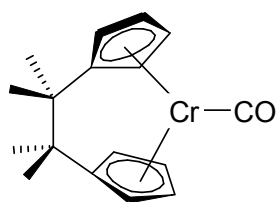
I also like to thank Prof. Dr. Bernd Wenclawiak for giving me the opportunity to perform the laboratory work at the University of Idaho as part of an exchange program between the Universität Siegen and the University of Idaho and for some financial support.

Also thanks to Dr. Brendan Twamley for resolving the X-Ray single crystal structures, Dr. Alexander Blumenfeld and Dr. Gary Knerr for obtaining NMR, IR and MS data. I would like to express my appreciation for all colleagues in the Shapiro Work Group and the Department of Chemistry at the University of Idaho for their kindness and help.

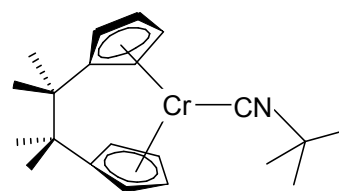
I also thank Dr. Matthew Johnston and Mark Engelmann for proofreading.

Thanks to the Departments of Chemistry at the University of Idaho and the University of Siegen as well as to the National Science Foundation for financial support.

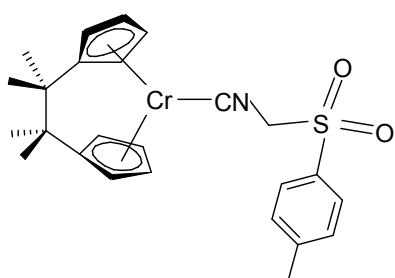
List of *Ansa*-Chromocene isocyanide Complexes



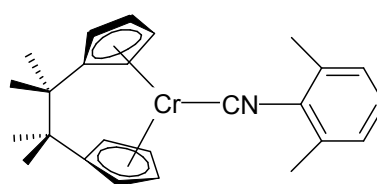
1b



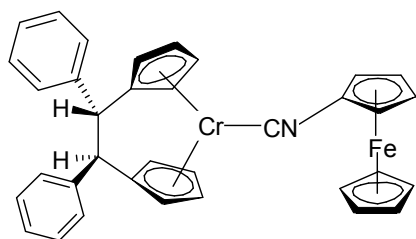
2b



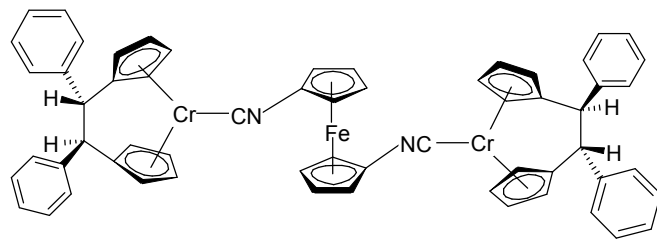
F1



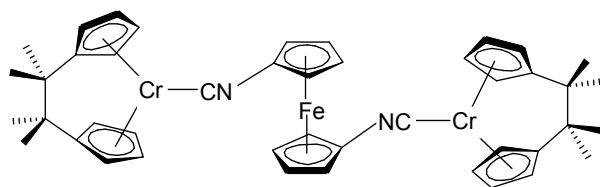
F2



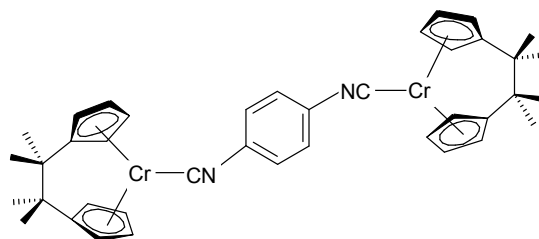
3



4a



4b



5